NASA CONTRACTOR
REPORT

NASA CR-61367

TEST AND EVALUATION OF APOLLO 14 COMPOSITE CASTING DEMONSTRATION SPECIMENS 6, 9, AND 12

TRW Systems Group
Redondo Beach,
California

September 1971

Final Report

Prepared for

NASA-GEORGE C. MARSHALL SPACE FLIGHT CENTER
Marshall Space Flight Center, Alabama 35812

TECHNICAL REPORT STANDARD TITLE PAGE

1. REPORT NO.	2. GOVERNMENT ACCESSION NO.	3. RECIPIENT'S CATALOG NO.
NASA CR-61367		

4. TITLE AND SUBTITLE	5. REPORT DATE
TEST AND EVALUATION OF APOLLO 14 COMPOSITE CASTING DEMONSTRATION SPECIMENS 6, 9, and 12: Final Report	September 1971
	6. PERFORMING ORGANIZATION CODE
7. AUTHOR(S)	8. PERFORMING ORGANIZATION REPORT #
9. PERFORMING ORGANIZATION NAME AND ADDRESS TRW Systems Group Redondo Beach California	10. WORK UNIT NO.
	11. CONTRACT OR GRANT NO. NAS 8-27085
12. SPONSORING AGENCY NAME AND ADDRESS National Aeronautics and Space Administration Washington, D. C. 20546	13. TYPE OF REPORT & PERIOD COVERED Contractor Report Final
	14. SPONSORING AGENCY CODE

15. SUPPLEMENTARY NOTES

Technical Monitor: Iva C. Yates, Jr., George C. Marshall Space Flight Center

16. ABSTRACT

Flight and Control Specimens 6, 9 and 12 from the Apollo 14 Composite Casting Demonstration were evaluated with respect to the degree of dispersion achieved for mixtures of immiscible materials under one gravity and low gravity environments. The Flight and Control Capsules 6, 9 and 12 contained paraffin and sodium acetate, paraffin, sodium acetate and argon and paraffin, sodium acetate and 100μm diameter tungsten microspheres, respectively. The evaluation and documentation utilized photographic and metallographic examinations, density measurements and droplet size and distribution determinations. In addition, theoretical analyses were performed in order to aid in the understanding of the fluid behavior of the specimens during processing and subsequent solidification. A comparison of evaluated data with the theoretical analyses reveals that although the immiscible materials were uniquely dispersed in a low gravity environment, non-uniform dispersions were obtained primarily due to insufficient initial mixing and an essentially unidirectional thermal gradient during cooldown.

17. KEY WORDS	18. DISTRIBUTION STATEMENT
	Iva C. Yates, Jr. Unclassified-unlimited

19. SECURITY CLASSIF. (of this report)	20. SECURITY CLASSIF. (of this page)	21. NO. OF PAGES	22. PRICE
Unclassified	Unclassified	66	$3.00

MSFC - Form 3292 (May 1969)

FOREWORD

This report was prepared by TRW Systems Group, Redondo Beach, California, and contains the results of the Phase I work accomplished during the period 16 April 1971 to 30 September 1971. The program was originated and is managed by the George C. Marshall Space Flight Center under the technical direction of Mr. I. C. Yates, Jr.

The work performed on the program was accomplished by the Advanced Technology Division of TRW Systems Group. Technical direction of the program is provided by the Materials Science Staff of the Research and Technology Operations. The Program Manager is Mr. R. L. Hammel and the Principal Investigator is Mr. J. L. Reger. Responsible technical personnel who supported this program are acknowledged below:

Mr. J. D. O'Keefe, Advanced Technology Staff Group
Mr. V. H. Reineking, Materials Science Staff
Mr. R. Valencia, Jr., Materials Science Staff

TABLE OF CONTENTS

TABLE OF CONTENTS (CONT'D)

1.0 INTRODUCTION

1.1 General

The purpose of these experiments was to demonstrate the dispersion of immiscible materials in a low gravity environment. This determination was accomplished by direct evaluation of both flight and control specimens, calculation of gravity and surface tension dominating forces, and comparison of the calculated data with the evaluation of the specimens.

1.2 Experiment Design

Each experiment consisted of a control specimen, where the materials were processed on Earth, and a flight specimen which was processed in space. The two specimens were then compared to determine the effect of gravity along with other factors on the degree of dispersion.

Three types of material combinations in the capsules were utilized. Flight and Control Specimens 6 contained 50 volume percent paraffin and 50 volume percent sodium acetate trihydrate, with an included tungsten mixing pellet. Flight and Control Specimens 9 contained 40 volume percent paraffin, 40 volume percent sodium acetate trihydrate, 20 volume percent argon and an included tungsten mixing pellet. Flight and Control Specimens 12 contained 40 volume percent paraffin, 40 volume percent sodium acetate trihydrate, 20 volume percent 100μm diameter tungsten microspheres and an included tungsten mixing pellet. (In the remainder of the report the word sodium acetate will be utilized instead of sodium acetate trihydrate for brevity, although the hydrated form is the actual chemical used.)

These combinations were chosen to assess the effect of processing in a near zero gravity environment on two and/or three phase immiscible mixtures, where the two main phases were immiscible liquids during processing and the third phase was either a gas or a solid. The procedure for processing these capsules was as follows: the capsule was inserted into the heater, heated for 10 minutes, the heater-capsule combination shaken for 90 seconds, and the combination was then inserted on the cooling pin connected to the heat sink until the temperature was 100°F or less. The cooling time was at least 30 minutes. After heating, processing and cooling, the solidified material could then be assessed for the degree of dispersion.

2.0 CHARACTERIZATION OF FLIGHT AND CONTROL SPECIMENS 6, 9 AND 12

2.1 General

The characterization of the control and flight specimens proceeded in three areas: photographic documentation of the intact and sectioned specimens, density determinations of the sectioned specimens, and droplet distribution of the sectioned flight specimens.

Figure 2-1 is a schematic representation of the photographic documentation procedure utilized to evaluate the degree of dispersion in the specimens. The surfaces of the intact specimens were polished and then photographed at various magnifications. The specimens were then sectioned, the side of each sectioned sample closest to the heat sink end polished and photographs at various magnifications were taken.

The density determinations were performed using an air comparison pycnometer, and the droplet distribution was measured using a microscope and a template to measure size and position within the sectioned samples.

2.2 Surface Characterization - Intact Specimens

The cut surfaces of the intact specimens were prepared by removing the saw marks with 2/0 and 4/0 sandpaper, and final polishing of the specimens on Buehler nylon polishing cloth.

The polished surfaces were then photographed at various magnifications. The entire surface was photographed at 1X and 10X magnification and selected areas were photographed at 50X. A Leitz "Aristophot" macro-camera was used to take the 1X and 10X photomacrographs. Oblique lighting using a polarized filter was found to give maximum contrast, although UV fluorescence and direct lighting with various compensating filters were also tried. A Reichart Research Metallograph, Model "MeF" was used to take the 50X photomicrographs. Most of the photomicrographs were taken using dark field illumination, although phase contrast, polarized light and bright field illumination techniques also were utilized.

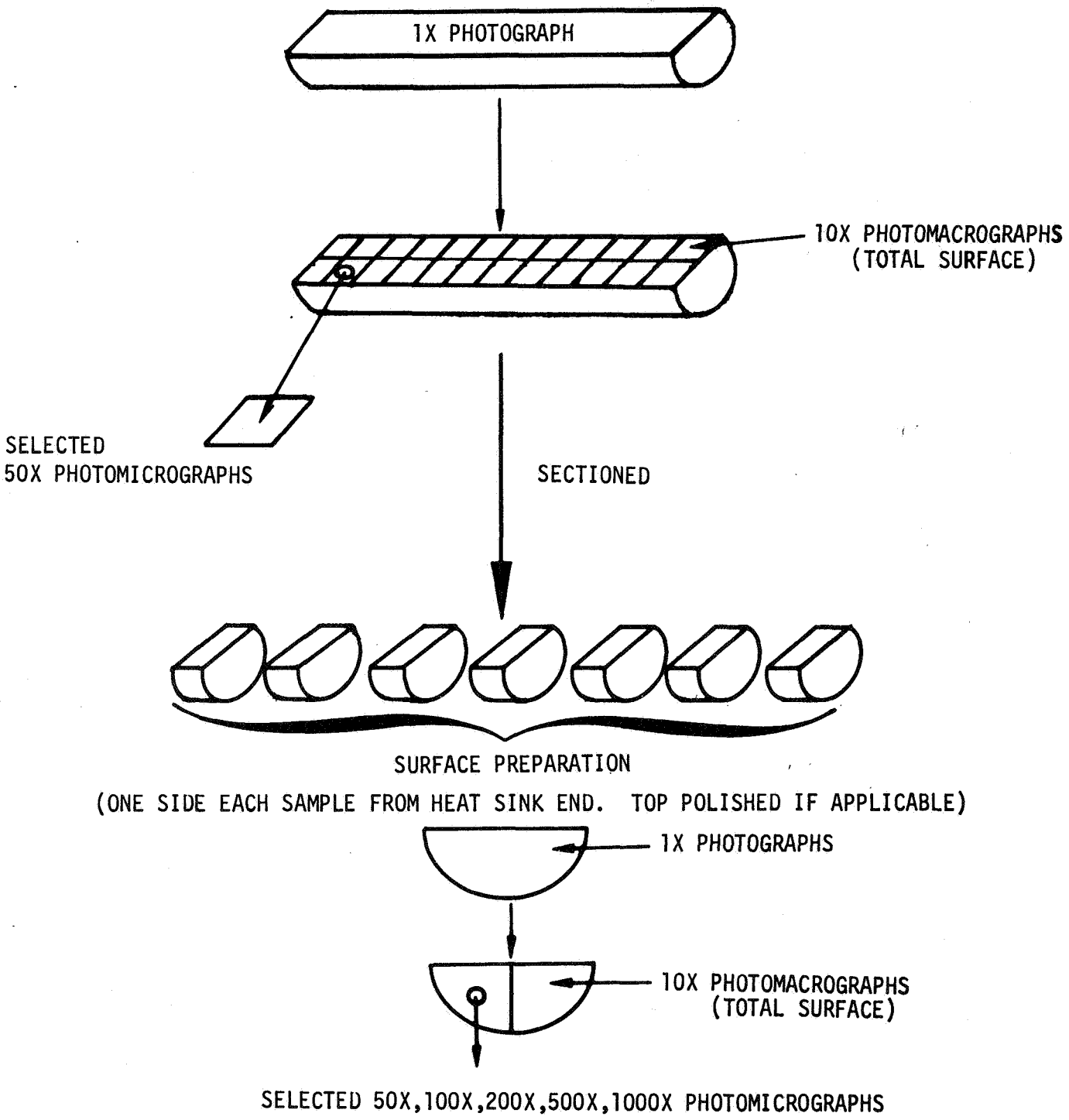

FIGURE 2-1. SCHEMATIC OUTLINE OF PHOTOGRAPHIC DOCUMENTATION PROCEDURE

Figure 2-2 shows the polished surfaces of both the control and flight specimens at 1X magnification. The arrows denote areas of interest and the surface appearance of the control and flight specimens are described below, and are shown in greater detail in Figures 2-3 through 2-11.

2.2.1 Control Specimen 6C-A-00

The paraffin and sodium acetate are segregated in the control specimen with the exception that the shrinkage tube is filled with sodium acetate (area 1). This probably occurred when the paraffin solidified, creating a partial vacuum at the top of the capsule and aspirated the still liquid sodium acetate into the shrinkage tube.

The translucent ellipsoid (area 2) below the shrinkage tube is a fine dispersion of air bubbles or vacuum voids in the paraffin, probably formed during the solidification and concomitant shrinkage of the paraffin.

The interface between the paraffin and the sodium acetate (area 3) is smoothly rounded with a radius of approximately 7.6 cm. The sodium acetate is randomly crystallized, with the finer crystals near the end closest to the heat sink.

2.2.2 Flight Specimen 6F-A-00

The sodium acetate and paraffin are partially segregated, however, there is some dispersion of sodium acetate in paraffin (area 1 and 2) and paraffin in sodium acetate (areas 3 and 4). A thin coating of sodium acetate surrounds most of the outside of the paraffin (area 5). There are two connected cavities in the paraffin, one hollow and the other nearly filled with sodium acetate (area 1). The sodium acetate spheres in the paraffin are reasonably uniform with the majority of the spheres being approximately 1.2 mm in diameter (area 2). The paraffin dispersion, however, are spheres with widely varying diameters. Area 3 is a sphere 2.5 mm in diameter and area 4 contains spheres approximately 0.025 mm in diameter. Some of the paraffin spheres in area 4 are distorted, indicating that there may have been a rather steep thermal gradient imposed longitudinally across the capsule during cooling. There are a number of

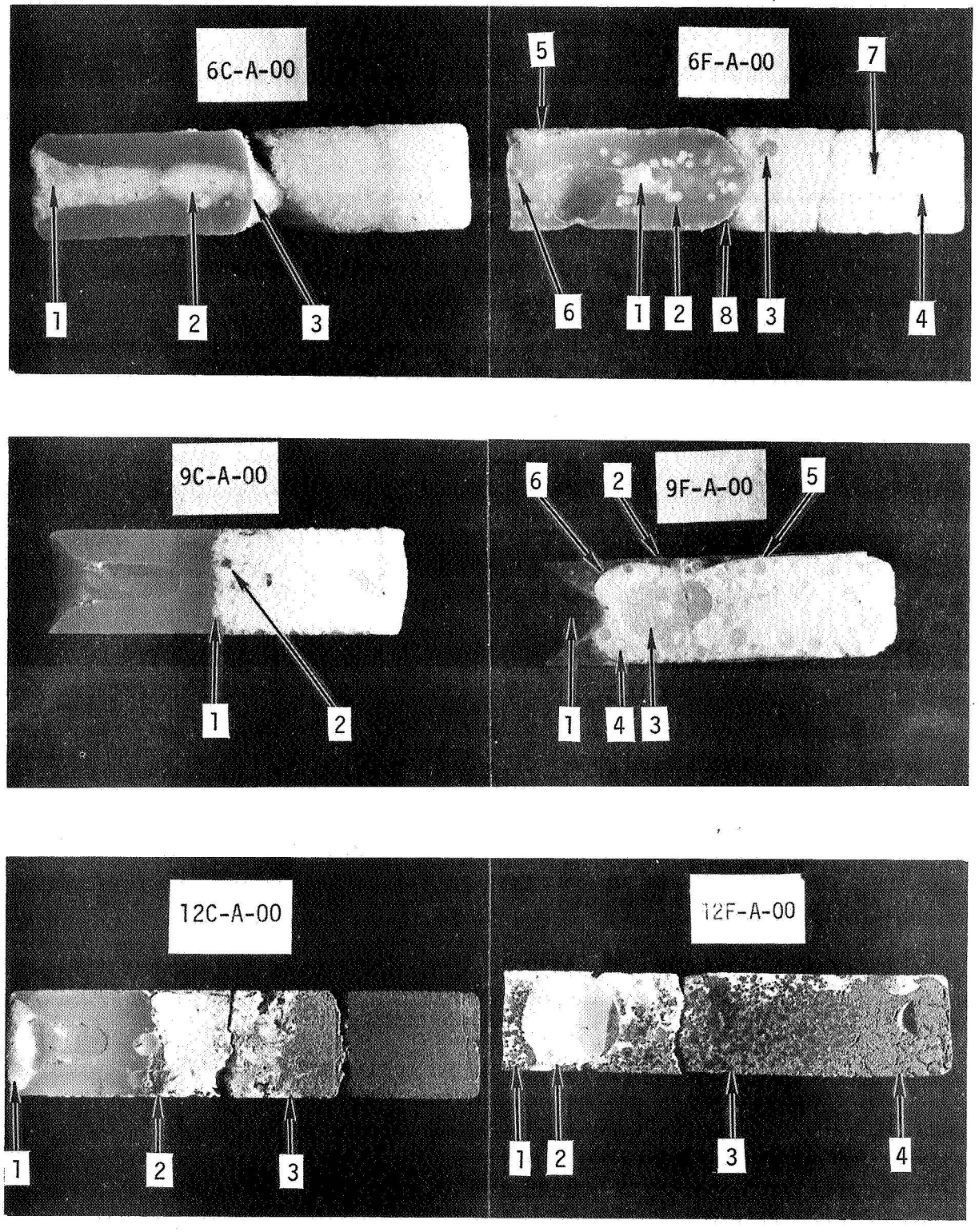

FIGURE 2-2. Photomacrographs of the Polished Surfaces of Control and Flight Specimens 6, 9 and 12. (1X Magnification)

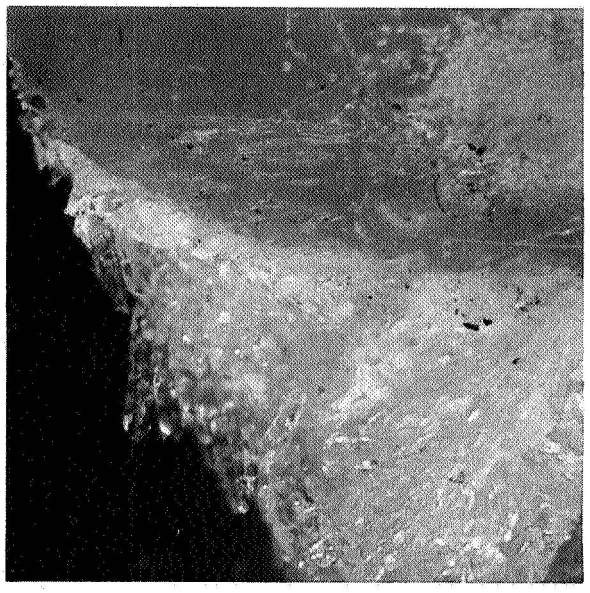

6C-A-00

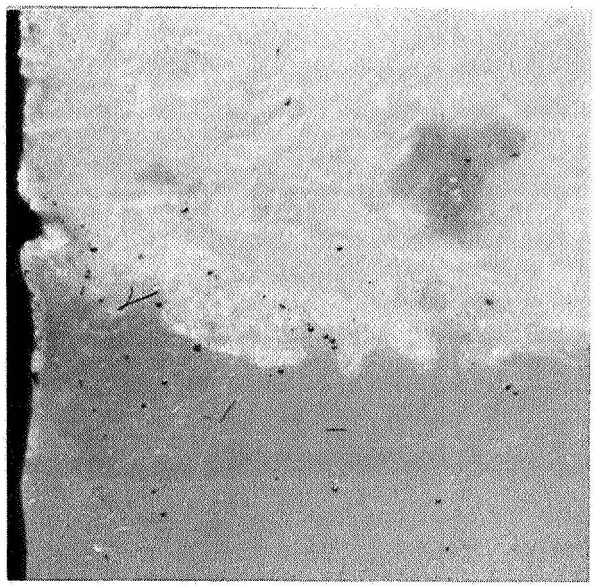

9C-A-00

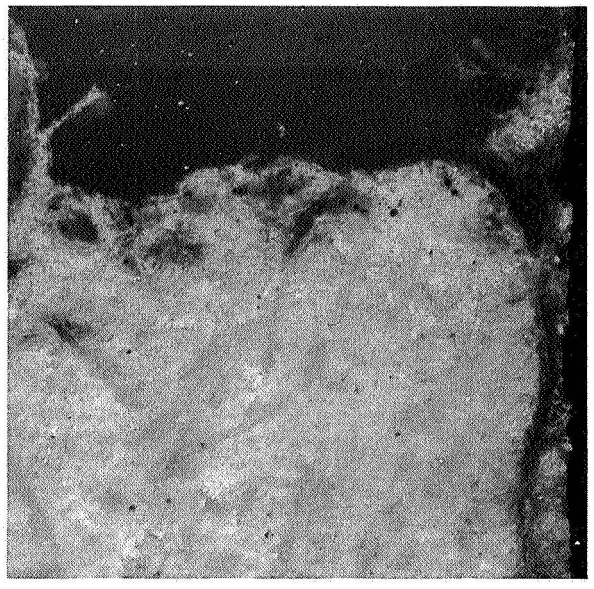

12C-A-00
Paraffin-Sodium Acetate

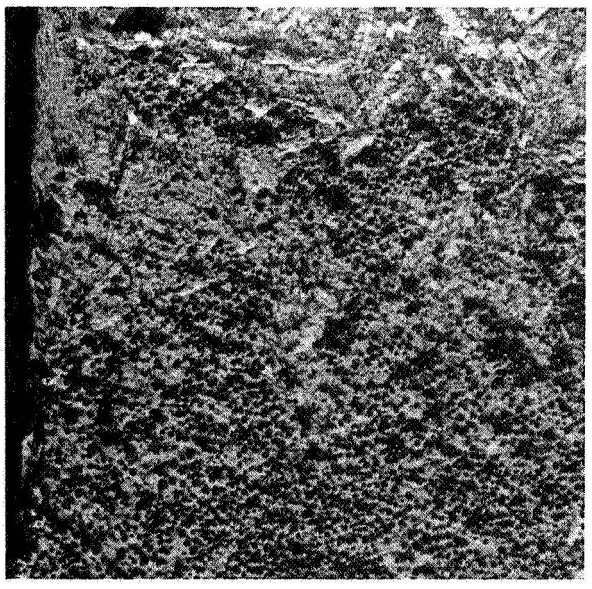

Sodium Acetate-Tungsten
Microspheres

FIGURE 2-3. Control Specimen Interfaces
(10X Magnification)

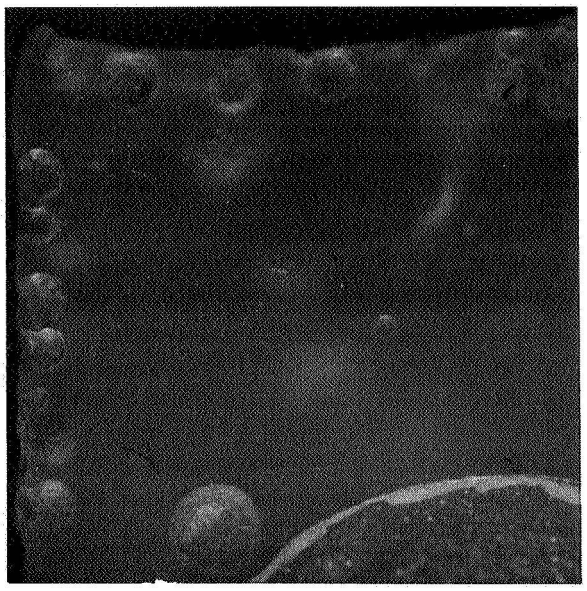

End Away From Heat Sink

5.5 cm From Heat Sink End

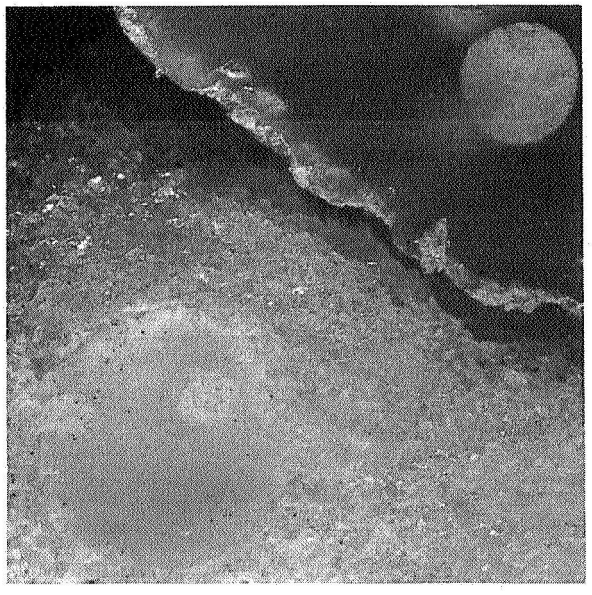

Interface

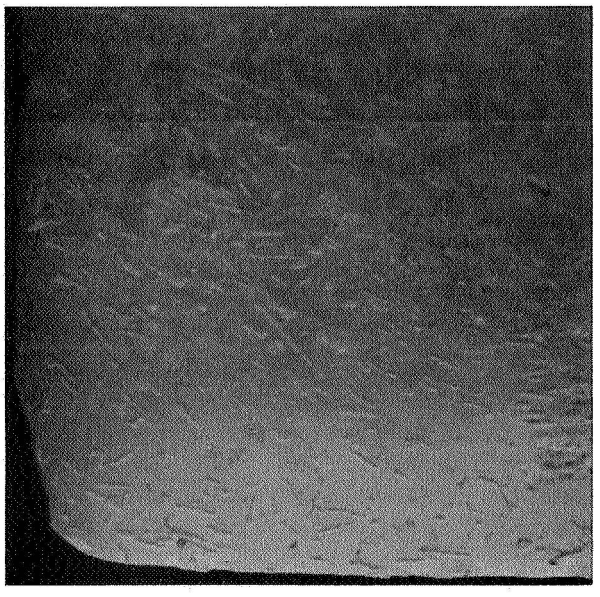

Heat Sink End: Dispersed Paraffin

FIGURE 2-4. Selected Photomacrographs of Flight Specimen 6F-A-00 (10X Magnification)

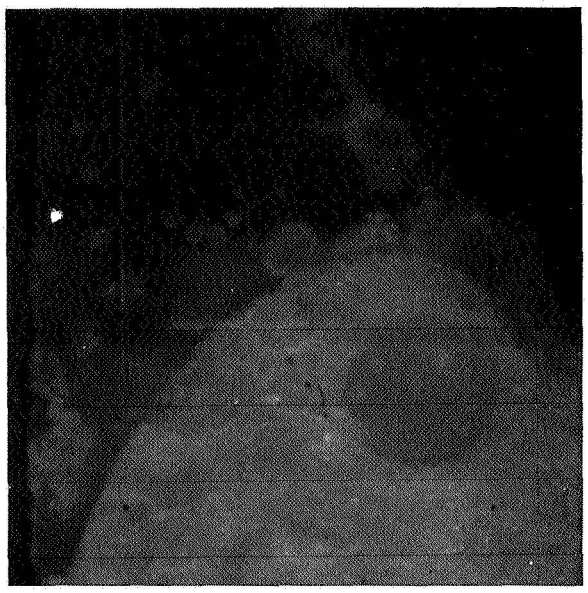

Shrinkage Cavity Away
From Heat Sink End

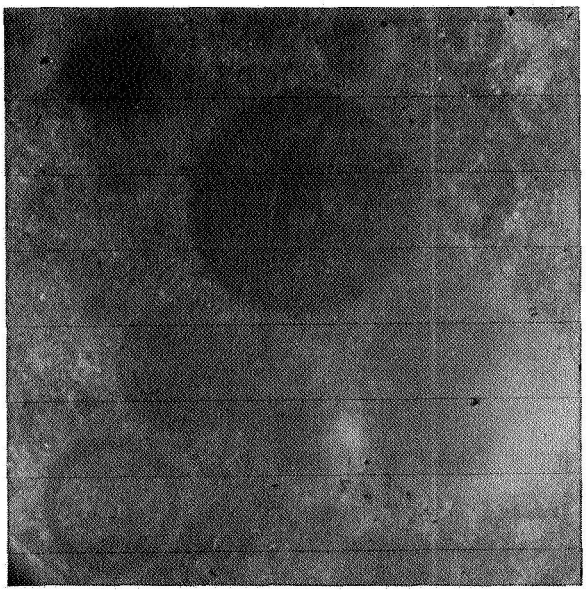

Duplex & Complex Dispersions
Near Center of Sample

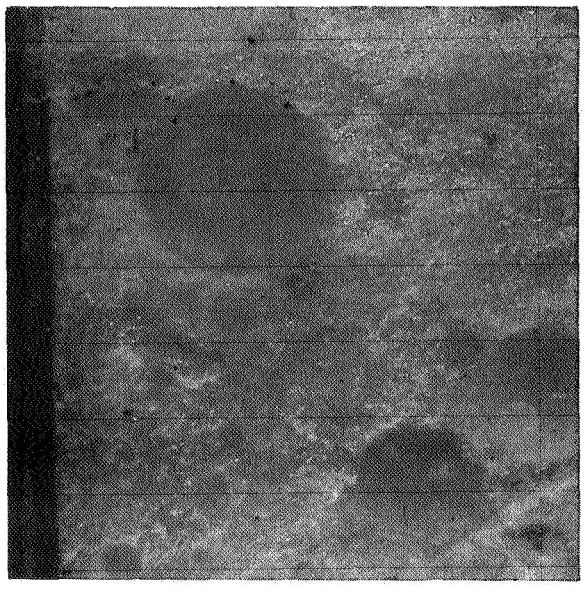

Duplex & Complex Dispersions
Near Center of Sample

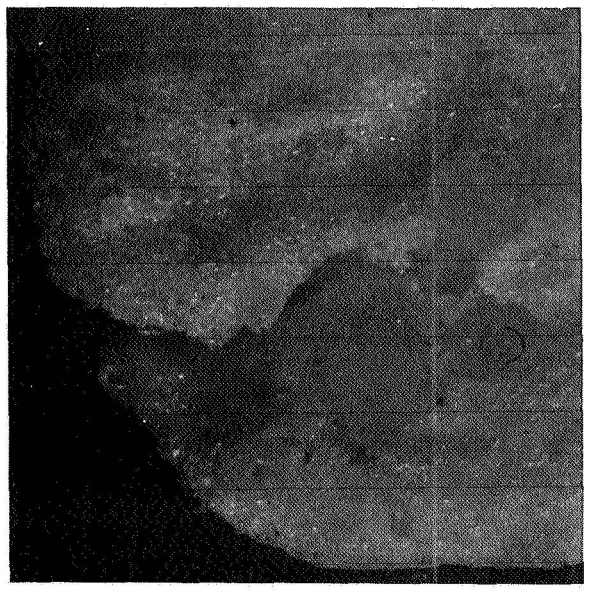

Heat Sink End

FIGURE 2-5. Selected Photomacrographs of Flight Specimen 9F-A-00 (10X Magnification)

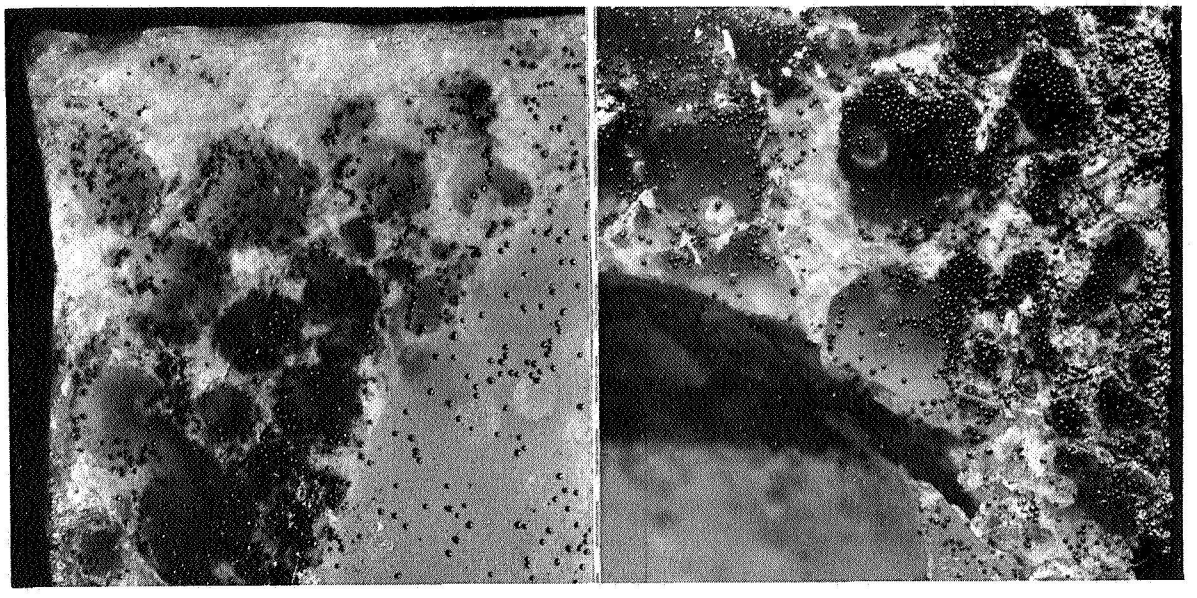

End Away From Heat Sink

Area Near Shrinkage Void

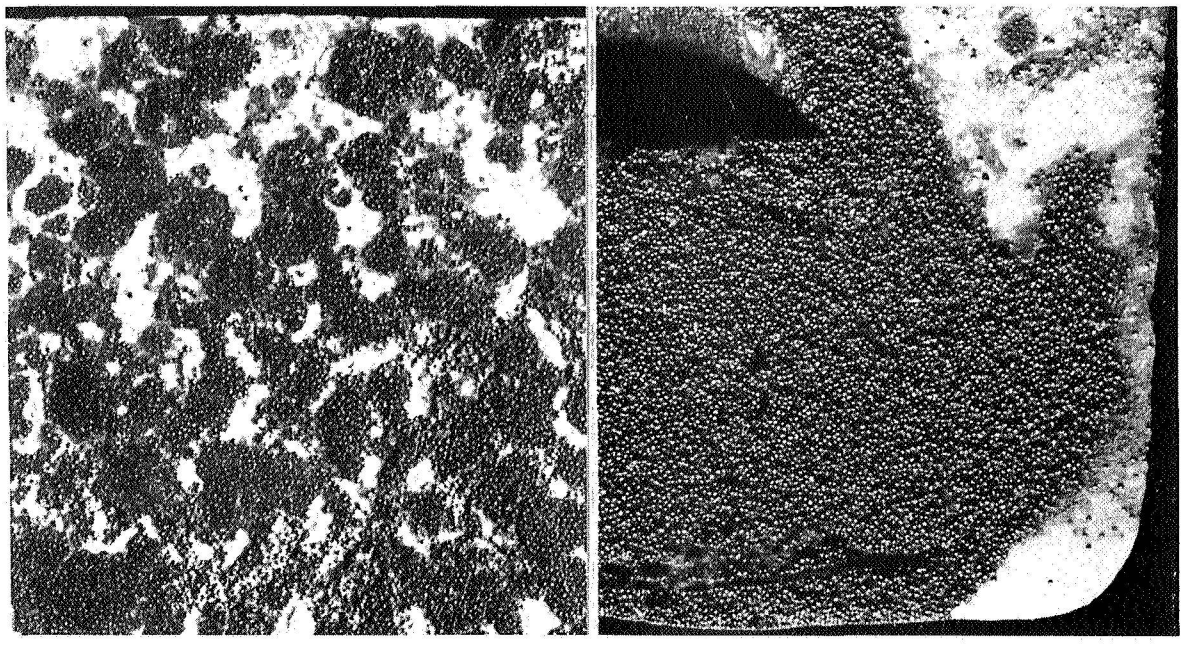

Representative Area
Near Center

Heat Sink End

FIGURE 2-6. Selected Photomacrographs of Flight Sample 12F-A-00 (10X Magnification)

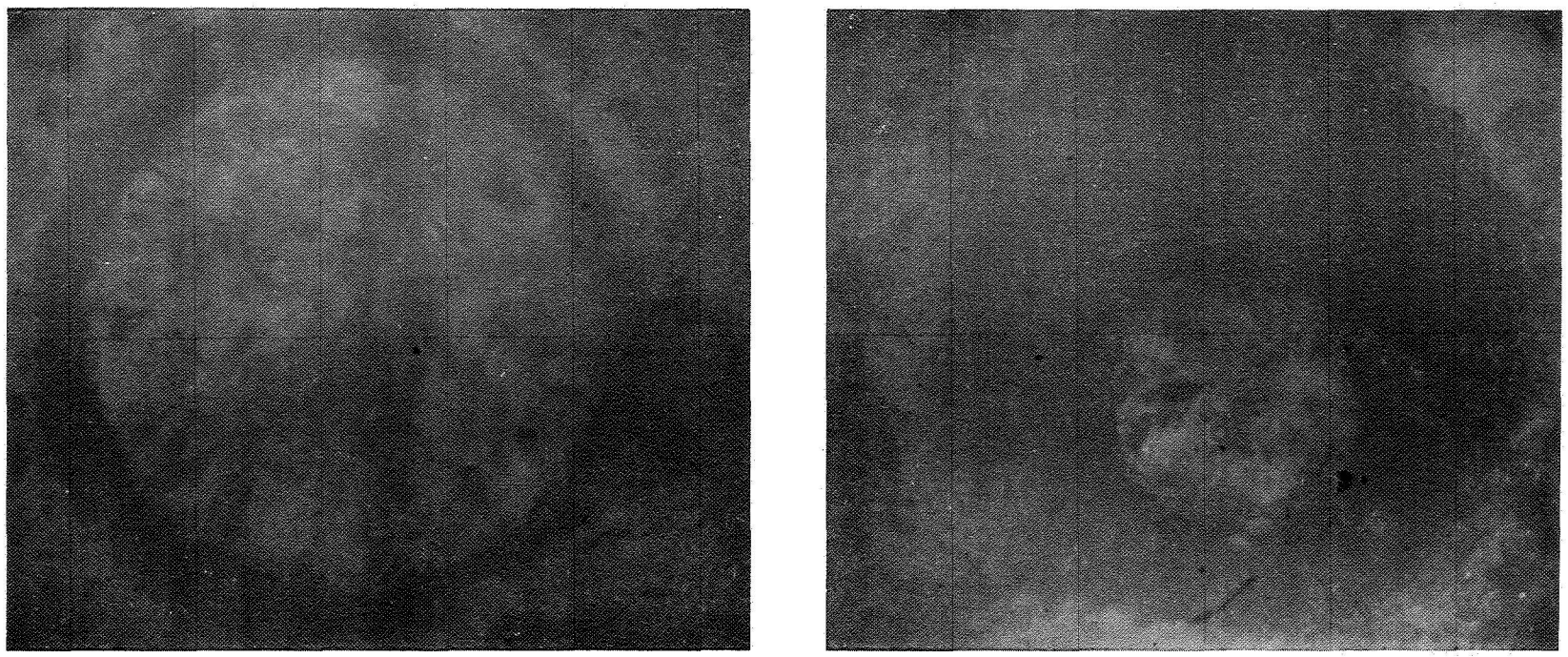

FIGURE 2-7. Photomicrographs of Flight Specimen 9F-A-00 Showing Duplex Dispersions (50X Magnification)

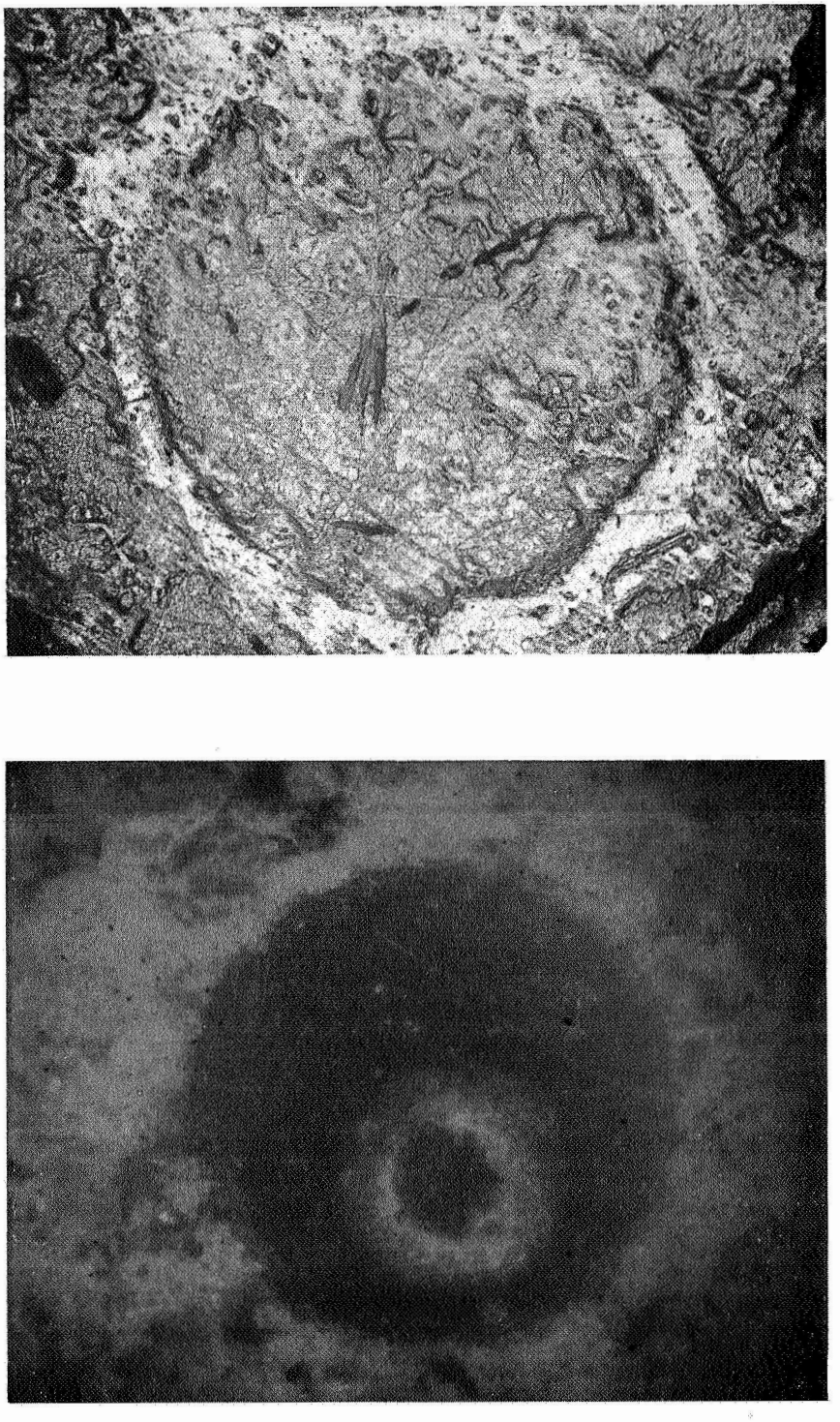

FIGURE 2-8. Photomicrographs of Flight Specimen 9F-A-00 Showing Complex Dispersions (50X Magnification)

Sodium Acetate in Paraffin
4.6 cm from Heat Sink End

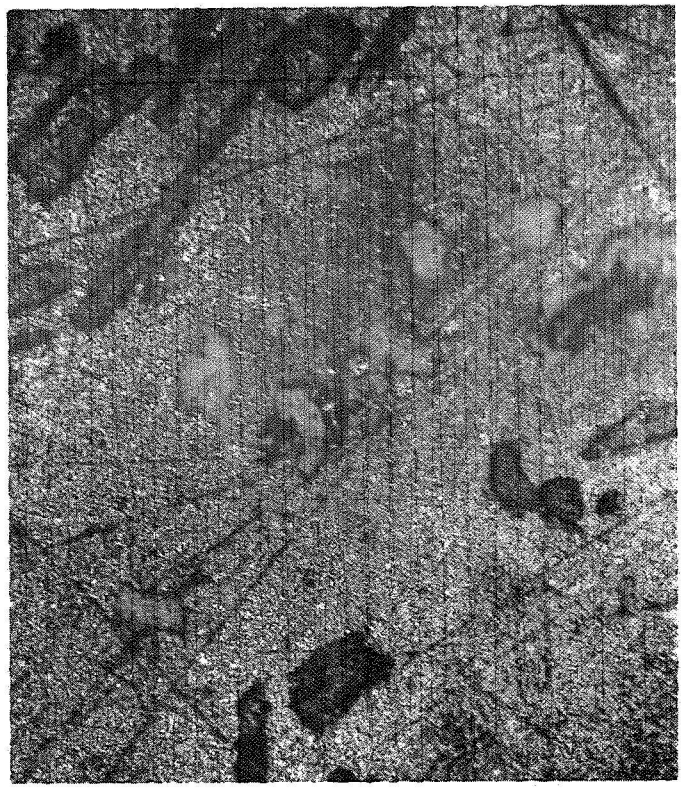

Paraffin in Sodium Acetate
Near Heat Sink End

FIGURE 2-9. Photomicrographs of Flight Specimen 6F-A-00
(50X Magnification)

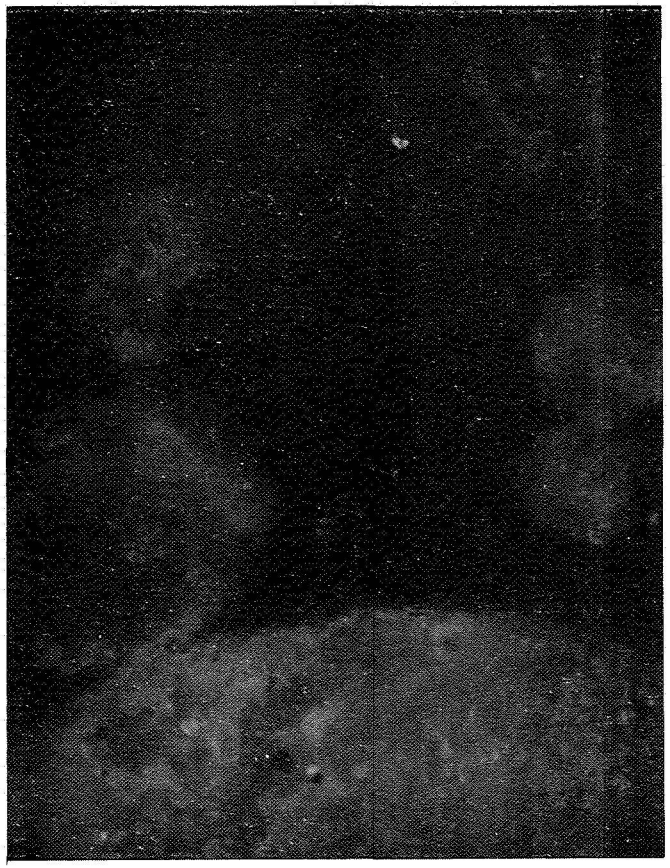

Sodium Acetate in Paraffin
Near Shrinkage Void

Paraffin in Sodium Acetate
at Heat Sink End

FIGURE 2-10. Photomicrographs of FTight Specimen 9F-A-00
(50X Magnification)

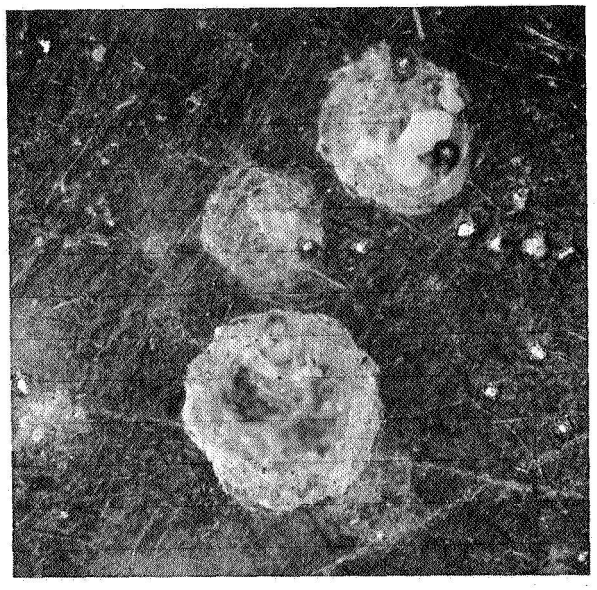

Sodium Acetate in Paraffin
7.5 cm from Heat Sink End

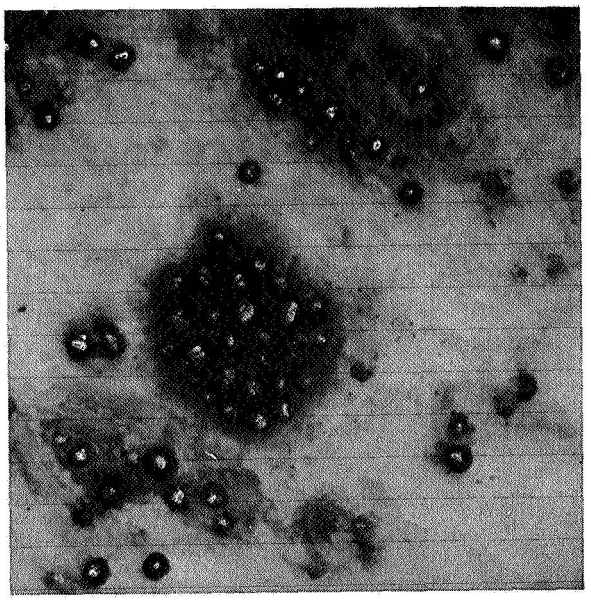

Paraffin/Tungsten Microspheres
in Sodium Acetate 1 cm from
Heat Sink End

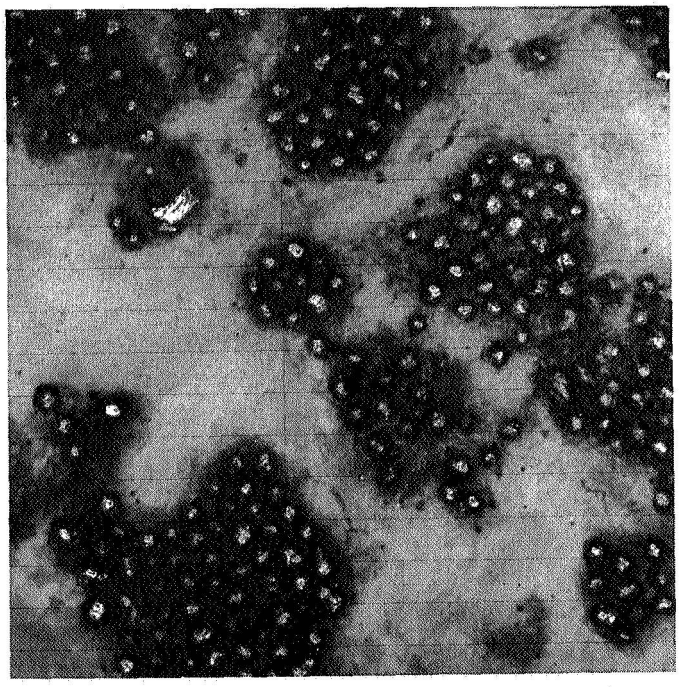

Representative Dispersion of Paraffin/
Tungsten Microspheres 3 cm from Heat
Sink End

FIGURE 2-11. Photomicrographs of Flight Specimen 12F-A-00
(50X Magnification)

elongated voids or air bubbles (area 6) near the top of the specimen (end furthest from the heat sink) which were probably formed during solidification of the paraffin. Area 7 has rather large crystals (2 - 5 mm) which are oriented at approximately 45° to the longitudinal centerline. The paraffin, sodium acetate interface (area 8) is much more sharply rounded that the interface in the control sample, having a radius of approximately 1 cm.

2.2.3 Control Specimen 9C-A-00

The paraffin and sodium acetate in the control sample are completely segregated, with an empty shrinkage tube, unlike 6C-A-00. This is probably due to the gas space in the capsule. The interface (area 1) is almost perfectly flat, with some rounding at the sides where the capsule was in contact with the material.

There is some contamination of the sodium acetate as shown in area 2, and there are a few tungsten microspheres randomly distributed in the paraffin. The sodium acetate is crystallized in a random manner, with a few large crystals in the center of the material.

2.2.4 Flight Specimen 9F-A-00

The sodium acetate and paraffin are almost completely dispersed. A thin layer of paraffin is located in the top of the capsule away from the heat sink, along with a small amount of sodium acetate (not shown). Thus the shrinkage tube (area 1) is actually a large gas pocket surrounded by paraffin. In addition, a thin layer of paraffin surrounds the entire dispersion and is indicated by area 2. Interspersed in the paraffin shell are small spheres of sodium acetate and a few voids or gas pockets.

The paraffin is primarily dispersed in the sodium acetate, except at areas 3 and 4. In area 3, three relatively large droplets of paraffin have coalesced and enclose some sodium acetate spheres. In area 4, a thin shell of paraffin encloses a sphere of sodium acetate. This is known as the "grapeskin effect" or duplex dispersion and has been observed in oil-water mixtures and in wet jet fuel being pumped through pipelines. Area 5

illustrates a "double grapeskin effect", or a complex duplex dispersion in that paraffin surrounds sodium acetate which in turn surrounds paraffin. Too small to be seen is the reverse type of dispersion. Droplet distribution is relatively random and diameters range from approximately 1 cm to 0.025 mm. The sodium acetate, paraffin interface (area 6) has a more pronounced curvature than 9C-A-00 and is reversed from the interfaces in 6C-A-00 and 6F-A-00.

The sodium acetate is very finely crystallized in a random orientation. There does not appear to be any appreciable gas dispersion, but this may be due to the thermal gradient during solidification. The presence of the paraffin dome at the top indicates that some solidification occurred at the top end during cooldown.

2.2.5 Control Specimen 12C-A-00

The paraffin, sodium acetate and tungsten microspheres are segregated with the exception of a small cap of sodium acetate with a few tungsten microspheres over the top of the shrinkage tube (area 1). The cap probably was formed in the same manner as mentioned for 6C-A-00.

The paraffin, sodium acetate interface (area 2) is slightly rounded, but not as smooth as that formed in the other two control samples. There are several droplets of paraffin embedded in the main body of the paraffin and a few tungsten microspheres present in the interface.

The sodium acetate, tungsten microsphere interface (area 3) is partially graded. Microscopic examination of the interface indicates that as the sodium acetate crystallized, some of the tungsten microspheres were displaced into the predominantly sodium acetate phase.

2.2.6 Flight Specimen 12F-A-00

There appear to be three types of sodium acetate, paraffin, tungsten microsphere dispersions. Area 1 is a dispersion of paraffin (containing 90% of the tungsten microspheres) into the sodium acetate. Area 2, containing the shrinkage cavity, is predominantly paraffin with some

sodium acetate dispersed into it. Area 3 is a tungsten microsphere, paraffin blend with a dispersion of sodium acetate. Area 4 appears to be similar to area 3, with a higher concentration of tungsten microspheres. Since the tungsten microspheres are preferentially wetted by the paraffin, the continuous phase is predominantly paraffin with the sodium acetate as the dispersant over most of the length of the specimen.

The dispersed droplets in areas 1 and 2 are predominantly spherical from 0.025 to 1 mm in diameter, but the dispersed phases elsewhere in the sample are distorted, presumably because of the crystallization of the sodium acetate. The sodium acetate is finely crystallized with a random orientation.

2.3 Surface Characterization - Sectioned Samples

All of the control and flight specimens were axially sectioned at 0.63 cm (0.25 inch) intervals starting from the heat sink end. Some difficulty was encountered at the breaks in the specimens, consequently there is an extra, undersized sample from the 6 and 12 control specimens and two from the 12 flight specimen. The lower half of specimen 6F-A-00 was very friable and tended to break when the razor saw was almost through. All of the other specimens were readily sectioned.

The sectioned samples were mounted for polishing by placing each individual sample in a Buehler No. 20-8151AB Bakelite Ring Form (2.54 cm O.D. X 2.22 cm I.D.) and potting with Maraset Epoxy Resin No. 656, which polymerizes at room temperature. This was done to prevent damage to the samples during polishing. Each sample was marked to prevent identification errors.

After the epoxy was cured, the samples were rough ground with Buehler No. 160 Carbimet paper. No. 320 and No. 600 soft paper were then used to remove the grinding marks and the final polish was done with Buehler nylon polishing cloth.

The widely varying hardness of the specimen materials caused some damage to the polished surfaces of the samples, but satisfactory photomicrographs

up to 1000X were taken and the morphological details of the samples could be observed easily.

All of the specimen samples were photographed at 1X and 10X, and selected area photomicrographs from 50X to 1000X were taken. The details observed are described below, and illustrated in Figures 2-12 through 2-21.

2.3.1 Control Samples 6C-A-01 through -12

The crystal habit near the heat sink end for the control samples is random with dispersed 0.5 - 1.5 mm crystals in the axial cut plane. After approximately 1.4 cm, the crystals tend to become finer and randomly oriented up to the sodium acetate-paraffin interface.

The interface area shows a relatively uniform transition from sodium acetate to paraffin, with a very small dispersion depth of approximately 0.5 mm maximum.

The paraffin is free of sodium acetate except for the filled shrinkage tube. The distortion of the voids toward the interior of the samples indicates that the postulation of aspiration of the sodium acetate into the shrinkage tube is valid.

2.3.2 Flight Samples 6F-A-01 through -13

The crystal habit of the sodium acetate near the heat sink end is primarily fine crystals randomly dispersed. The crystal habit changes rather abruptly approximately 0.5 cm from the end, with the crystals becoming oriented toward the center of the specimen. The orientation angle changes gradually from approximately 45° to 90° (parallel to the axial plane) 2.5 cm from the heat sink end.

Numerous paraffin inclusions are dispersed throughout the sodium acetate rich region. Most of the paraffin dispersions are spherical in shape, but a number of distorted spheres and elongated ellipsoids are present in the area where the sodium acetate is directionally oriented. This would indicate rather steep thermal gradients and concomitant directional solidification of the sodium acetate. Photomicrographs at 500X and 1000X

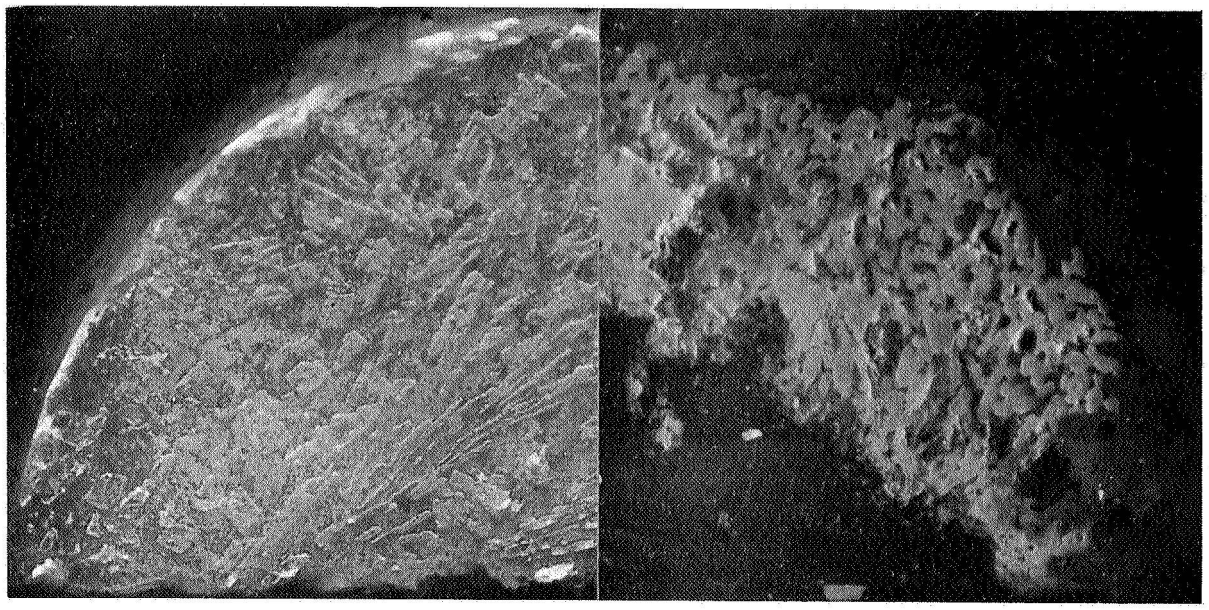

6C-A-01
Heat Sink End

6C-A-07
Paraffin-Sodium
Acetate Interface

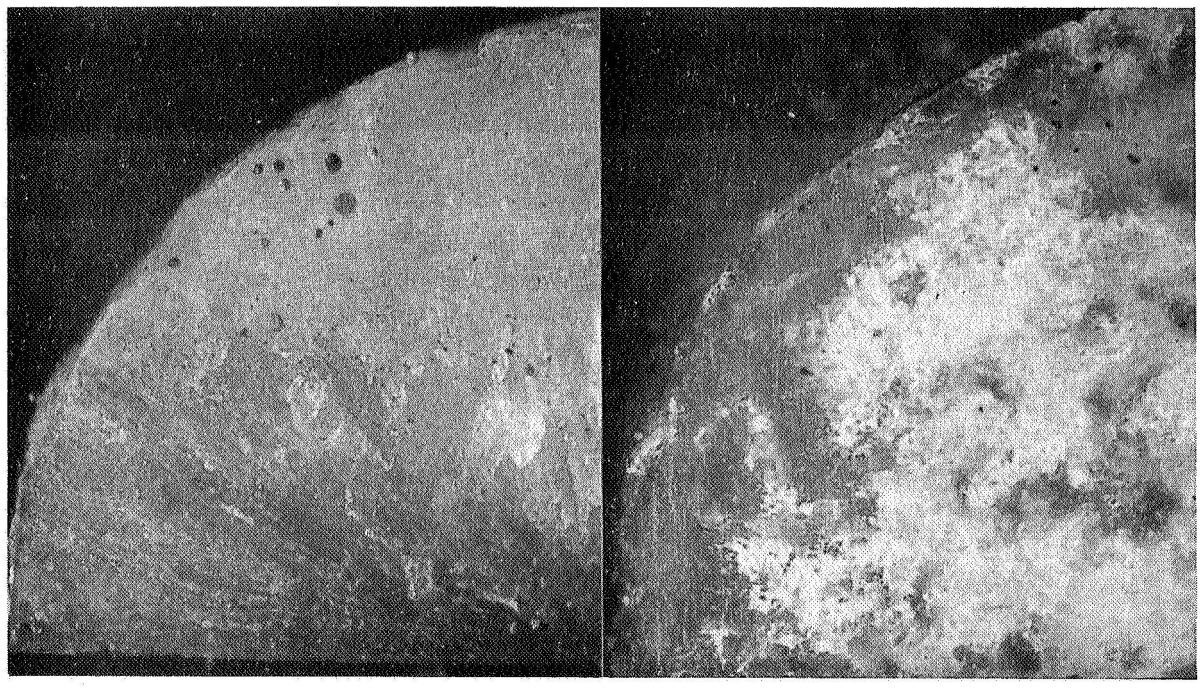

9C-A-01
Heat Sink End

9C-A-06
Paraffin-Sodium
Acetate Interface

FIGURE 2-12. Photomacrographs of Control Specimens 6C-A and 9C-A (10X Magnification)

6C-A-01
Heat Sink End

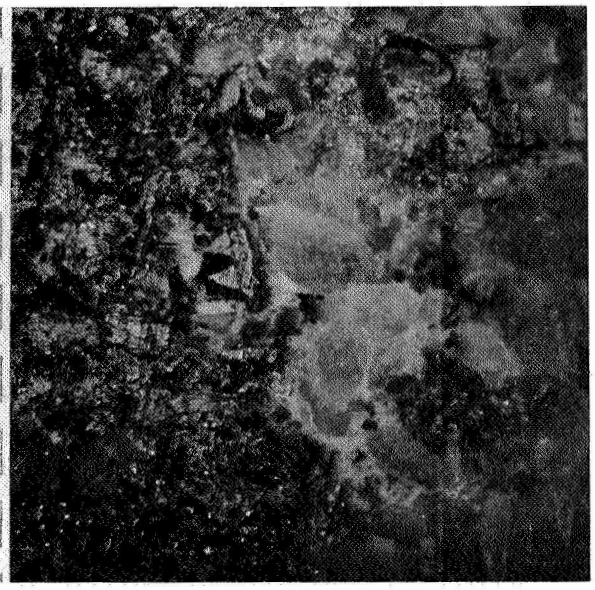

6C-A-07
Paraffin-sodium
acetate interface

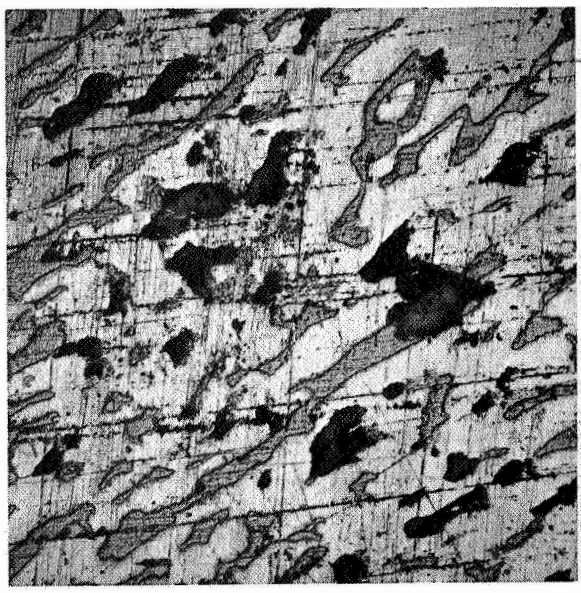

9C-A-01
Heat Sink End

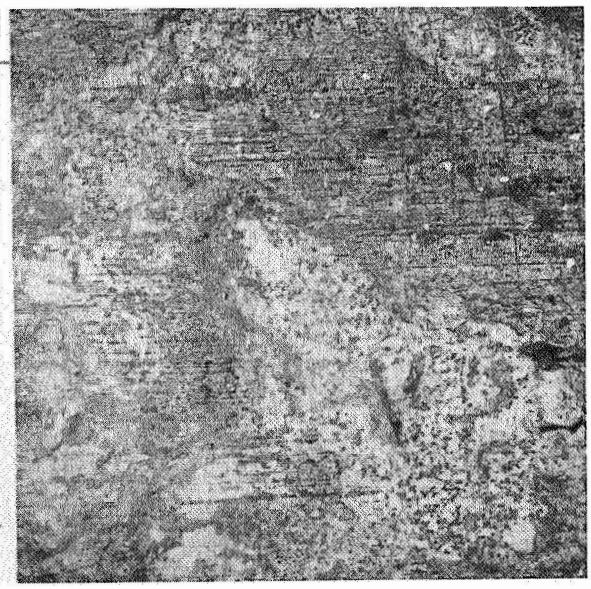

9C-A-06
Paraffin-Sodium
acetate interface

FIGURE 2-13. Photomicrographs of Control Specimens 6C-A and 9C-A (50X Magnification)

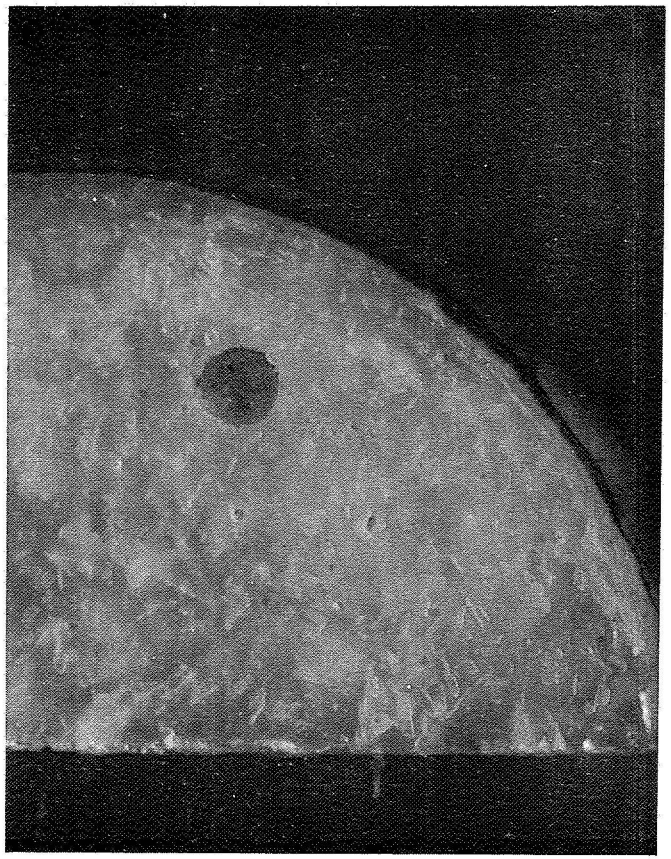

10X Magnification

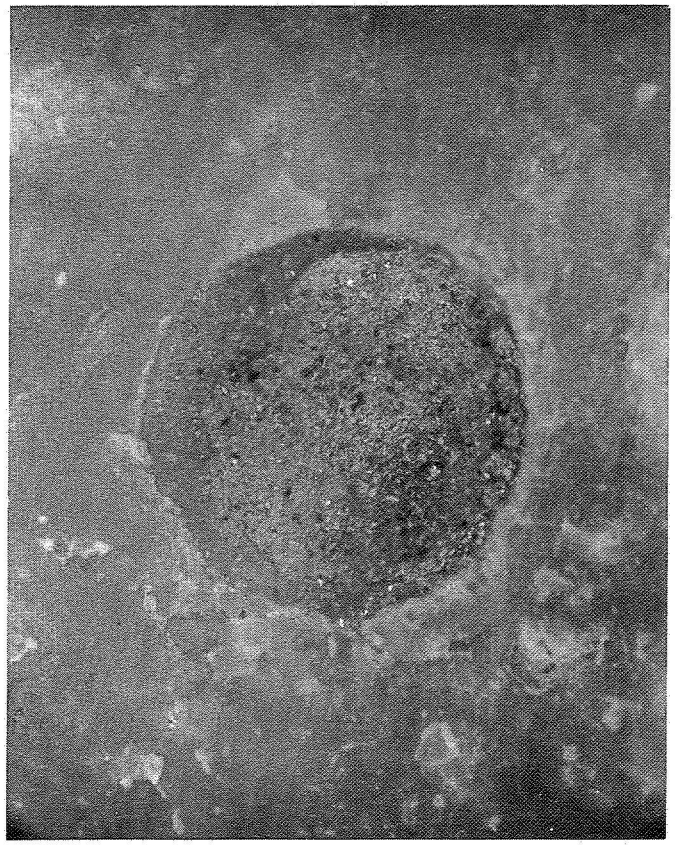

50X Magnification

FIGURE 2-14. Flight Specimen Sample 6F-A-01
Showing Paraffin Inclusion

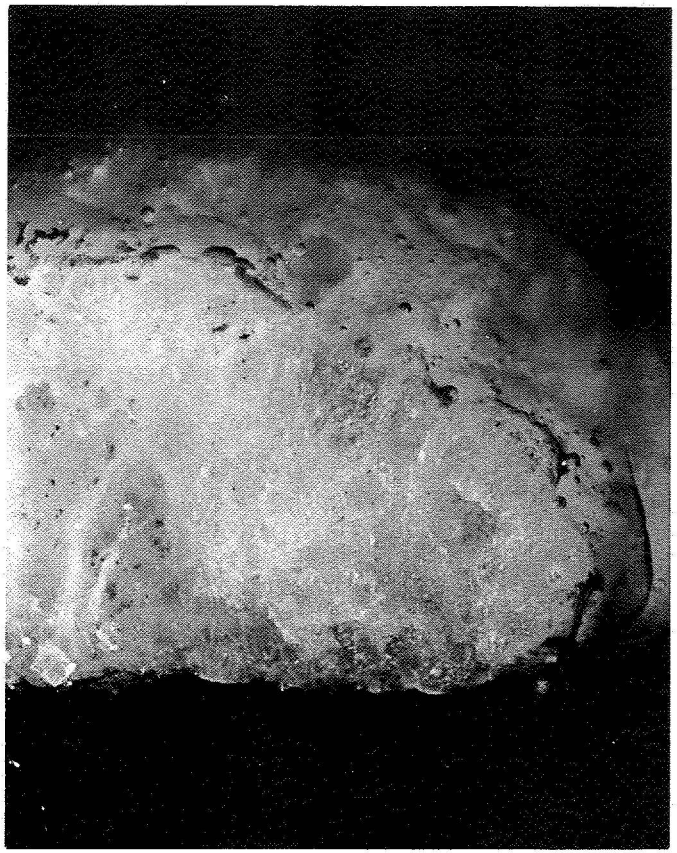

10X Magnification

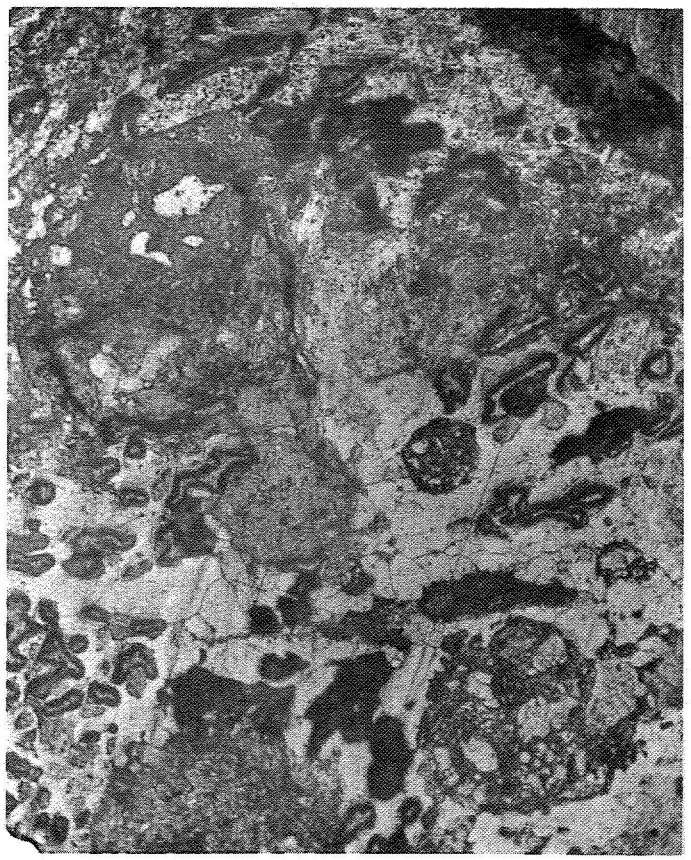

50X Magnification

FIGURE 2-15. Flight Specimen Sample 9F-A-01
Showing Paraffin Inclusions

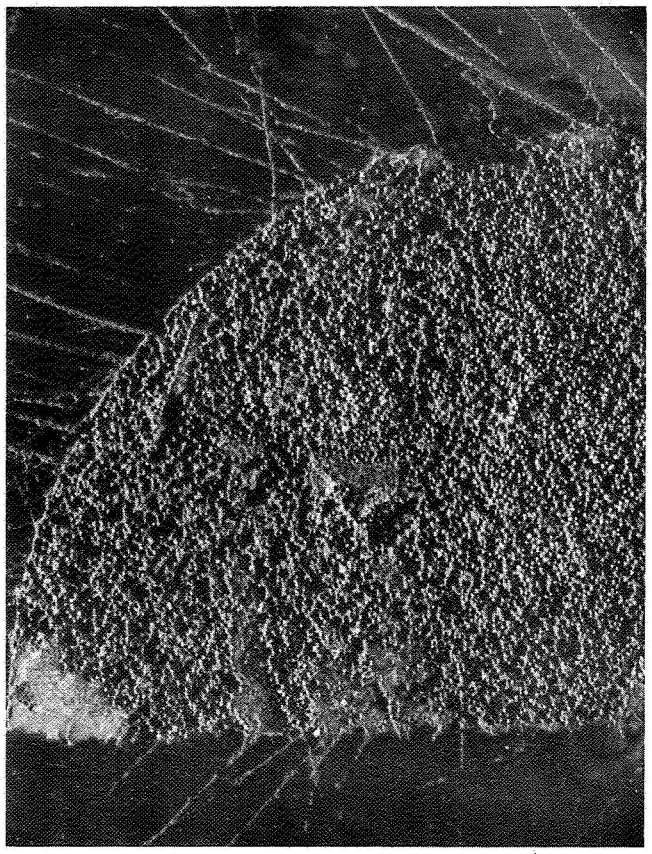

10X Magnification

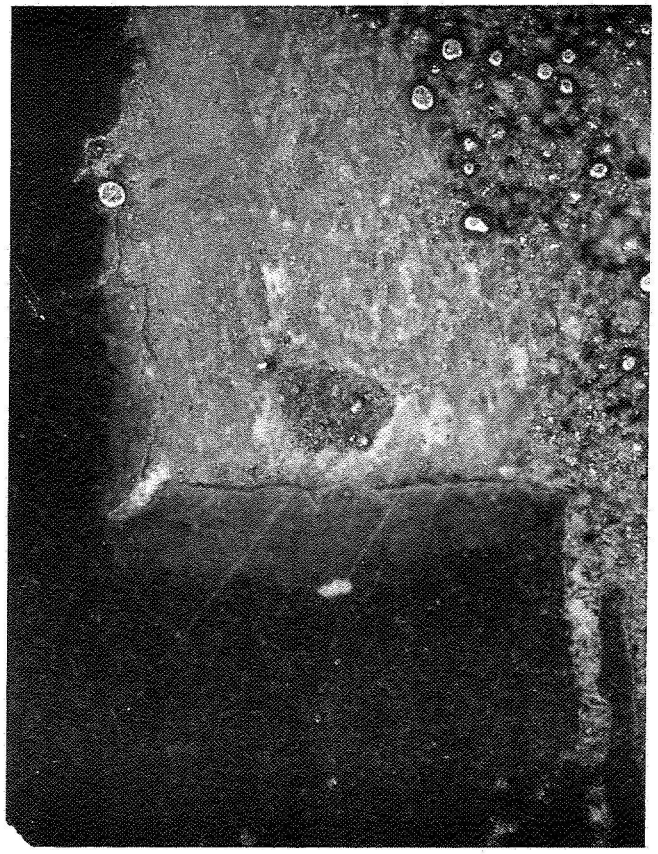

50X Magnification

FIGURE 2-16. Flight Specimen Sample 12F-A-01 Showing Paraffin Inclusion

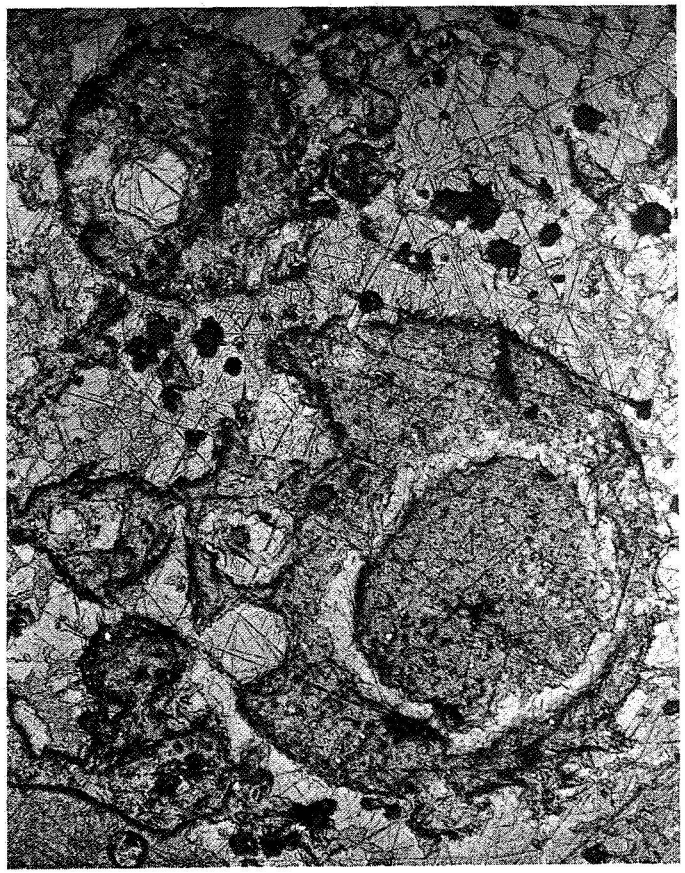

9F-A-07

9F-A-04

FIGURE 2-17. Photomicrographs of Complex Dispersions in Flight Specimen 9F-A (50X Magnification)

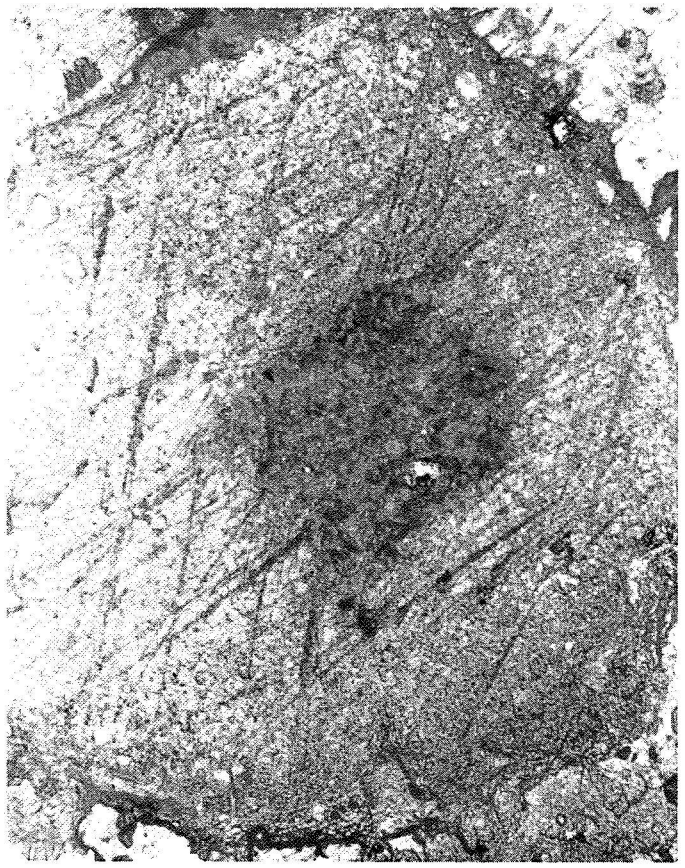

6F-A-07

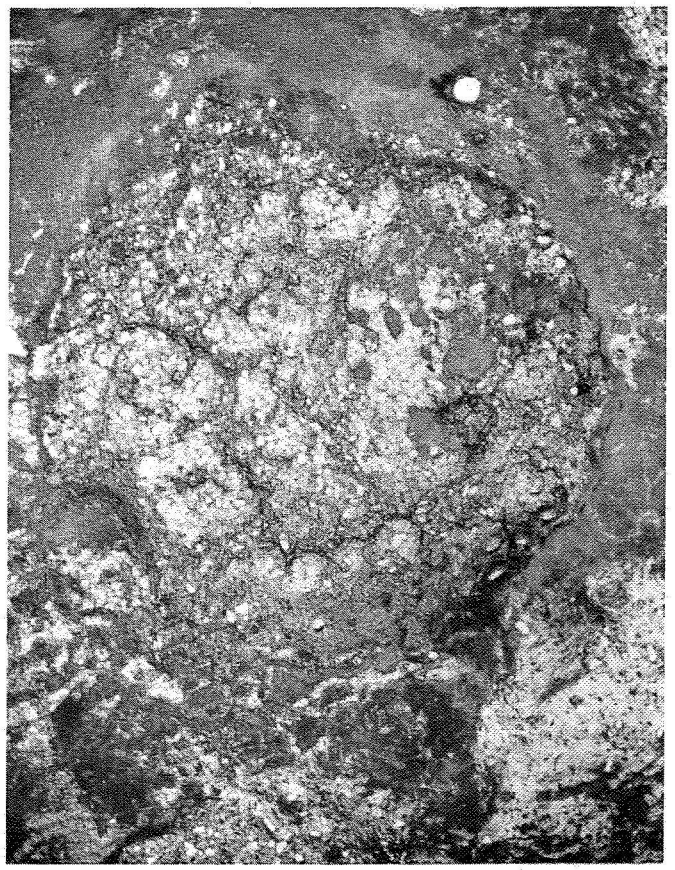

12F-A-09

FIGURE 2-18. Photomicrographs of Duplex Dispersions in Flight Specimens 6F-A and 12F-A (50X Magnification)

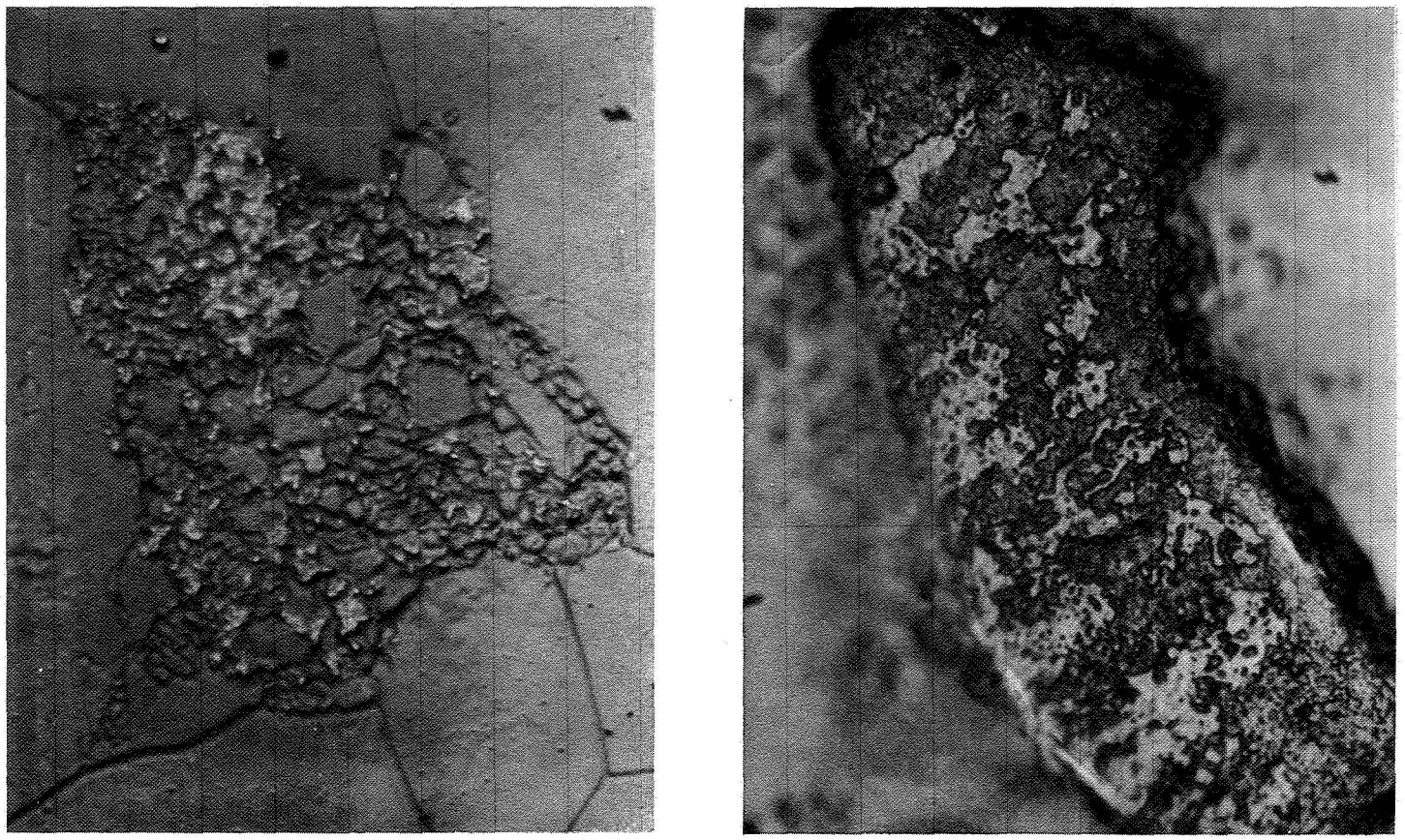

6F-A-02

6F-A-05

FIGURE 2-19. Photomicrographs of 1μm Dispersion Areas in Flight Specimen 6F-A (1000X Magnification)

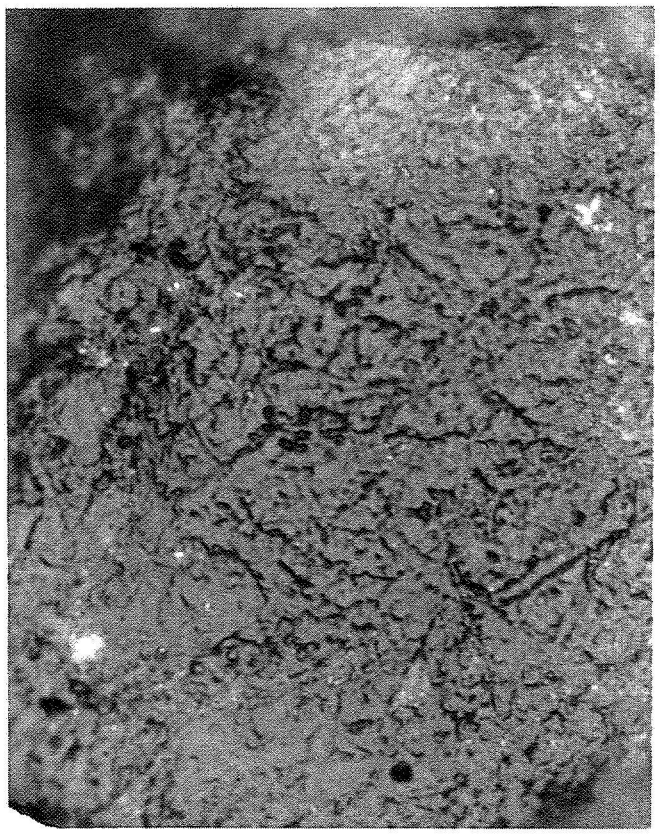

12F-A-04

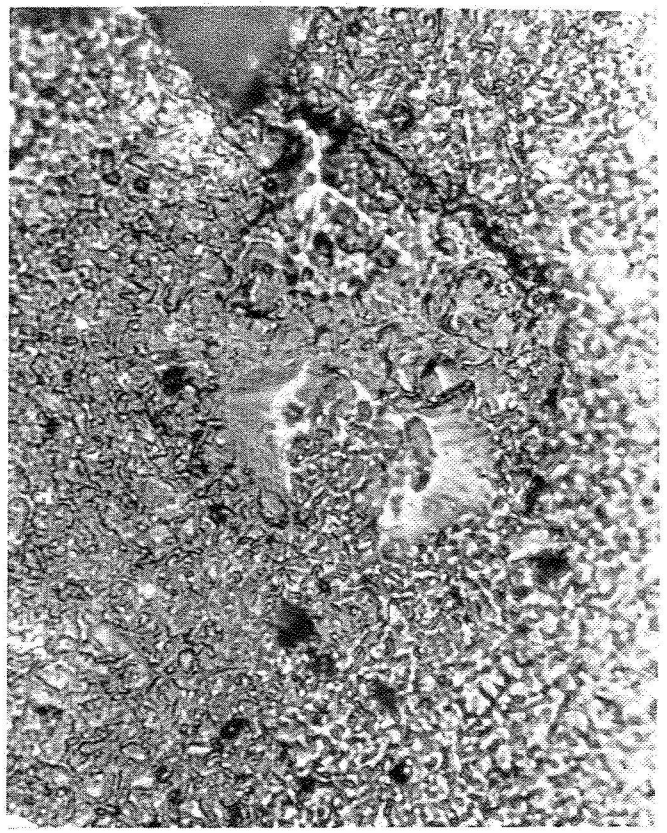

12F-A-09

FIGURE 2-20. Photomicrographs of 1μm Dispersion Areas in Flight Specimen 12F-A (1000X Magnification)

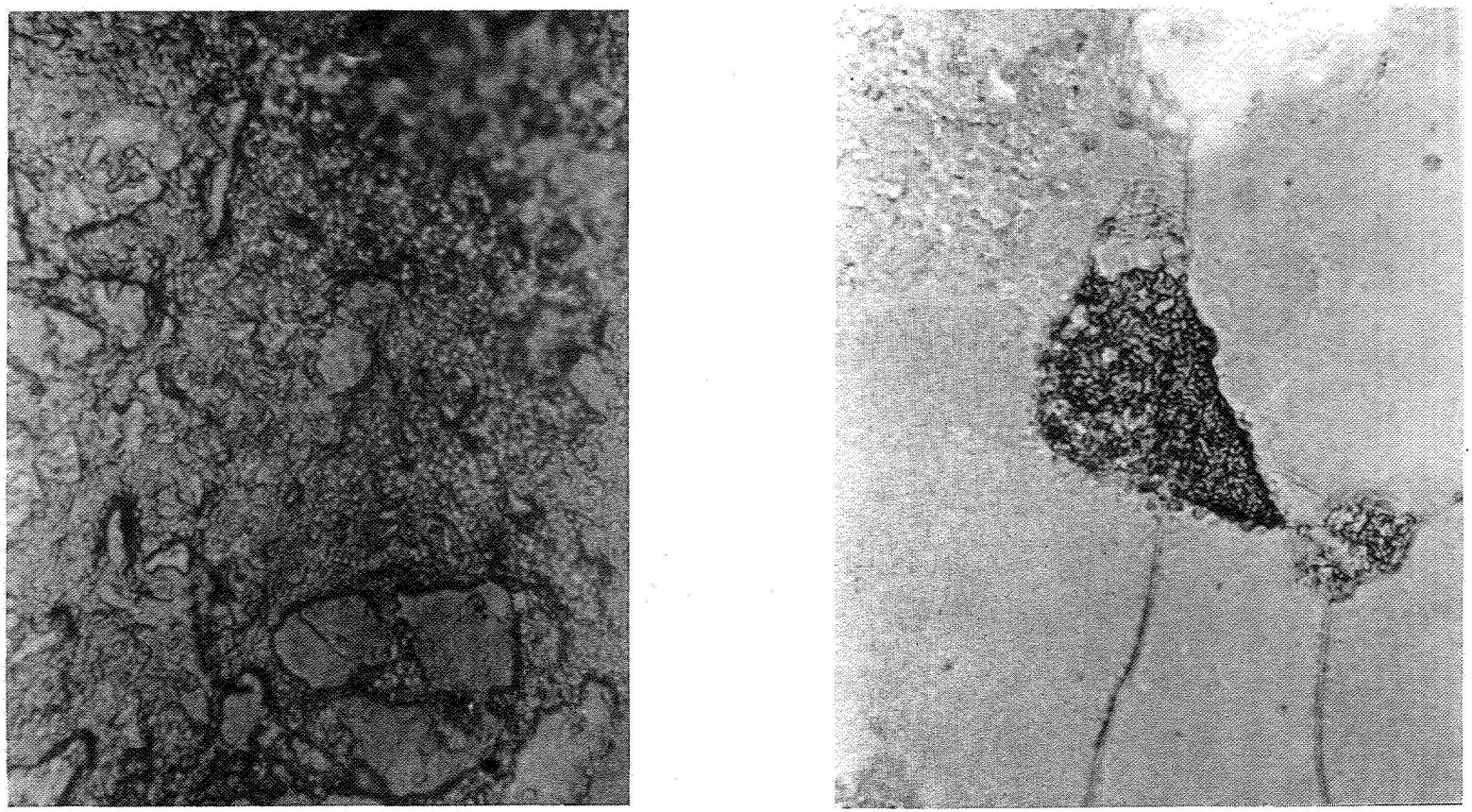

FIGURE 2-21. Photomicrographs of 1μm Dispersion Areas in Flight Specimen Sample 9F-A-01 (1000X Magnification)

show extremely fine, irregularly shaped dispersions of sodium acetate and paraffin (1μ or less) in the grain boundaries of the sodium acetate crystals. It is not known if the solidification forced the dispersions to the grain boundaries or whether these dispersions were nucleation sites. In general, the spherical paraffin dispersions range from 4 mm to 1μ in diameter. Smaller diameter spheres are suspected, but have not been resolved optically. One duplex dispersion of sodium acetate in a paraffin sphere located in the sodium acetate matrix was found, similar to those found in flight specimen 9.

The sodium acetate dispersions in the paraffin rich region are relatively uniform spheres, the majority having diameters between one and two millimeters.

2.3.3 Control Samples 9C-A-01 through -10

The sodium acetate near the heat sink end consists of small, random crystals for approximately one centimeter. Crystals having 2 - 4 mm lengths are randomly dispersed for approximately the next 1.5 centimeters, and then tend to become finer up to the sodium acetate-paraffin interface.

The interface area shows a relatively uniform transition, with a dispersion depth of approximately 0.5 mm as in the case of control specimens 6, and the sodium acetate and paraffin are completely segregated.

2.3.4 Flight Samples 9F-A-01 through -10

Each sample surface of flight specimen 9 shows dispersions of sodium acetate in paraffin or paraffin in sodium acetate. The majority also contain duplex dispersions, and in many instances, more complex dispersions of sodium acetate and paraffin.

The dispersions for the most part are spherical, although some of the sodium acetate in the duplex dispersions have irregular, crystalline shapes. Photomicrographs at 1000X show dispersions of 1μ or less.

The dispersed phase in these cases is predominantly irregularly shaped sodium acetate crystals.

The spherical dispersions range in diameter from 8 mm to approximately 1μ, although there may be smaller dispersions not optically resolvable.

2.3.5 Control Samples 12C-A-01 through -13

The sectioned samples exhibited similar morphological details as was shown on the surface of the unsectioned specimen.

The tungsten is primarily segregated in the first 2.5 cm from the heat sink end, and the tungsten-sodium acetate interface dispersion depth is approximately 8 mm. The sodium acetate region is predominantly crystallized in a fine, random orientation and exhibits a porous structure. There are a few moderate sized (0.5 mm) sodium acetate crystals near the sodium acetate-paraffin interface, which has a dispersion depth of approximately 5 mm. Some tungsten microspheres are randomly dispersed throughout the specimen samples, with a higher concentration located at the top of the shrinkage tube along with some sodium acetate.

2.3.6 Flight Samples 12F-A-01 through -14

There are three main types of dispersions present within flight specimen 12 as was mentioned in Section 2.2: (1) a tungsten microsphere, paraffin blend with dispersions of sodium acetate, (2) a tungsten microsphere, paraffin blend dispersed in sodium acetate, and (3) sodium acetate dispersed in paraffin. These dispersion types occur within various areas of the samples and are described below.

The dispersion of sodium acetate in the tungsten microsphere, paraffin blend is predominant in the first 4.5 cm of length from the heat sink end. The concentration of tungsten microspheres decreases away from the heat sink end and the dispersion type changes to the tungsten microsphere, paraffin blend dispersed in sodium acetate for approximately 1 cm up to the shrinkage cavity and at the top of the specimen. The

shrinkage cavity is surrounded by a paraffin sphere containing a dispersion of sodium acetate.

The sodium acetate dispersed in paraffin is spherical, but the majority of the other two types of dispersions are either distorted spheres or irregular in shape. This is in contrast to flight specimens 6 and 9, where the dispersions are predominantly spherical. Since the tungsten microspheres are preferentially wetted by the paraffin, this blend has the tendency to form a continuous phase and become a three dimensional, non-spherical random network.

The size distribution of the spherical dispersions ranges from .01 to 1.3 mm in diameter. Several areas containing dispersions of 1μ particles have been found, although not as many as in Flight Specimens 6 and 9. This may be due to the influence of the tungsten microspheres. Several duplex dispersions of sodium acetate in paraffin surrounded by sodium acetate have been found.

2.4 Density Determination

After sectioning, the specimens were weighed on a Sartorius-Werke Analytical microbalance. A Beckman Model 930 Air Comparison Pycnometer was used to determine the volume of each specimen.

Figure 2-22 is a plot of the density versus sample position for all of the control and flight specimens. These density values should be accurate to ±3 percent, in terms of instrumentation error. Cellular porosity was noted in some sections, which would give a volumetric reading higher than was actual, and consequently a lower density value.

The main trend in the control specimens was a relatively sharp drop in density from the bottom or heat sink end to the top. The rise in density near the top of control samples 6 and 12 is due to the presence of sodium acetate in the shrinkage tube. Porosity near the center of control sample 6 and 12 caused the relatively gradual density transition as contrasted to the density transition of control specimen 9.

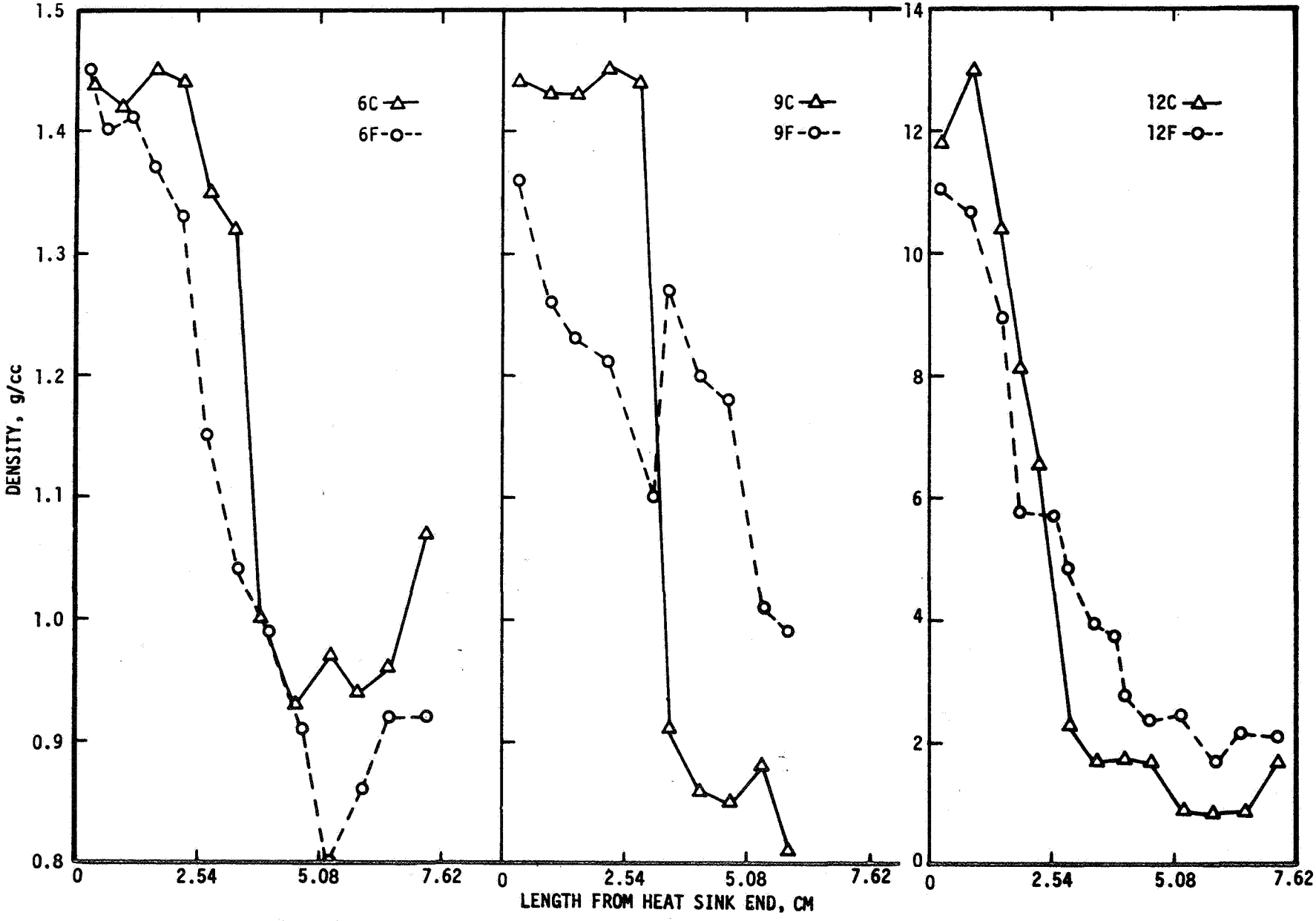

FIGURE 2-22. Density versus position for Control and Flight Specimens 6, 9 and 12.

The flight specimens all exhibited a more gradual density transition gradient as compared to the control specimens, with the exception of the top of flight specimen 6. The low density values again were caused by voids in the paraffin. Flight specimen 9 showed the greatest degree of dispersion, as illustrated in Figure 2-2. The density fluctuations near the center of the specimen are due to the large, localized paraffin-sodium acetate spheres in the center of the specimen.

2.5 Droplet Distribution of the Sectioned Flight Specimens

Each section of Flight Specimens 6, 9 and 12 was microscopically examined utilizing a template and an eyepiece filar to determine the droplet size and distribution of the materials contained in each specimen. The template used was a Gurley Lovins Microslide Field Finder No. 7100 and consists of a rectangular array of 1 mm square grids with 0.1 mm fiducial marks. The template and filar enabled droplet sizes down to 0.01 mm in diameter to be measured conveniently. Smaller droplet sizes were neglected since the depth of field prevented accurate distribution and diameter determinations.

Inasmuch as a differential temperature gradient existed radially between the edge and the center of the specimens, as well as longitudinally along the sample, three arbitrarily chosen regions were utilized to determine if there was a radial thermal effect as well as in the longitudinal direction. The first region was chosen to be the outer three millimeters, the second region the next three millimeters, and the third region the remaining center of the sample. Figure 2-23 schematically illustrates the template and the designated regions.

The measurements were performed as follows: the template was placed on the specimen with the corner of the specimen located at N-1 and the bottom edge aligned horizontally with the template. The specimen was then scanned vertically from numbers 1 through 18. Each droplet diameter was measured and the location noted. These diameters are probably smaller than actual, since the sectioning did not necessarily pass through the exact center of each droplet, however the diameter trend and distribution

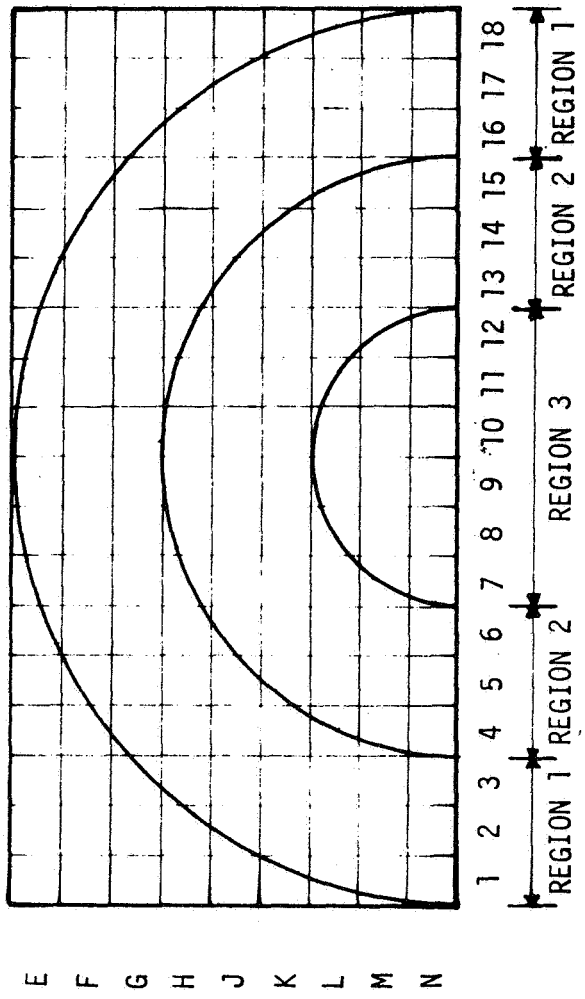

FIGURE 2-23. Template and Arbitrarily Designated Regions for Droplet Size and Distribution Measurement.

should be correct. For large droplets that significantly overlapped two (or more) regions, the droplet was counted as present in all overlapped regions. The results are presented in Figures 2-24 through 2-26 in terms of the droplet diameter multiplied by the number seen in each of the axially numbered samples. Each figure separates the three radial regions in which the droplet was located. The number located below or to the side of the symbol denotes the number of droplets counted of that diameter. In this manner the volumetric concentration and distribution of droplets longitudinally and radially in each specimen can be assessed. Duplex and more complex dispersions were considered separate droplets within a micro-matrix, and both materials were counted. An overall estimate of the droplet distribution in the specimens can be seen in the X-ray photographs in Figure 2-27, taken at MSFC.

The distribution of paraffin and sodium acetate droplets in specimen 6 is rather sharply spacially delineated. From Figure 2-24 it can be seen paraffin droplets were axially limited to the heat sink half of the sample whereas the sodium acetate was found only in the remaining half. The sodium acetate size/frequency factor is narrower in spread than the paraffin. No radial variation in either the paraffin or sodium acetate distribution is seen. However, some suggestion of a systematic increase in diameter of the paraffin droplets is seen in all three radial regions as the axial sections range from -01 through -07, the increase occurring with distance from the heat sink end. A number of dispersions near the heat sink end were distorted, and only the ones which were spherical or reasonably spherical in shape were counted; thus the droplet count from sections -01 through -05 is lower than the actual dispersion. Droplet size ranges were considerably varied, due either to initial lack of dispersion during mixing, or agglomeration during solidification.

Specimen 9 shows a much greater spacial distribution of observable paraffin and sodium acetate drops than specimen 6. Figure 2-25 shows a broad distribution of both types of droplets occurred with exception of a narrow region at the heat sink end which only contained paraffin drops and a narrow region at the other end containing only sodium acetate drops. As with specimen 6, a smaller spread in size frequency occurs for the sodium

FIGURE 2-24.
DROPLET DISTRIBUTION OF FLIGHT SPECIMEN 6F-A-01 THROUGH-13

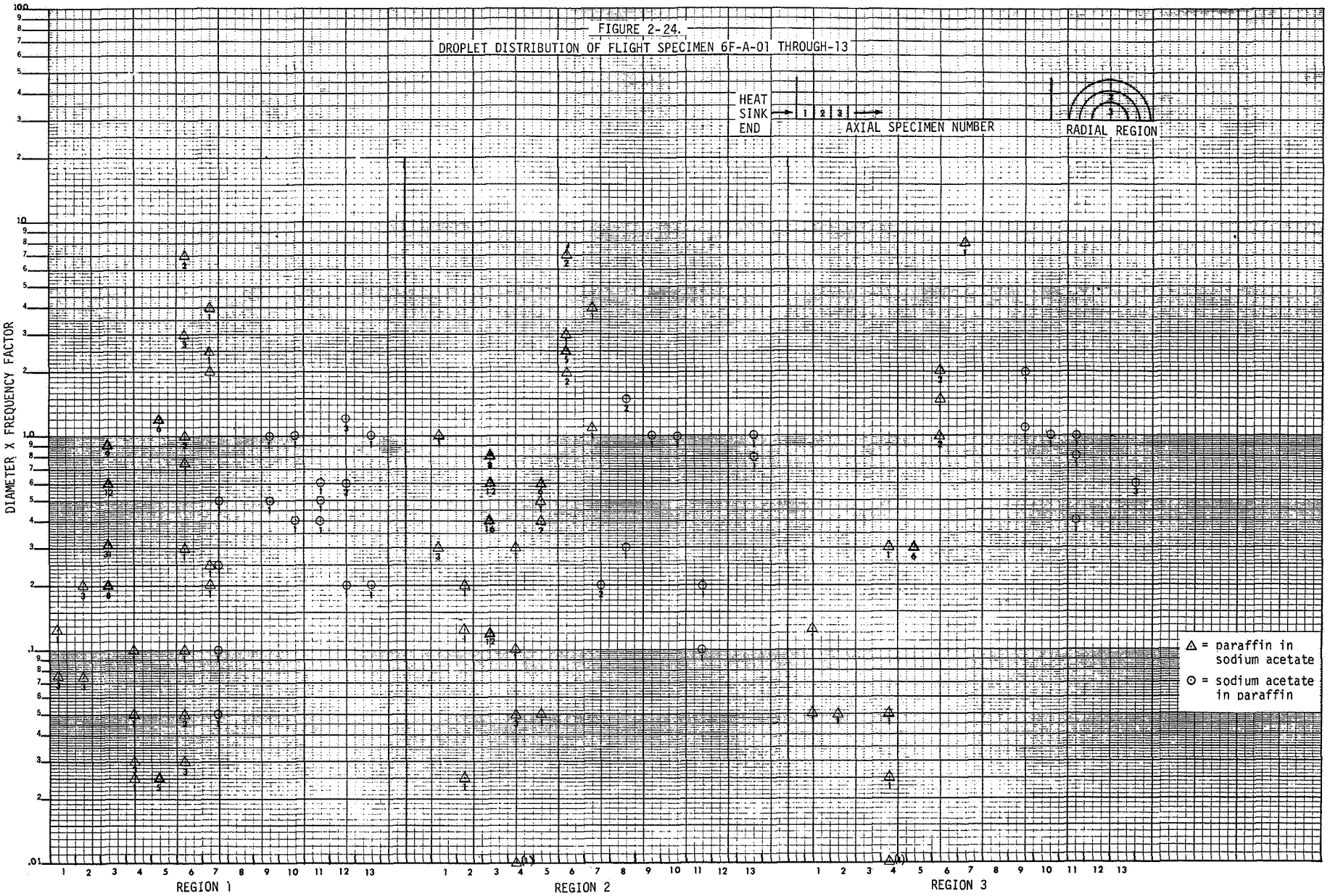

FIGURE 2-25.
DROPLET DISTRIBUTION OF FLIGHT SPECIMEN 9F-A-01 THROUGH-10

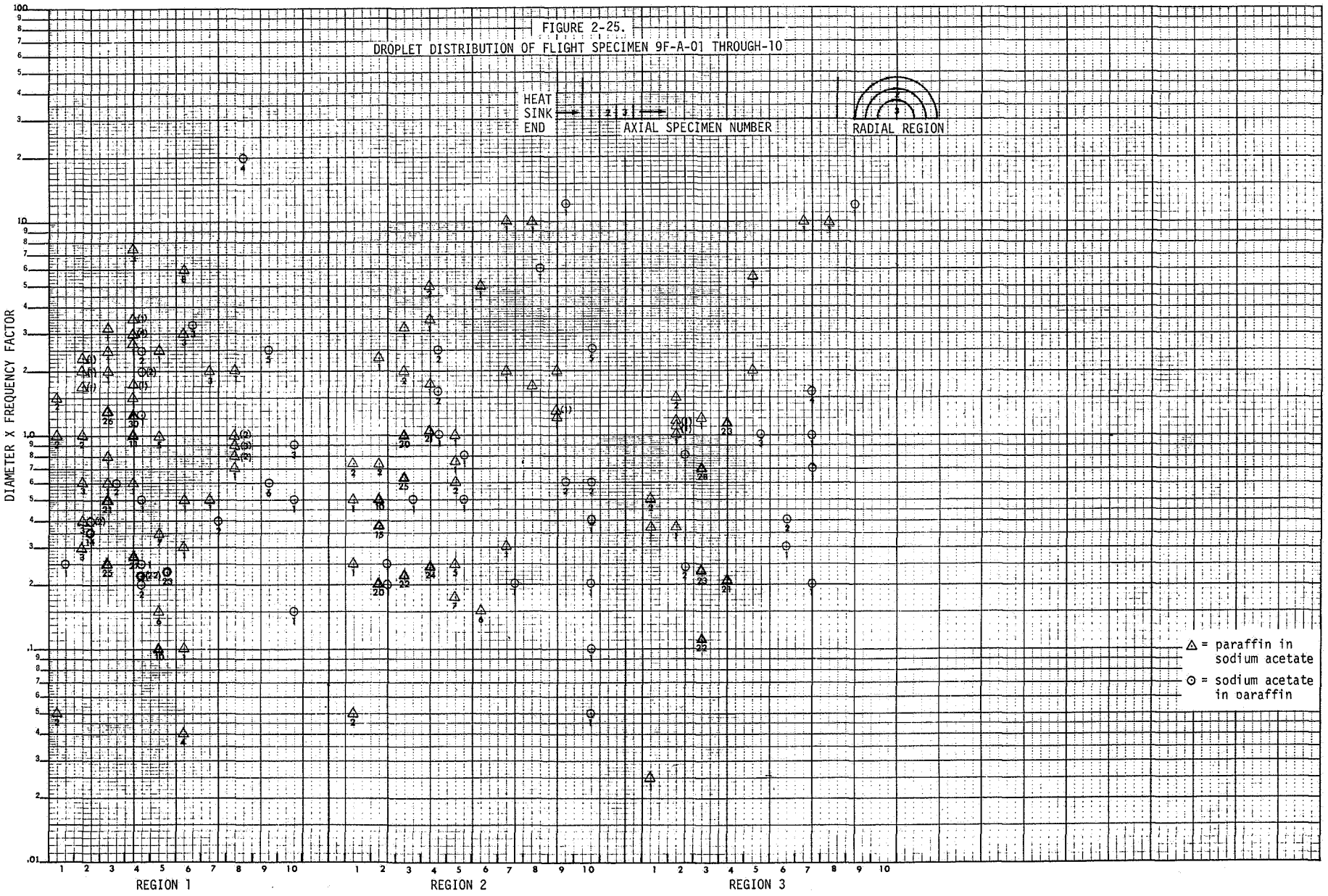

FIGURE 2-26.
DROPLET DISTRIBUTION OF FLIGHT SPECIMEN 12F-A-01 THROUGH-14

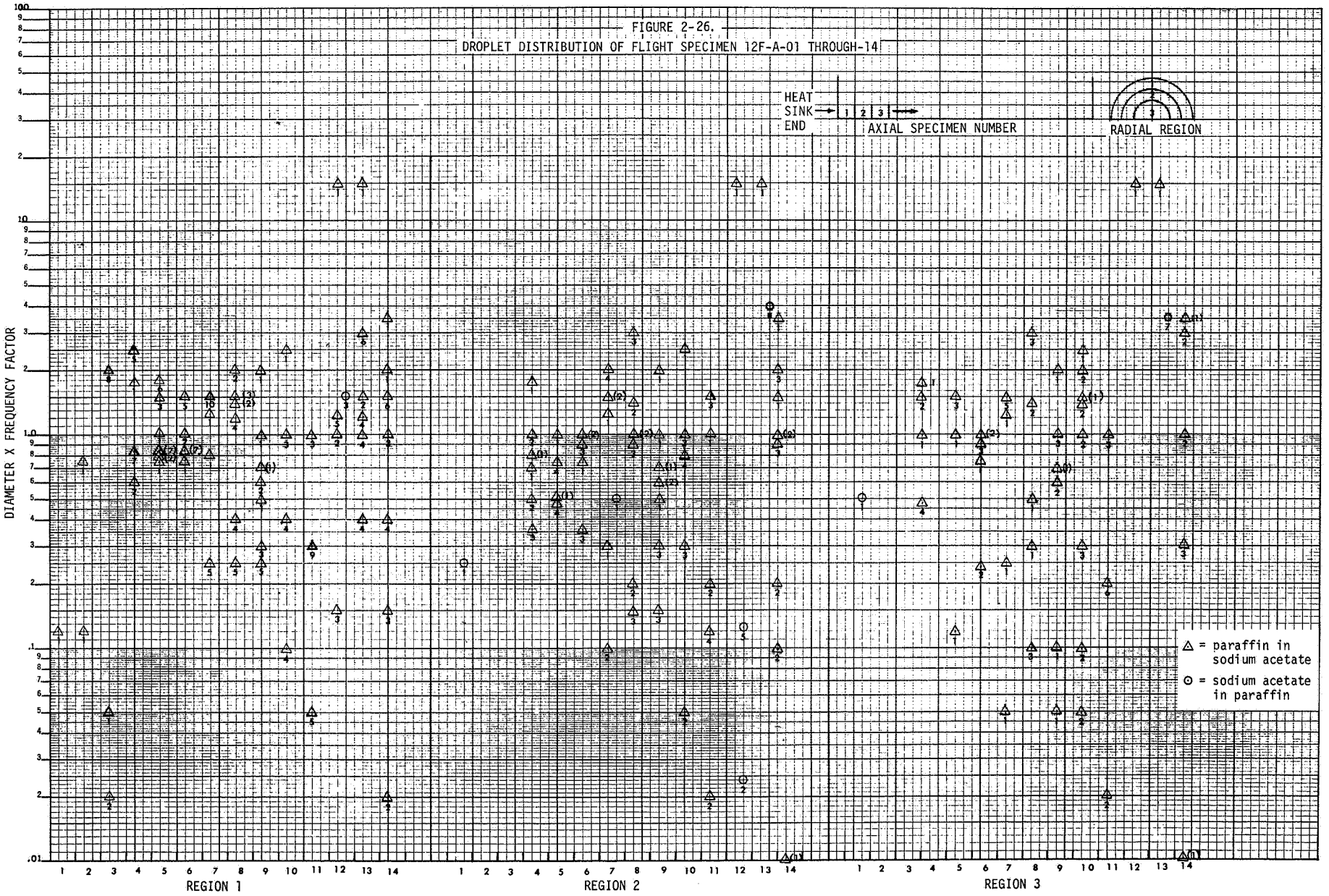

CONTROL

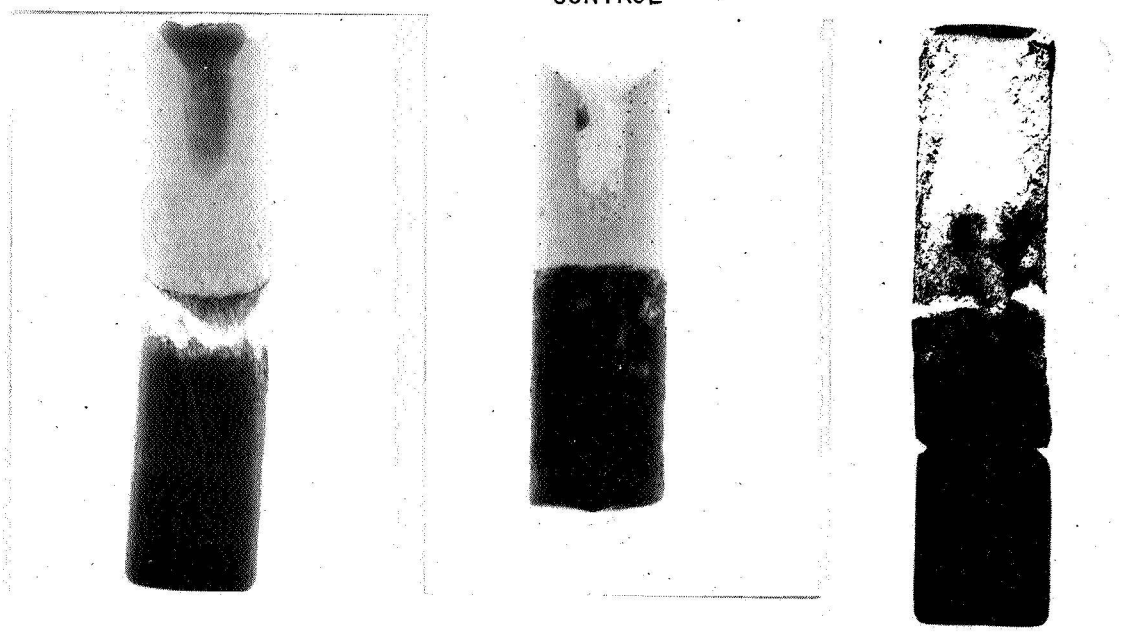

6C-A-00 9C-A-00 12C-A-00

FLIGHT

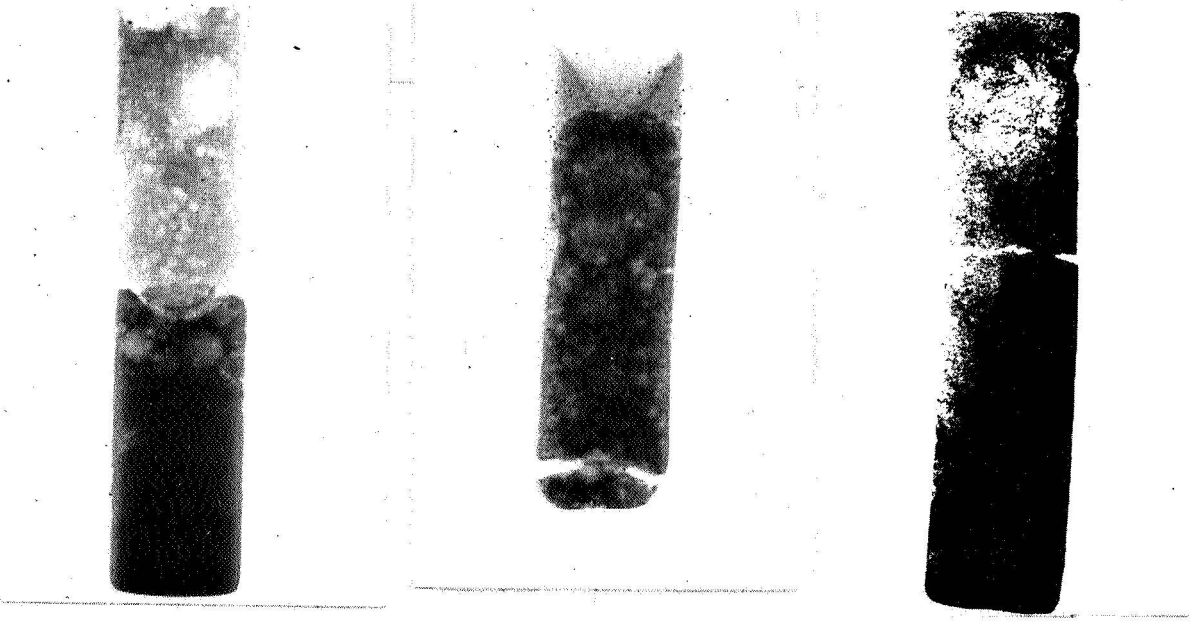

6F-A-00 9F-A-00 12F-A-00

FIGURE 2-27. X-Ray Photographs of Flight and Control Specimens 6, 9 and 12 (1X Magnification)

acetate than the paraffin. The suggestion of a possible increase in the size/frequency factor for the paraffin with increasing distance from the heat sink may be seen but is less obvious than in sample 6. Overall dispersion of the two materials in this sample as noted in the X-ray, photomicrographs and density measurements is verified by the droplet distribution counts.

Flight Specimen 12 was primarily a dispersion of paraffin and paraffin-tungsten microspheres. Since the tungsten microspheres were preferentially wetted by the paraffin, the droplet distribution shown in Figure 2-26 is predominantly a paraffin-tungsten microsphere aggregation. A number of the droplets were distorted, and as for Flight Specimen 6, only those droplets which were spherical or nearly so were counted.

The droplet dispersion was reasonably uniform throughout the three regions, indicating little radial movement, but there does appear to be a trend of increasing droplet size in the longitudinal direction away from the heat sink end. This specimen had the fewest droplet dispersions of any of the three flight specimens, due primarily to the tendency of the paraffin-tungsten microsphere phase to form a continuous network rather than discrete, dispersed droplets.

Several general conclusions regarding droplet observations include:

1. No droplets were present in any of the control samples. Thus droplet formation is strictly associated with mixing and solidification under reduced gravity.
2. Paraffin droplets exhibited a spacial distribution which exclusively included the heat sink end of the capsules and shows a tendency toward larger sizes as the distance increases In general, the number of paraffin droplets were increasingly diminished at the far end. Paraffin droplets were excluded from the far end.
3. Sodium-acetate droplets are excluded from the heat sink end and tend to predominate more as the distance is increased.

4. The distribution of paraffin droplet sizes is significantly broader than that observed for sodium acetate.
5. Preferential wetting of tungsten microspheres by paraffin markedly reduced the formation of sodium-acetate droplets.
6. The variation in droplet distribution between samples 6, 9 and 12 appears to reflect:
   a. The degree of initial mixing
   b. The imposition of an axial thermal gradient during solidification
   c. Possible influence of imposed body forces

However, the qualitative and quantitative aspects of such correlations remain to be experimentally verified.

2.6 Physical Property Determinations

In order to perform the theoretical analyses presented in Section 3.0, the density, surface tension and viscosity of paraffin and sodium acetate were measured from 60°C (140°F), close to their melting points, to 93°C (200°F), which was approximately the maximum temperature experienced by the capsule during initial processin . Filtered, Baker Analytical Grade sodium acetate trihydrate and Americal Oil Co. N.F. grade paraffin were used for the experiments. The results are shown in Table 2-1.

The density of each material was measured by filling a Weld pycnometer with the molten fluid, equilibrating to the desired temperature and then sealing them. The pycnometer was then cooled to room temperature and weighed. Three separate determinations were made at each temperature. It is estimated that the accuracy was good to better than $\pm$1%.

The viscosities were determined using a Ubbelohde viscometer, with both the viscometer and the fluid material equilibrated at the temperature of interest. Again, three determinations were made at each temperature and the accuracy is estimated to be better than $\pm$1%.

TABLE 2-1

Density, Surface Tension and Viscosity of Sodium Acetate and Paraffin at Various Temperatures

Temperature:	60°C (140°F)	71°C (160°F)	82°C (180°F)	93°C (200°F)
Property				
Density, g/cc				
Paraffin	0.781	0.774	0.767	0.760
Sodium acetate	1.276	1.266	1.257	1.246
Kinematic Viscosity, Centistokes				
Paraffin	8.538	6.795	5.343	4.425
Sodium acetate	9.350	6.660	4.828	3.709
Surface Tension, dyne/cm				
Paraffin	25.5	24.5	23.4	22.8
Sodium acetate	59.9	56.2	54.2	52.4
Interfacial Tension, dyne/cm				
paraffin–sodium acetate	26.8	25.3	24.2	23.1

The surface tension of each material, and the interfacial tension of sodium acetate and paraffin in combination were measured using a Model 21 Fisher Surface Tensiomat. Resistance wire heated beakers with partially covered tops were used to contain the fluids. Three measurements were taken at each temperature, and the accuracy is estimated to be better than $\pm$5%, from referee determinations made on triple distilled water and reagent grade methanol.

In addition to the above measurements, solid densities and latent heats of fusion were measured for sodium acetate and paraffin, and literature values of the thermal conductivity for both substances were found. These values are shown in Table 2-2.

TABLE 2-2

Density, Thermal Conductivity and Latent Heat of Fusion of Sodium Acetate and Paraffin

	Density, g/cc at 20°C	Thermal Conductivity cal/cm sec °C	Latent Heat of Fusion cal/g
Sodium Acetate	1.44	2.3×10^{-2}	66
Paraffin	0.85	5.7×10^{-4}	37

3.0 THEORETICAL ANALYSIS

3.1 General

Photographs of the returned capsules exhibit the results of a complex mechanical and thermal history. Because of this situation, the following analysis proceeds from a series of simple models to gain insight into the dominating phenomena to more complex models which attempt to predict various aspects of the capsules' thermal and mechanical histories. A discussion of some of the phenomena occurring from the time the capsules were shaken until the contents solidified is presented below.

3.2 Fluid Behavior in a Low Gravity Environment

The fluids in the capsules were mixed and dispersed by shaking the capsules with an included mixing ball in a complex manner. MSFC-supplied movies of neutral bouyancy fluids undergoing motions similar to the above capsules shows that the fluid obtains a circulatory motion both radially and axially. From the equation of motion for a rotating viscous fluid, an estimate of the characteristic times associated with the induced circulatory flow can be obtained. The equations of conservation of mass and momentum are

$$\nabla \cdot \tilde{q} = 0 \tag{1}$$

and

$$\frac{\partial}{\partial t}\tilde{q} + \tfrac{1}{2}\nabla(\tilde{q}\cdot\tilde{q}) + (\nabla \times \tilde{q}) \times \tilde{q} + \underline{2\Omega \times \tilde{q}} + \underline{2\tilde{\Omega} \times \tilde{q}} + \tilde{\Omega} \times (\tilde{\Omega} \times r) = -\frac{1}{\rho}\nabla P + \tilde{F} - \underline{\nu\nabla \times (\nabla \times \tilde{q})} \tag{2}$$

where $\tilde{q}$ is the particle velocity measured in a coordinate system rotating with constant angular velocity, $\tilde{\Omega}$, and $\tilde{r}$, t, P, ρ, ν and $\tilde{F}$ represent respectively the position vector, time, pressure density, kinematic viscosity and body force per unit mass.

An important dimensionless parameter which is a measure of relative magnitude of the viscous forces to coriolis forces (underlined terms in equation 2) is the Eckman number (Ref. 1).

$$E = \frac{\nu}{\Omega L^2} \quad , \tag{3}$$

where L is a characteristic length. For the interaction of the fluid with a rotating container, there are three phases of development of the induced flow: the development of a viscous boundary layer, the spin-up of the fluid and the viscous decay of residual effects. These phases occur with approximate characteristic times given by

$$\begin{aligned} t_B &\simeq \frac{1}{\Omega} \quad , \\ t_{SU} &\simeq \frac{1}{\Omega E^{\frac{1}{2}}} \quad , \\ t_V &\simeq \frac{1}{\Omega E} \quad , \end{aligned} \tag{4}$$

where t_B, t_{SU} and t_V are the times for boundary layer growth, spin-up and viscous decay respectively. These times are plotted in Figure 3-1 as a function of characteristic circulation frequency using the mean fluid properties of paraffin and sodium acetate.

An examination of Figure 3-1 reveals that for a characteristic frequency of 1 sec^{-1}, the assumed astronaut shaking frequency, the characteristic time for boundary layer growth is 1 sec, spin-up is 4 sec and viscous decay is 16 sec. Spin-up is a stable flow configuration, however, spin-down or the deceleration of the fluid by a stationary container is not stable, and becomes turbulent. Because of this instability, spin-down times cannot readily be calculated. However, the spin-up time should be an upper bound on this spin-down time.

The above calculations estimate the effects of viscous and coriolis effects of the fluid motions. We would now like to assess some of the effects of surface tension forces. A measure of the relative importance of the surface tension forces to the acceleration forces is the Bond number (Ref. 2).

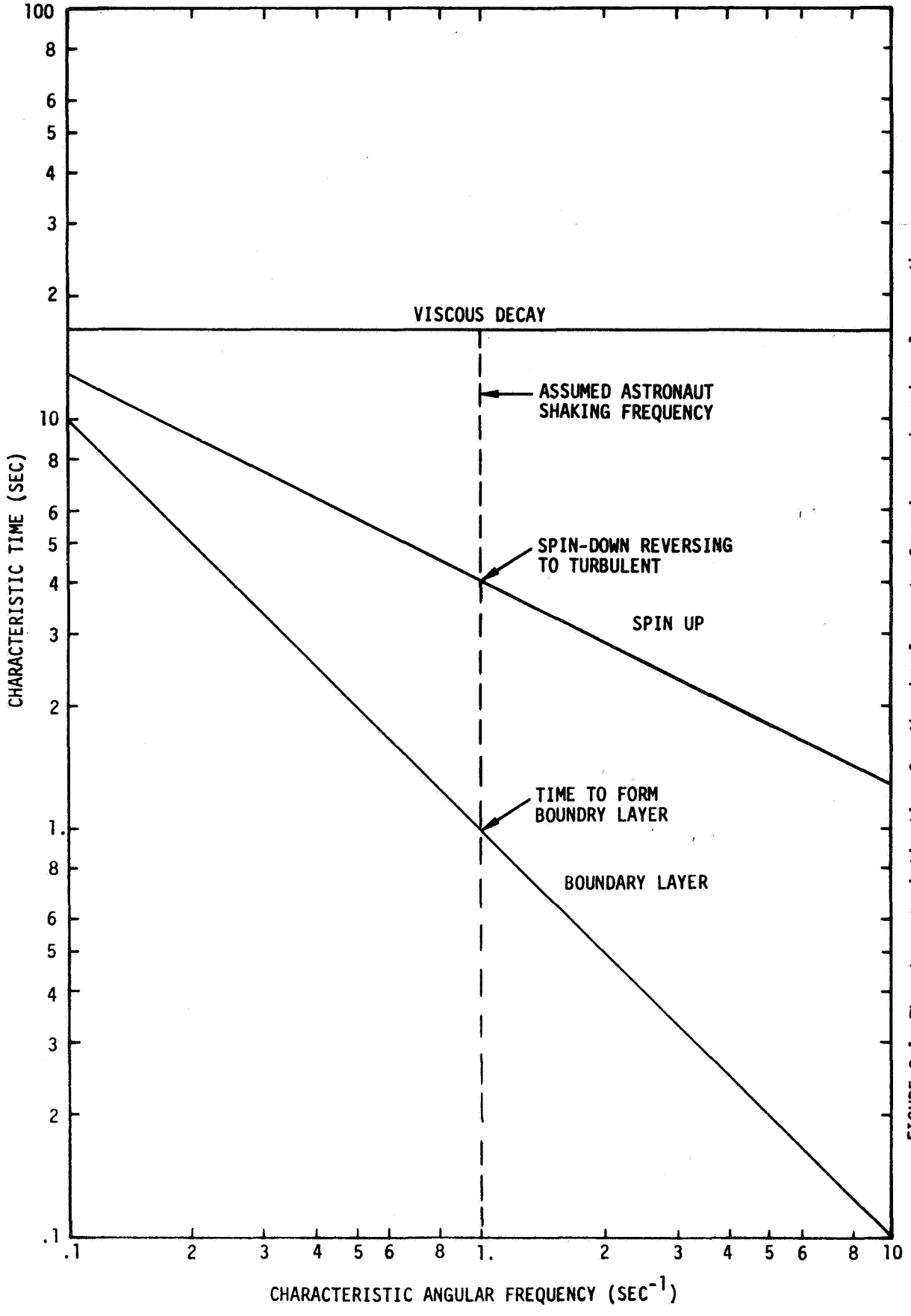

FIGURE 3-1. The characteristic time for the development of a viscous boundary layer, the spin-up of the fluid and the viscous decay of residual effects as a function of the characteristic angular frequency of the flow.

$$B_o = \frac{\Delta\rho\ g\ L^2}{\sigma} \tag{5}$$

where g is the local acceleration, $\Delta\rho$ the density difference and σ is the surface tension. The Bond number for paraffin-sodium acetate as a function of acceleration is shown in Figure 3-2. For Bond numbers much less than 1, the motion of the fluid is capillary dominated and for magnitudes greater than 1 the motion is body force or gravity dominated.

For the paraffin-sodium acetate system to be capillary dominated the accelerations should be less than $10^{-2}\ g_e$ or 0.098 M/sec^2.

In the capillary dominated regime, it is of interest to know what would be the characteristic time for the fluid system to recover to an equilibrium capillary configuration when an imposed body force is rapidly removed. An estimate of this time (Ref. 3) is given by

$$t_{eg} = .15 \left(\frac{\sigma L^3}{\rho}\right)^{\frac{1}{2}} \tag{6}$$

For the paraffin-sodium acetate capsules this time is of the order of .1 sec., indicating that the system reverts rather rapidly to the capillary dominating regime.

Single or small numbers of liquid and/or solid particles immersed in a fluid and subjected to an acceleration field will rapidly reach a limiting velocity called the Stokes velocity,

$$V_s = \frac{2}{9}\ \frac{\Delta\rho\ g\ a^2}{\mu}\ , \tag{7}$$

where μ is the dynamic viscosity and "a" the particle radius. This velocity was calculated for a range of sizes of sodium acetate particles in paraffin as a function of acceleration and also for 50 micron radius tungsten spheres in sodium acetate and paraffin and are illustrated in Figs. 3-3 & 3-4.

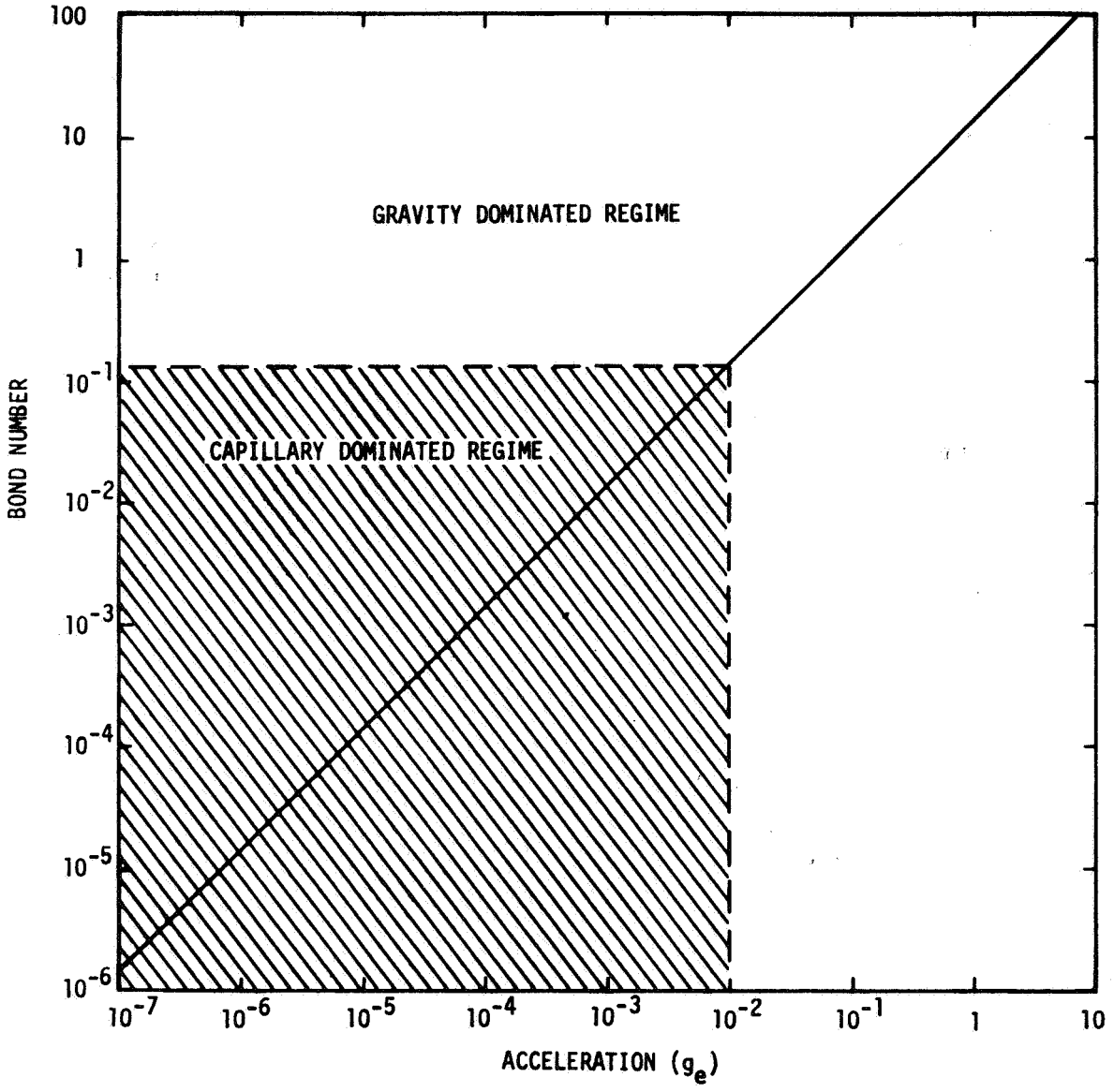

FIGURE 3-2. The Bond number as a function of acceleration enviroment for a paraffin-sodium acetate system.

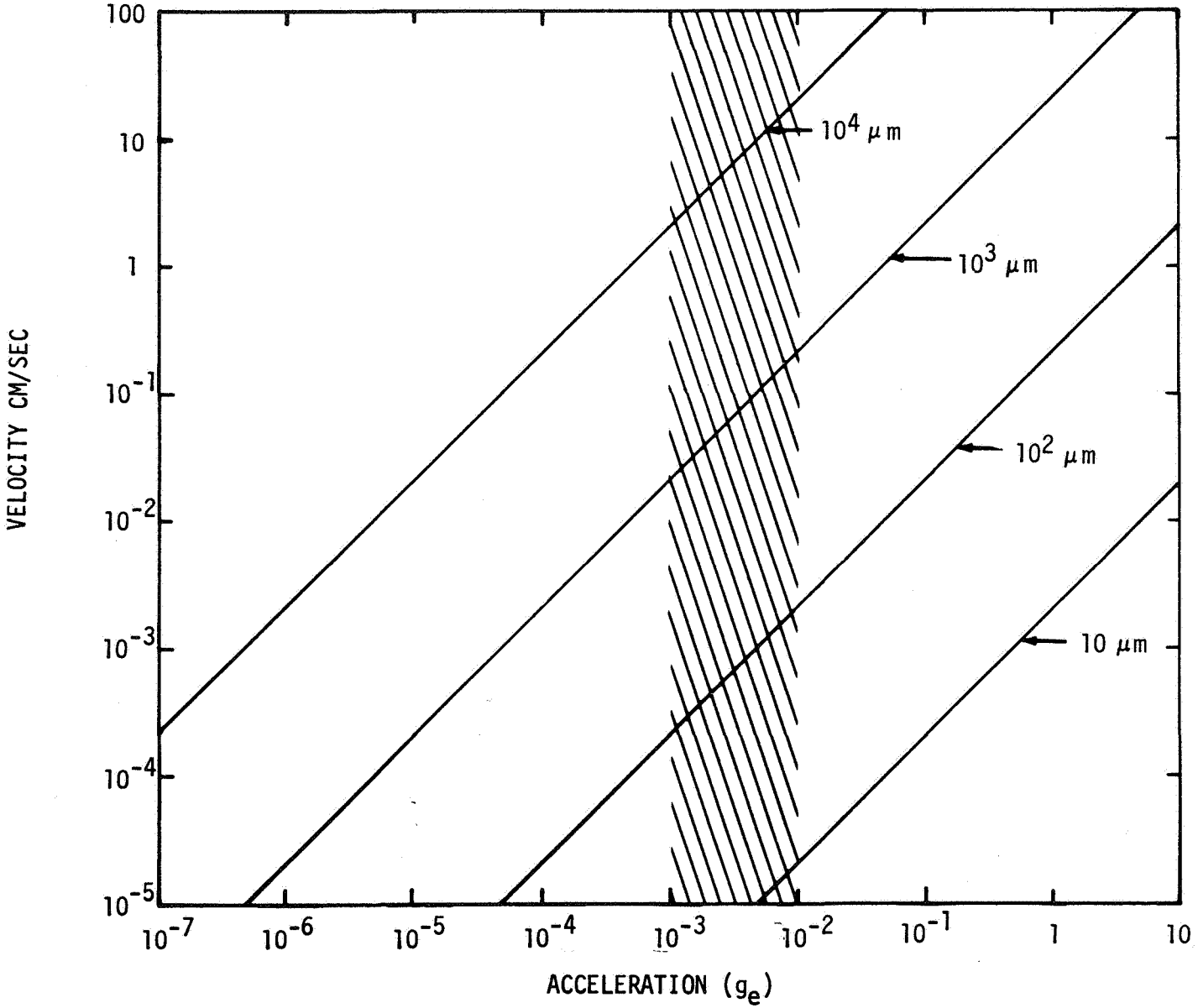

FIGURE 3-3. The Stokes velocity of sodium acetate particles of various radii in paraffin as a function of acceleration environment.

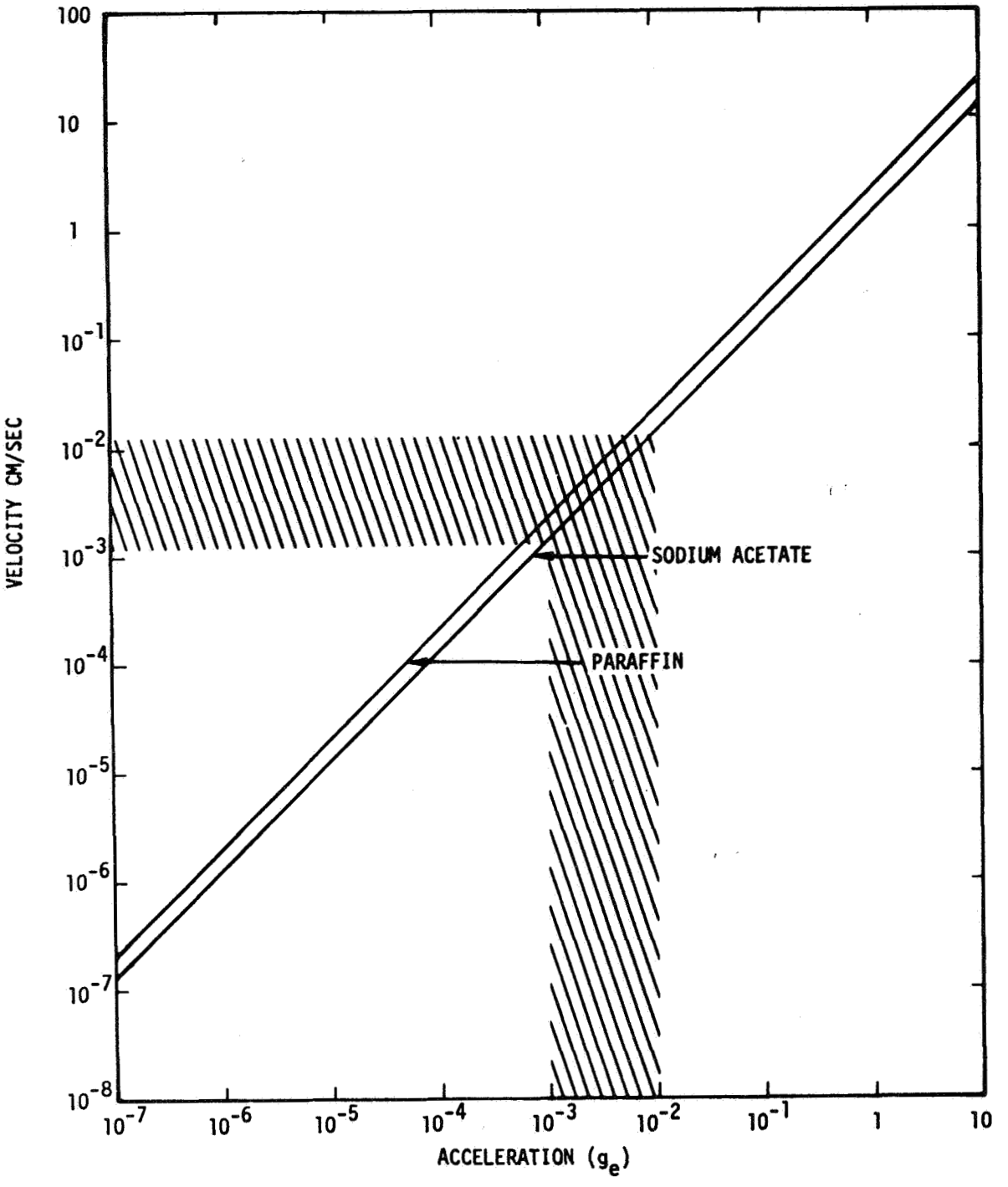

FIGURE 3-4. The Stokes velocity of 50 micron radii tungsten spheres in paraffin and sodium acetate as a function of acceleration environment.

During the shaking and dispersing of the fluid mixtures, many droplets will impinge upon the capsule walls. In order to predict the maximum size of droplet that would be stable in the acceleration environment, the stability calculations of reference 4 were applied to a paraffin-sodium acetate system and is illustrated in Fig. 3-5. For example, a 10^{-2}g field and contact angle of 30° imply that droplets are unstable when the volume of the droplets are greater than 35 cm^3. The obvious implication here is that wall bound drops would remain bound in a low gravity acceleration environment. Since individual wall bound droplets were not observed in any of the specimens, droplet coalescence or some other mechanism must have prevented this phenomenon from occurring.

3.3 Thermal Analysis

Low gravity convection, whether surface tension or buoyancy driven, and immiscible droplet motions are all functions of the thermal history of the system. The thermal history is complicated by inhomogeneity of the immiscible mixture, phase changes, moving fluid surfaces within the container and several possible modes of mass transfer. In this light, a simple one-dimensional heat transfer model was chosen in order to provide a basis for assessing the magnitude of the more complex phenomena. The model assumes the capsule, fluid mixture and copper sleeve to be represented by a finite homogeneous cylinder which is insulated on all sides except for one end, denoted as Region 1. Connected to the uninsulated end of the Region 1 is a semi-infinite insulated aluminum rod, Region 2.

At time equal to zero the temperature in the capsule is assumed to be equal to the temperature immediately after shaking the capsule and the temperature profile is assumed to be uniform. The temperature in the heat sink is assumed to be ambient. The derivation of the solutions to the heat equation in regions 1 and 2 is given in Appendix A. The thermal properties of region 2 were those of aluminum with a conductivity of $.504 \frac{cal}{cmsec°C}$ and diffusivity of $.872 \frac{cm^2}{sec}$. In region 1 the mean thermal properties were adjusted until agreement was obtained with the measured temperature histories at the top of the capsules. These values for the conductivity and diffusivity were found to be $.0146 \frac{cal}{cmsec°C}$ and

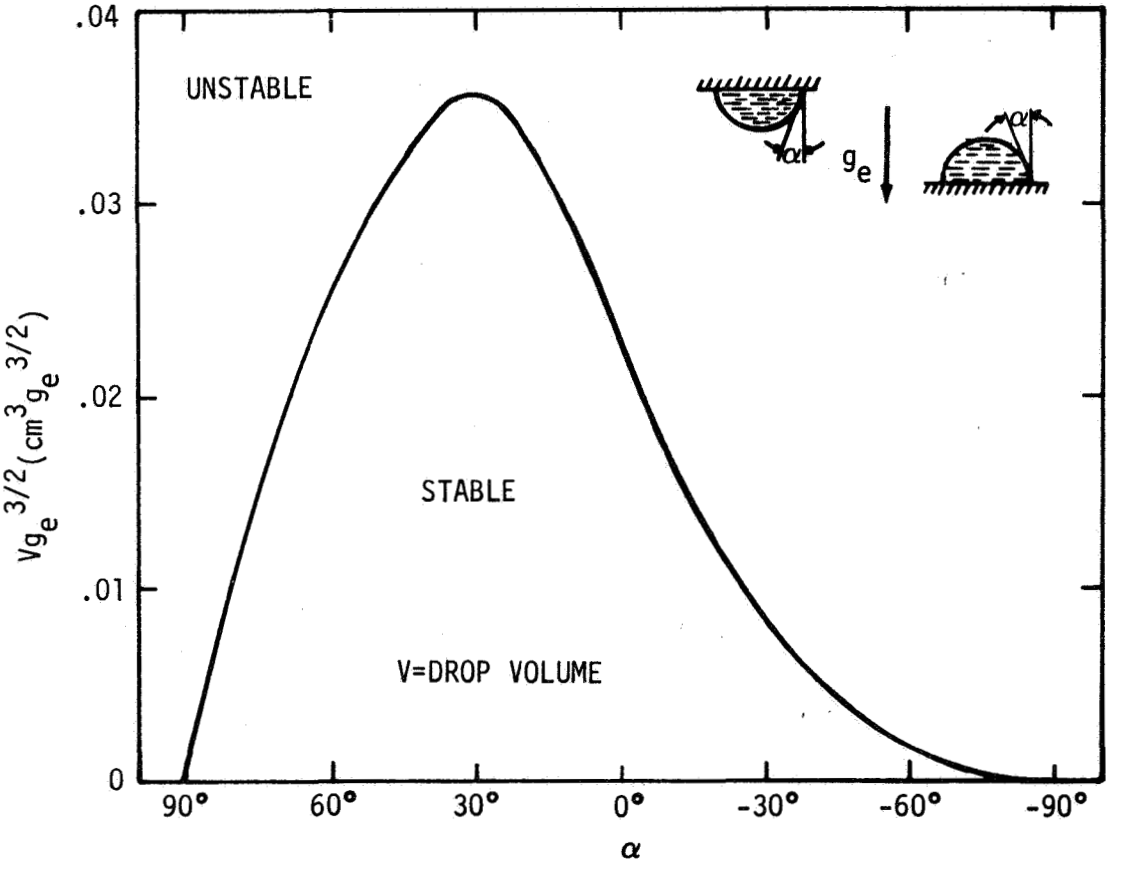

FIGURE 3-5. The stability of droplets or bubbles in a paraffin sodium acetate system as a function of the contact angle α.

.02 $\frac{cm^2}{sec}$ respectively, and were the same in all cases indicating that the matrix material was the dominating factor in the thermal transfer. The measured thermal histories for tests 9C and 12C are presented in Figures 3-6 and 3-7. Since the thermal profile of 6C was intermediate to 12C and 9C, the thermal histories of 9C and 12C were taken as the upper and lower boundaries, respectively. The circled points on the figure are the computed temperatures at various times. The agreement is very good considering the simplicity of the model. The thermal profiles at 100, 360, 720 and 1440 sec (after heater power was turned off) for tests 9C and 12C are given in Figures 3-8 and 3-9, utilizing the heater/capsule initial temperature at power turn-on as the baseline. The melting temperature of sodium acetate is 58°C and for paraffin it ranges from 54 to 58°C. From the analyses solidification occurs at times on the order of 900 sec.

3.4 Surface Tension and Bouyancy Driven Convection Force Analyses

The possibility of surface tension and/or bouyancy driven convection during the cooling cycle was investigated. Both the Marangoni and Rayleigh numbers were found to be negative. These numbers were calculated by assuming the fluid to be homogeneous and not containing droplets of included material. From this standpoint, the fluid in the capsules would be absolutely stable and would not convect. (Ref. 5). However, as shown in the following sections, the inherent inhomogeneity of the dispersed fluid gives rise to other potential modes of mass transfer.

The fluid particles in the capsules were subjected to both temperature gradients and small acceleration fields. Both of these conditions will give rise to droplet particle motions and therefore mass transfer. Previously calculated Stokes velocity for various particle radii were done as a function of acceleration levels in the absence of thermal gradients, as shown in Figure 3-3. However, it has been found experimentally that thermal gradients influence the motion of small bubbles and that they are accelerated towards regions of higher temperature. In Ref. 6 the limiting velocity of a particle in both a constant acceleration and thermal gradient field was theoretically calculated and found to be

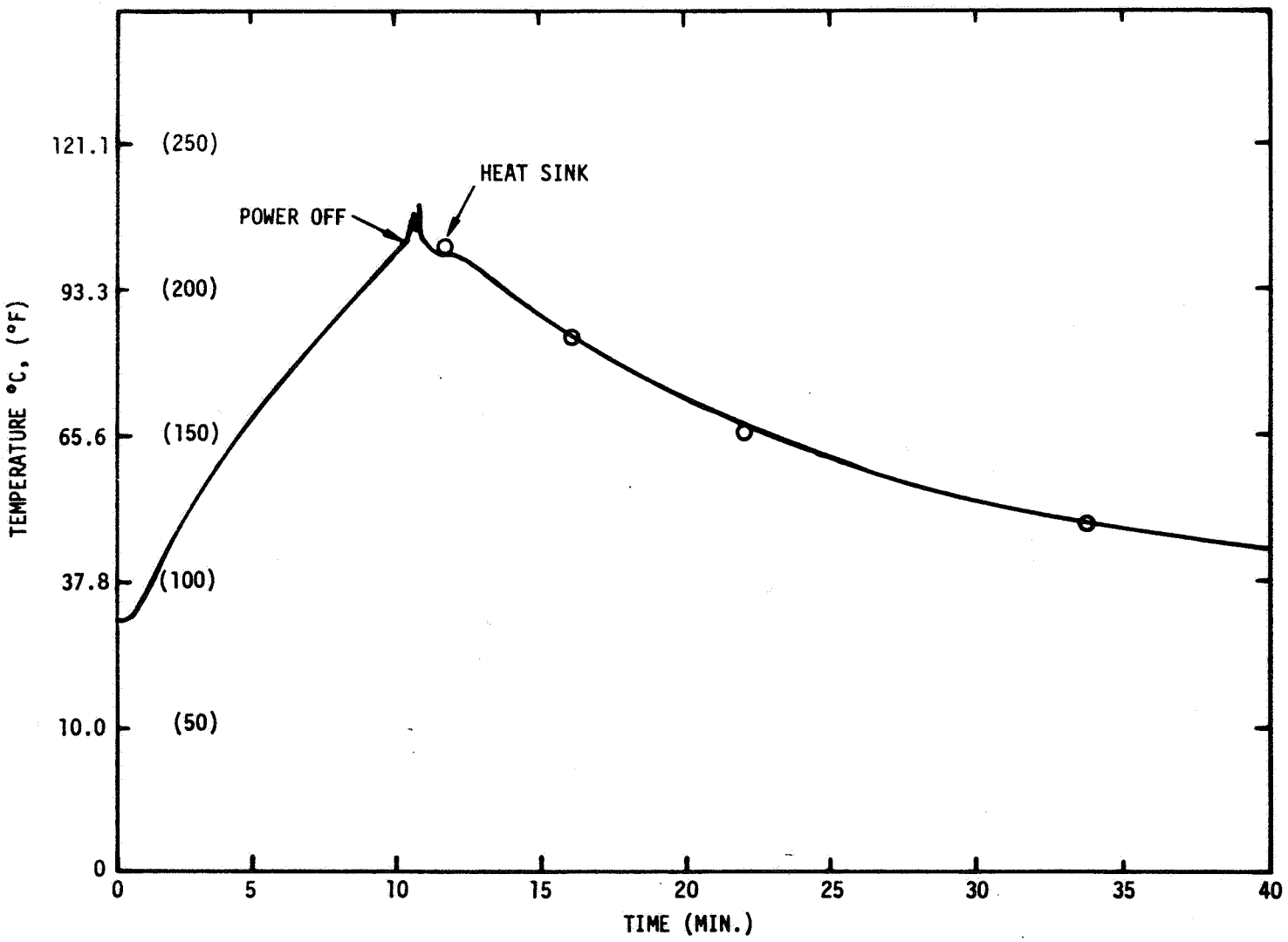

FIGURE 3-6. Measured thermal history of experiment 9c.
The circled points are the calculated temperatures.

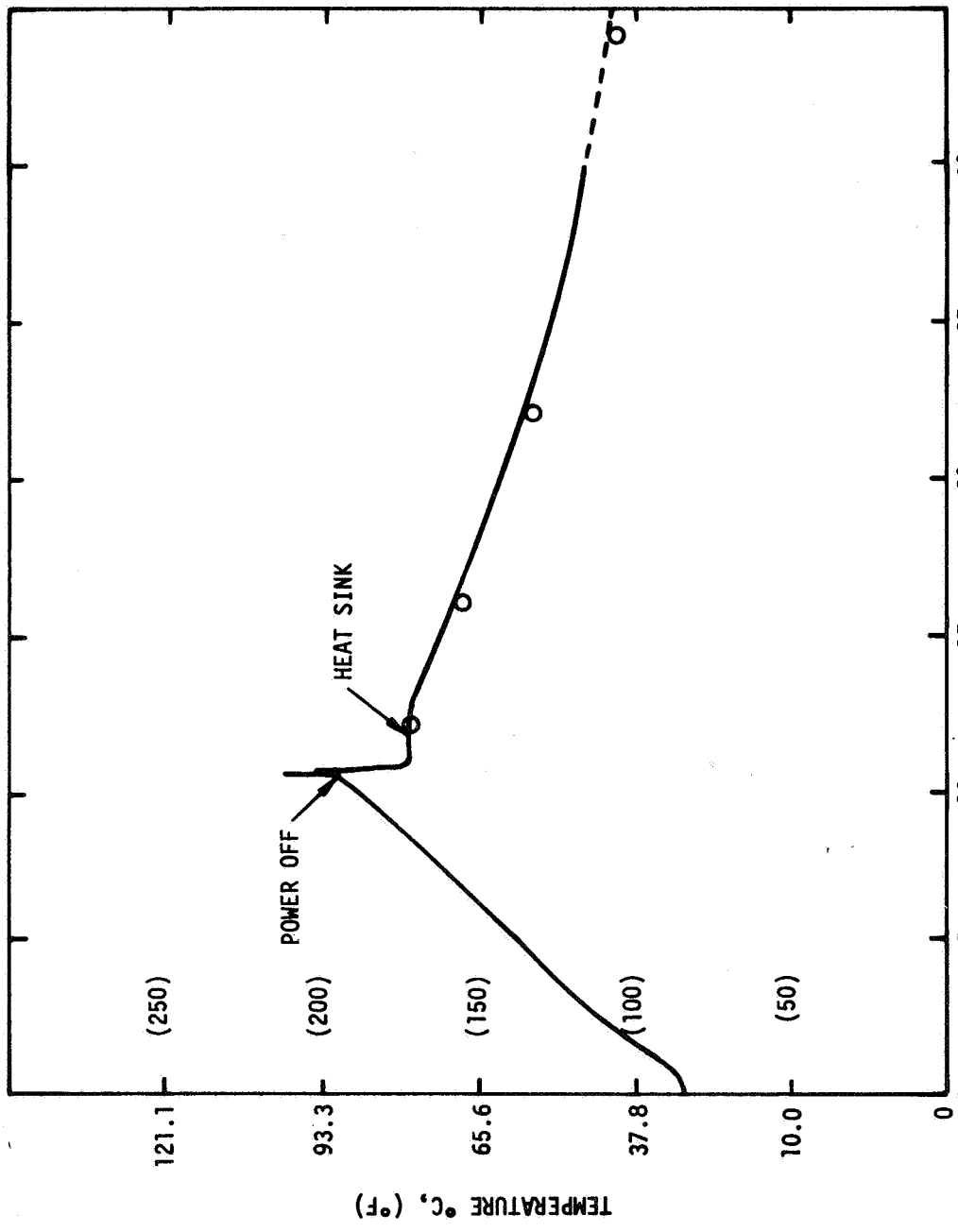

FIGURE 3-7. Measured thermal history of experiment 12c.
The circled points are the calculated temperatures.

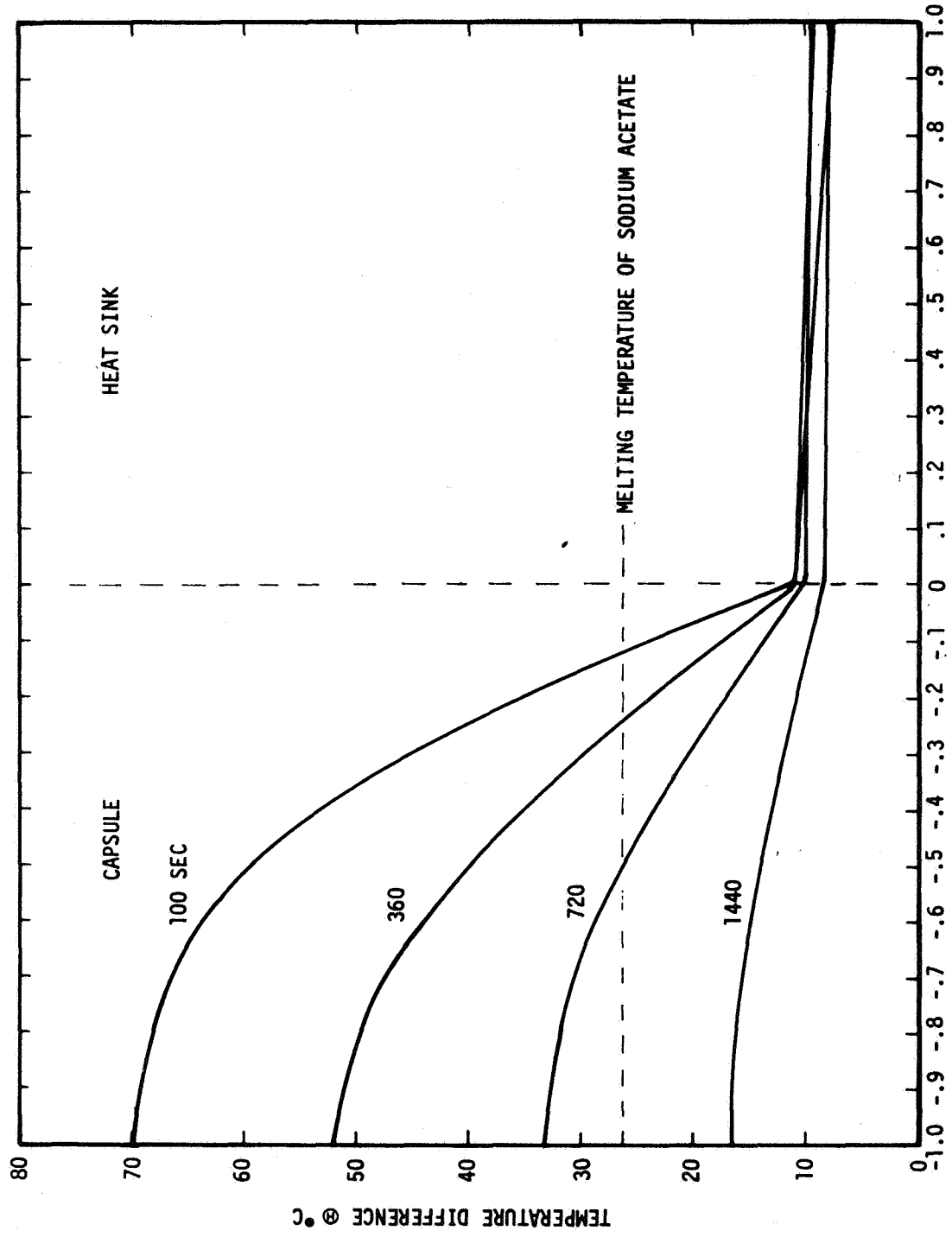

FIGURE 3-8. Calculated thermal profile of experiment 9c at various times. L is defined as length of capsule.

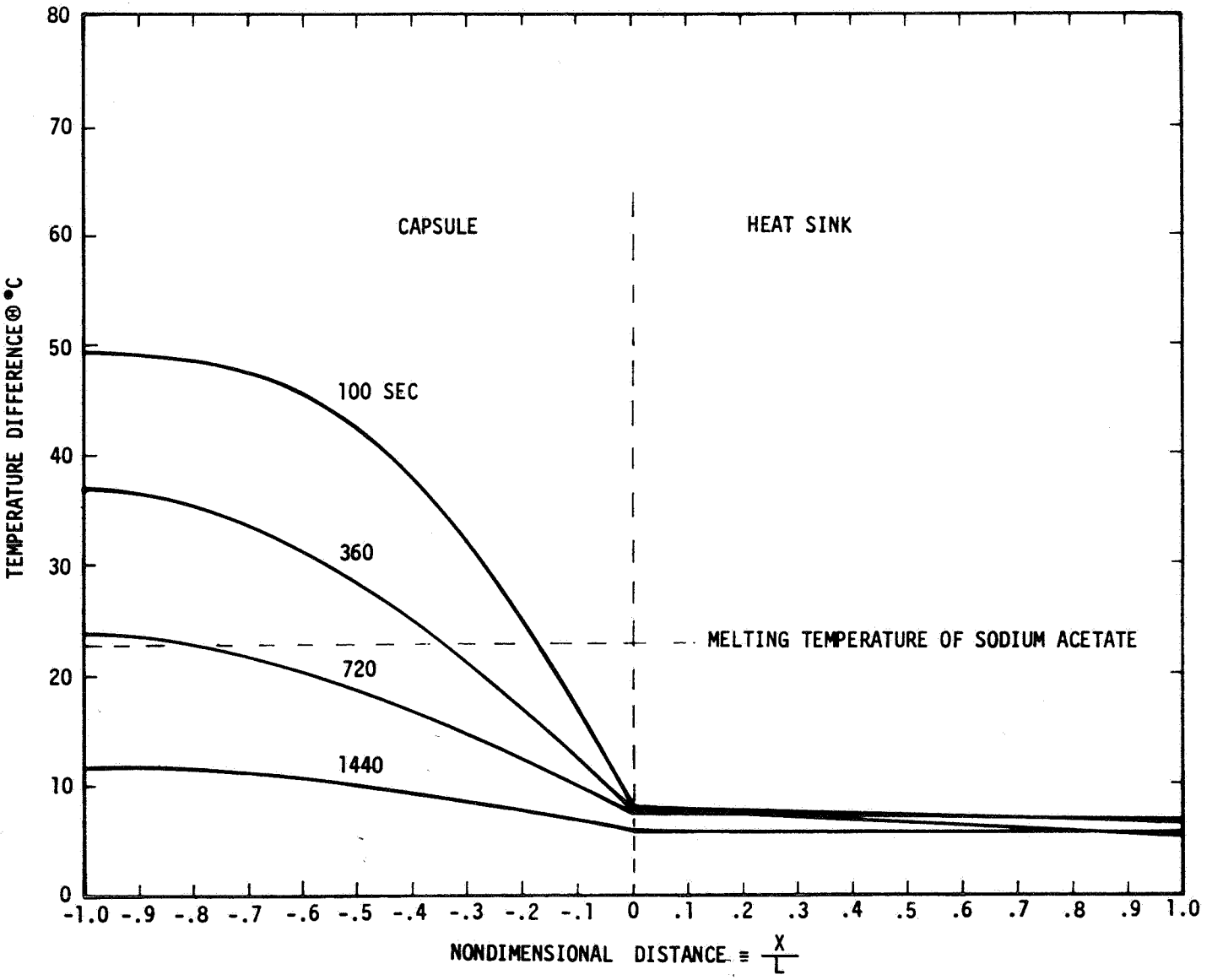

FIGURE 3-9. Calculated thermal profile of experiment 12c at various times.

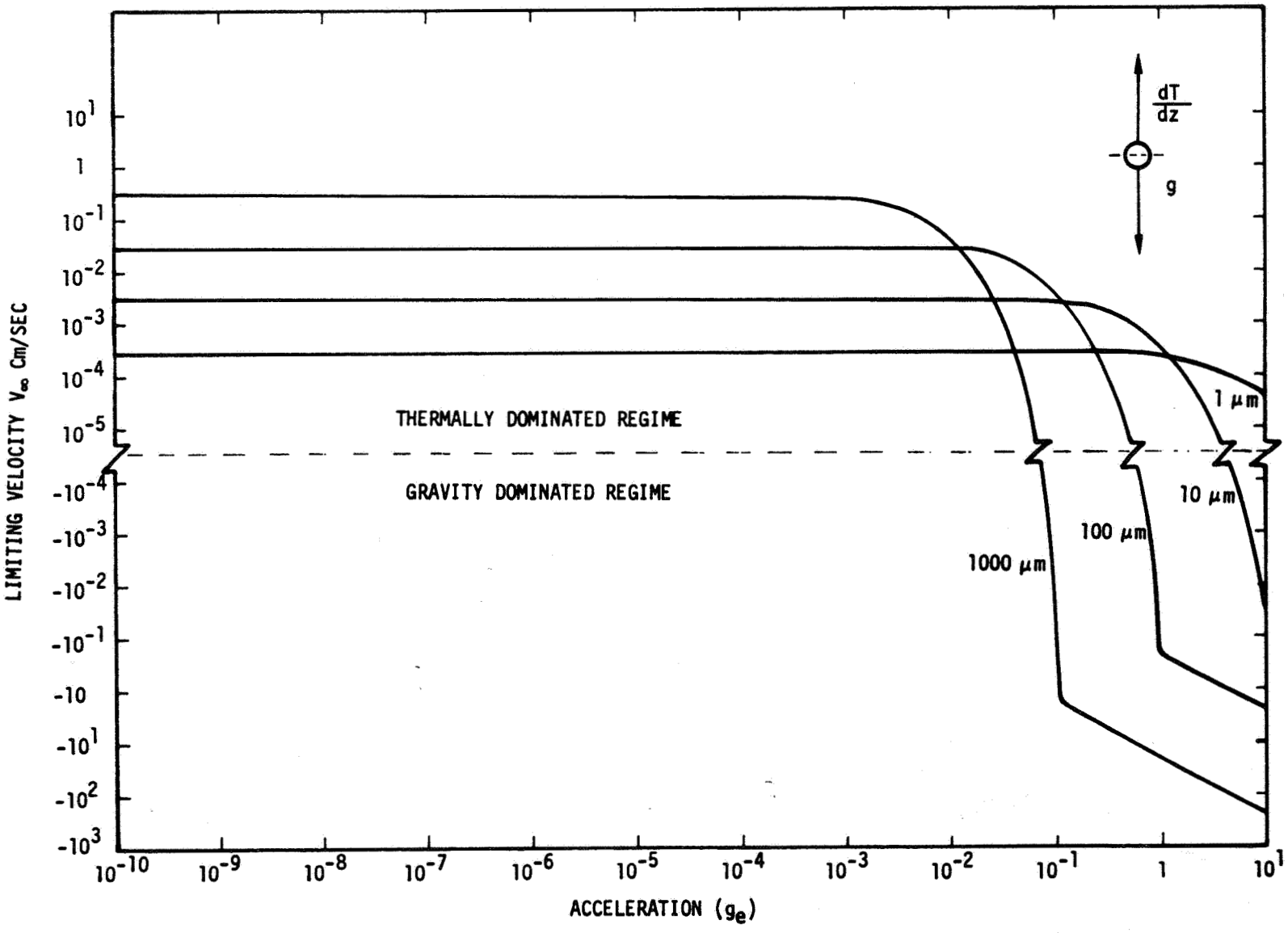

FIGURE 3-10. The limiting velocity of various radii sodium acetate droplets in paraffin as a function of acceleration. The temperature gradient was 10°C/cm.

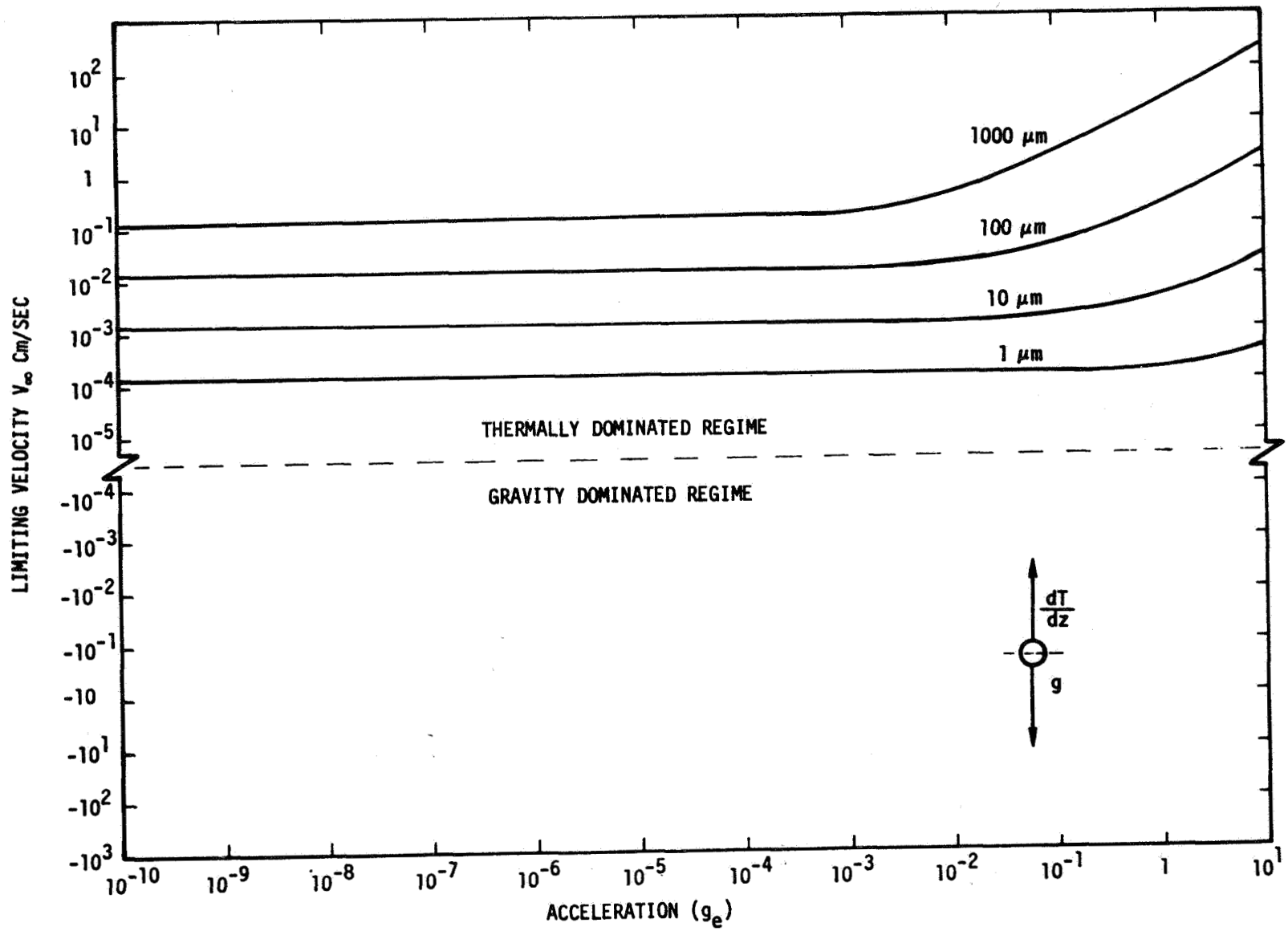

FIGURE 3-11. The limiting velocity of various radii paraffin droplets in sodium acetate as a function of acceleration. The temperature gradient was 10°C/cm.

$$V_\infty = \frac{2}{3\mu}\left[3\mu a \frac{d\sigma}{dT}\frac{dT}{dz}\left(2+\frac{k'}{k}\right)^{-1} - (\rho - \rho')\, g a^2 (\mu + \mu')\right] \qquad (8)$$
$$(3\mu + 2\mu')^{-1}$$

where k is the thermal conductivity and the primes denote the material property outside the bubble. This velocity has been computed as a function of acceleration level for both sodium acetate in paraffin and paraffin in sodium acetate and is displayed in Figures 3-10 and 3-11. The temperature gradient in these calculations was taken to be 10°C/cm, and was opposite to the acceleration vector. For sodium acetate droplets in paraffin it is interesting to note that the particle velocity reverses direction depending upon the magnitude of the acceleration field, whereas the bouyancy forces are reversed for paraffin droplets in sodium acetate due to gravity.

3.5 Particle Motion

The motion of groups of particles whether solid or fluid differs considerably from the motion of a single particle. The theoretical understanding of the motion and forces and group of particles in terms of first principles is not well understood, however, there are many accurate emperical relationships between particle velocity and particle concentration. One such function for particle velocity

$$V_p = V_\infty\ (1 - \alpha)^n, \qquad (9)$$

where V_∞ is the limiting velocity and α is the particle concentration. For rigid spheres, n = 4.65 and the velocity is zero when the spheres pack together at a concentration of $\alpha \simeq .64$.

In the case of bubbles or droplets, n has a value of 2. When particles agglomerate or flocculate n has values ranging from 20 to 30. The particle velocity divided by the Stokes velocity as a function of particle concentration for several values of n is shown in Figure 3-12. For example, in the experiments, the volume concentration of tungsten spheres was .2, this corresponds to a velocity for the group of particles which is .35 times the limiting single particle velocity.

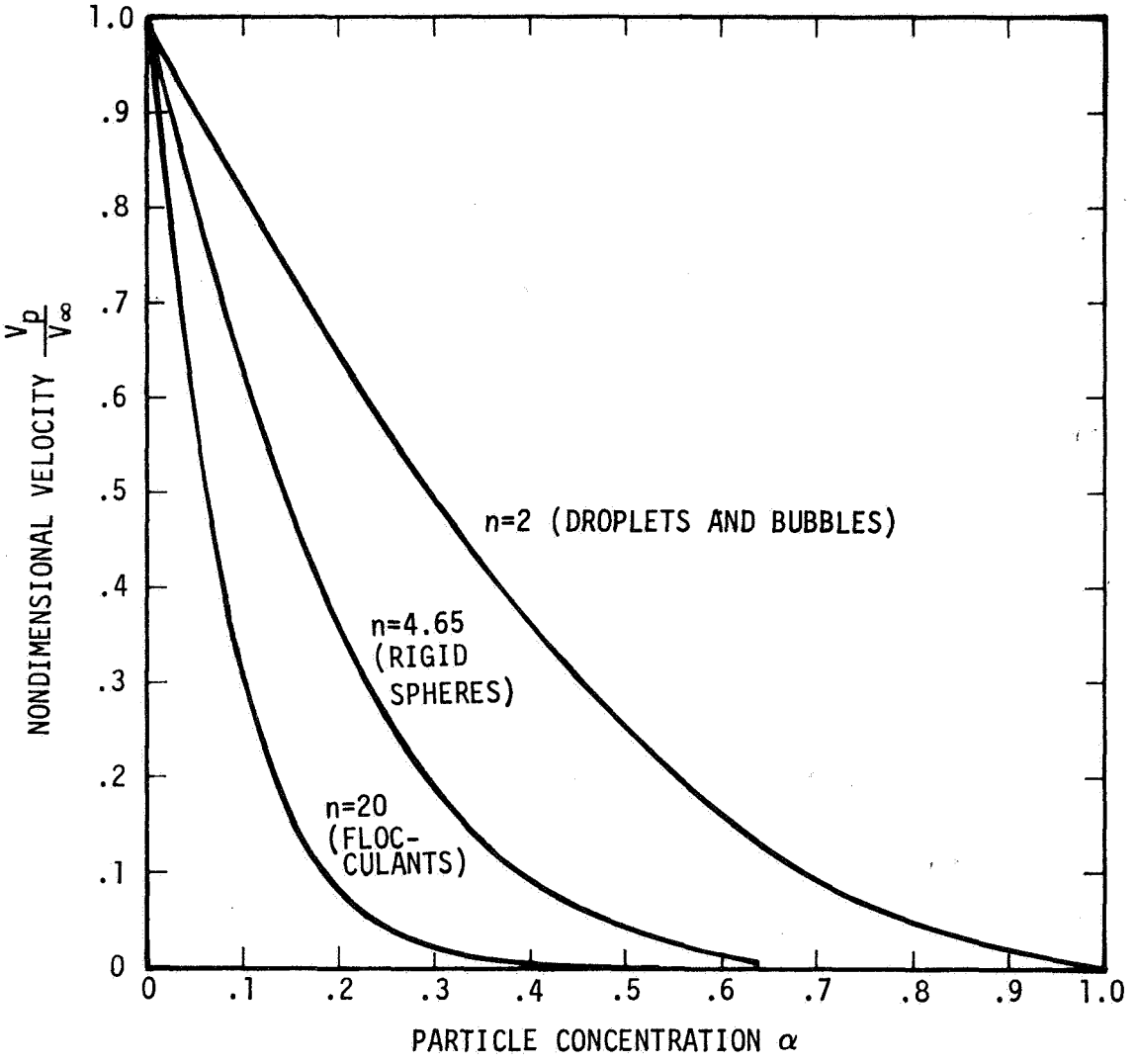

FIGURE 3-12. The velocity of a group of particles divided by the single particle limiting velocity as a function of particle volume concentration.

The global dynamics of dispersions of fluids or solid particles in thermal and/or acceleration fields can be analyzed in terms of sedimentation theory. In the following the drift flux model of sedimentation will be used to calculate the particle concentration histories. (Ref. 7). An important parameter in determining the time scale for this event is the limiting particle velocity. Again, note that the direction of this velocity will depend upon the relative magnitude of the thermal gradients and acceleration fields.

The settling process of an initially uniform suspension of particles subjected to a uniform body (acceleration) force field typically proceeds as follows. As settling starts to occur, a homogeneous fluid will appear at the top and a close packed sediment will appear at the bottom. These regions are labeled A and D respectively in Figure 3-13. The region B remains at the initial uniform particle concentration. Depending upon the initial particle concentration and the change in particle flux with concentration, there may be a region C in which the particle concentration is not uniform. If the particles are approximately the same size, then there will be a sharp discontinuity between regions A and B and C and D. The motion of these discontinuities are described by a concentration shock velocity. If there is no region C, then the settling process is governed by the shock trajectories of the interfaces of AB and BD and terminates when these shock fronts collide. If there is a region C, then at some time during the settling, region B will disappear and the event will terminate when the boundary of AC collides with CD. The evolution of the concentration in region C is determined by the concentration wave velocity and not the shock wave velocity since the particle concentration in this region is continuous.

The drift flux model has its basis in separated flow theory. In separated flow theory the motions of each of the constituents of a fluid are followed. The drift flux model however chooses variables in which the relative motion rather than the absolute individual motions are paramount. The derivations of the theory will not be given here but the following key variables will be defined. The total volumetric flux j, is the volumetric flow rate per unit area. The flux of each component of the flow is

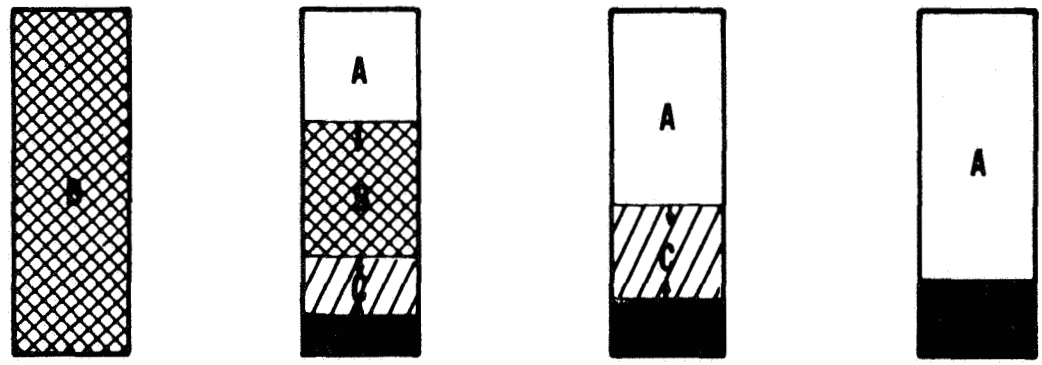

FIGURE 3-13. The settling process of an initially uniform suspension of particles subjected to a uniform body force field.

$$j_f = (1 - \alpha)\, v_f \tag{10}$$

$$\text{or} \quad j_s = \alpha\, v_s \tag{11}$$

where v_f and v_s are the various component flow and shock velocities respectively. The relative velocity between components is

$$v_{sf} = (v_s - v_f) = - v_{fs} \,, \tag{12}$$

and the drift velocity, defined as the difference between the component velocities and the average is as follows

$$v_{fj} = v_f - j \tag{13}$$

$$v_{sj} = v_s - j \tag{14}$$

The drift flux, which is the volumetric flux of a component relative to a surface moving at the average velocity is

$$j_{sf} = \alpha\, (v_s - j) \tag{15}$$

$$j_{fs} = (1 - \alpha)\, (v_f - j) \tag{16}$$

$$\text{or} \quad j_{sf} = j_s\, (1 - \alpha) - \alpha j_f = - j_{fs} \tag{17}$$

The drift flux velocity as a function of concentration has been measured for a wide variety of flow configurations. The following function describes this data quite well.

$$j_{fs} = V_\infty \alpha (1 - \alpha)^n \tag{18}$$

The exponent n here corresponds to same conditions as the previously defined n.

The sedimentation or settling process proceeds as a result of propagating shock waves and continuity waves. These shock and continuity waves refer to propagating discontinuities and gradients in the particle concentrations. The shock velocity is given in terms of the drift flux velocity by

$$U_s = \frac{(j_{fs})_1 - (j_{fs})_2}{\alpha_1 - \alpha_2} \quad , \tag{19}$$

and the continuity wave velocity by

$$U_w = - \frac{d}{d\alpha} (j_{fs}) \ . \tag{20}$$

In the following, two general cases of sedimentation will be analyzed, that of the motion of rigid spheres and liquid drops in a matrix fluid. The drift flux velocity as a function of concentration is sufficient information to determine the sedimentation dynamics. The drift flux velocity for rigid spheres is shown in Figure 3-14. Note that at a concentration of $\alpha = .64$ that the spheres pack and the flux is zero. The shock wave velocity (Eq. 19) for the interface AB has been calculated and shown in Figure 3-15, and similarly the continuity wave velocity (Eq. 20) which controls the concentration in region C is shown in Figure 3-16. The time history of the interfaces AB and AC was calculated using Wallis' generalized representation of sedimentation, (Ref. 8), and is shown on Figure 3-17. The volumetric concentration of rigid spheres was .2. These values correspond to specimen 12 with the tungsten microspheres. The solutions are presented in terms of reduced height and reduced time. For a given acceleration level and therefore limiting velocity, the sedimentation history is determined. For example, in a one gravity

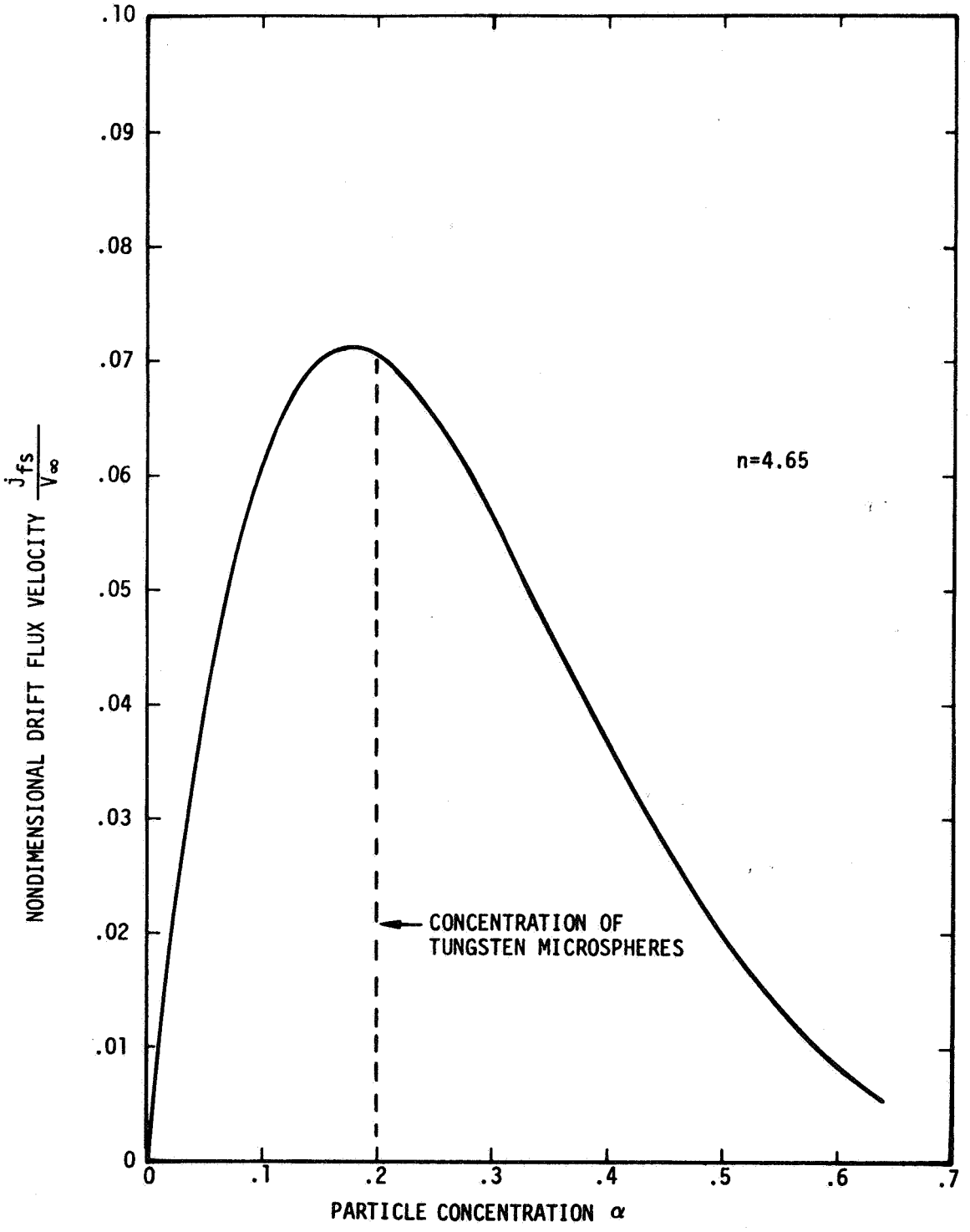

FIGURE 3-14. The drift flux velocity of rigid spheres as a function of particle volumetric concentration.

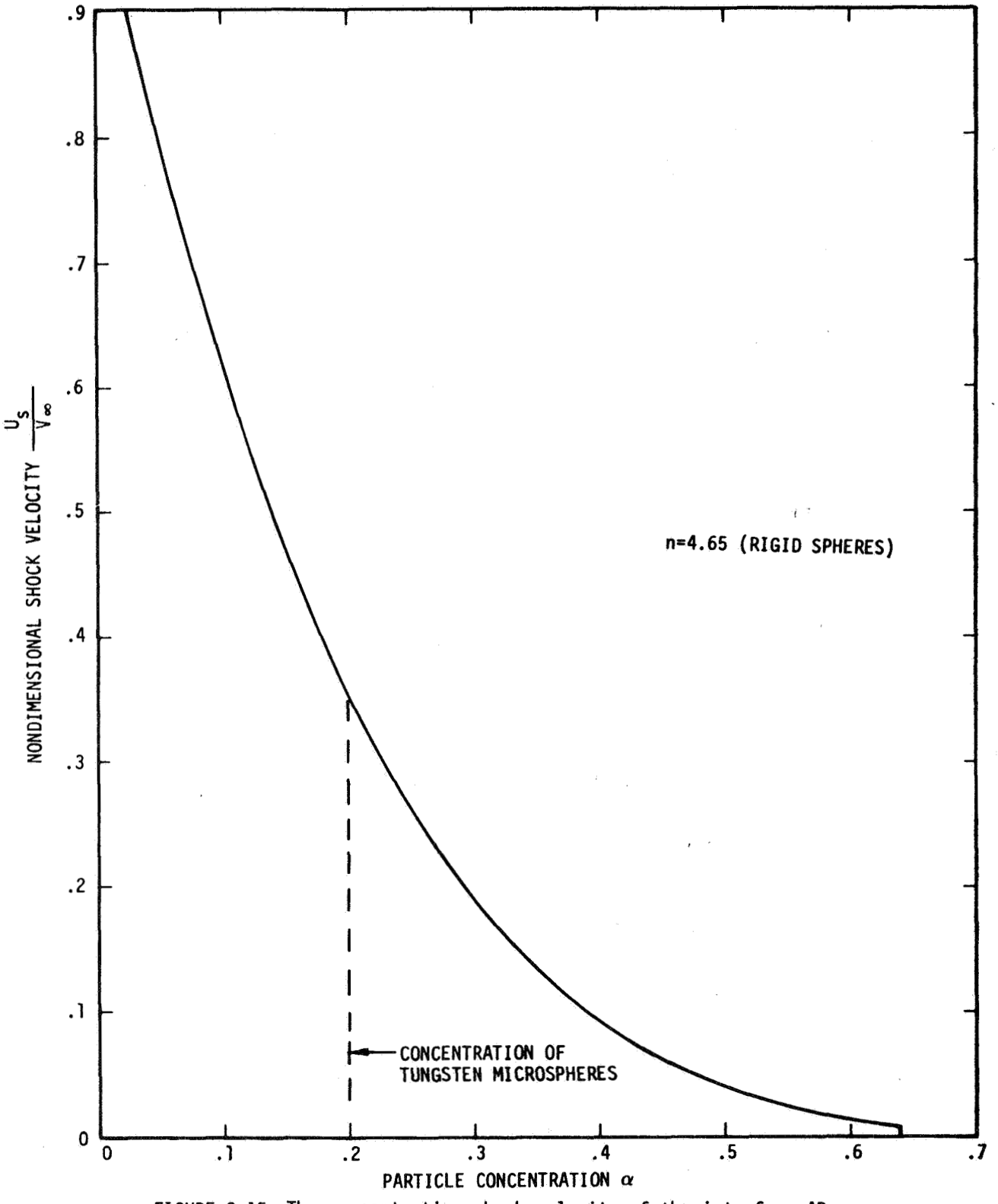

FIGURE 3-15. The concentration shock velocity of the interface AB as a function of particle volumetric concentration.

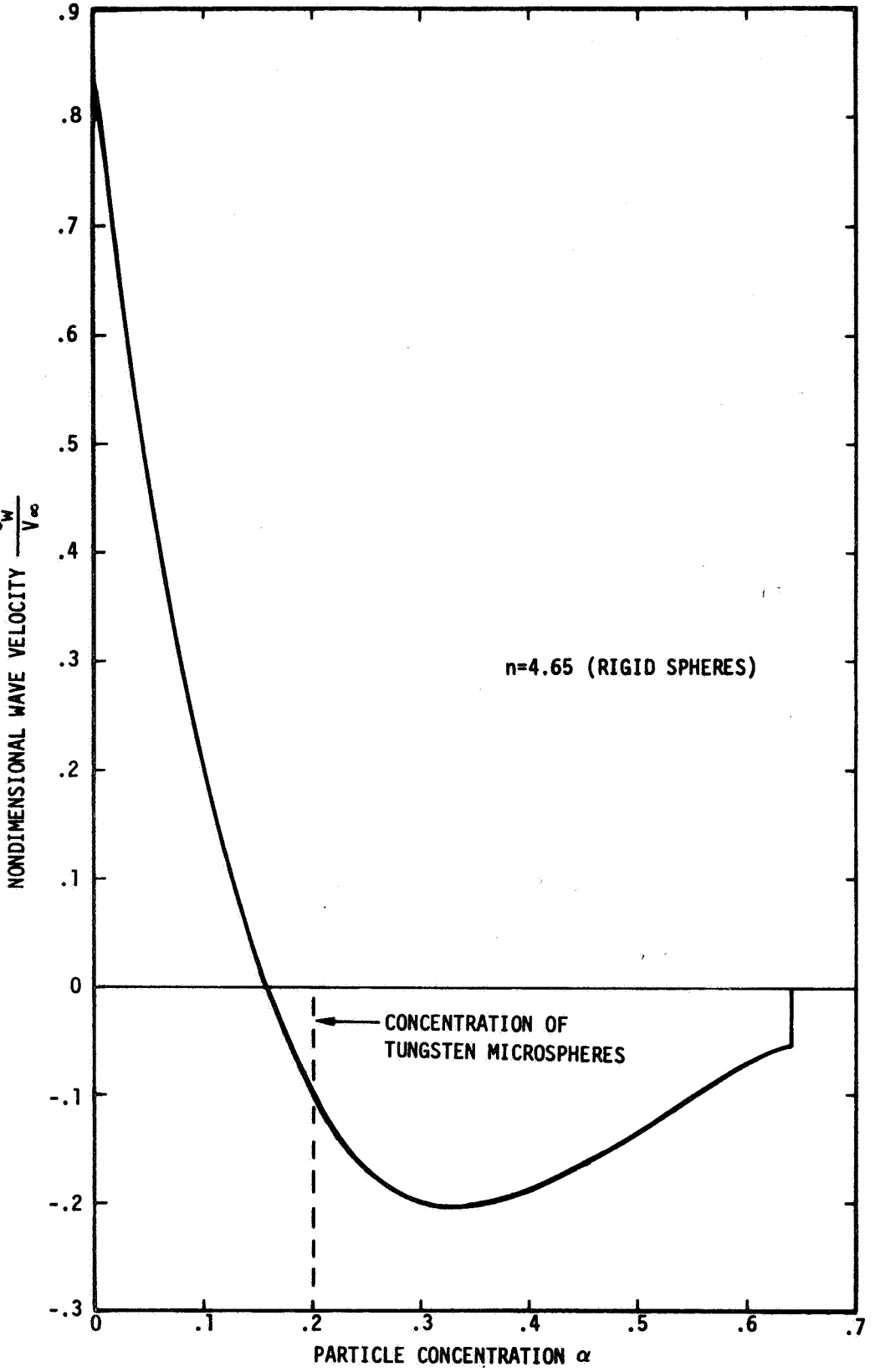

FIGURE 3-16. The continuity wave velocity as a function of particle volumetric concentration.

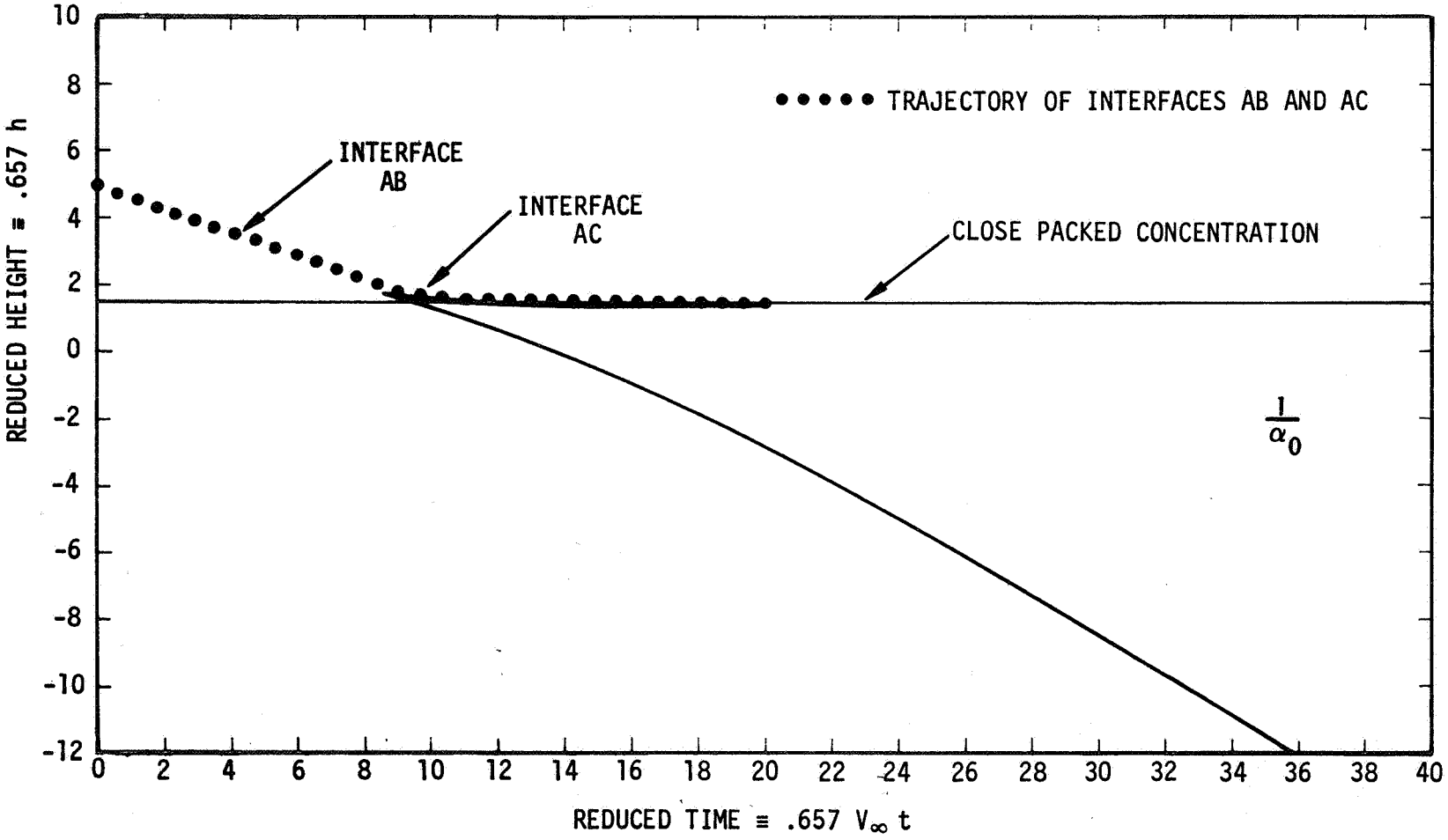

FIGURE 3-17. The time history of sedimentation of tungsten microspheres with an initial volumetric concentration of .2.

acceleration field the limiting velocity of tungsten microspheres in paraffin is 1.87 cm/sec. The time for settling to the limiting concentration of .64 is approximately 10 seconds. (See Figure 3-4). This is much shorter than the cooling time of the capsules. In a 10^{-4} g_e acceleration field the limiting velocity is 1.87 X 10^{-4} cm/sec and the settling time would be on the order of 10^{+3} seconds. This time is of the same order as the solidification time and therefore complete sedimentation would not be expected in this case. Note that for this initial concentration of .2, that there exists an area of non-uniform concentration (region C).

The second case to be considered is that of the motion of liquid drops in a matrix fluid. The exponent n for this situation is 2 and the volumetric concentration was allowed to very from 0 to 1. (Ref. 9). The drift flux velocity, shock velocity of the interface AB and the continuity wave velocity were calculated as before. These results are presented in Figures 3-18, 3-19 and 3-20.

The settling history of the interfaces AB and AC is shown in Figure 3-21. The volumetric concentration was taken to be .5, which would be representative of the three series of experiments. In these cases, for an imposed one gravity acceleration field, with an average particle size of 100μm, the settling time would be on the order of 75 seconds for a sodium acetate particle in paraffin. At the other extreme, when the imposed acceleration field is less than 10^{-3} g_e and the thermal gradient is 10°C/cm then the sedimentation time for a 100μ sodium acetate droplet in paraffin would be on the order of 500 seconds. Since the complete solidification time is approximately 900 seconds, incomplete segregation should be observed in these experiments conducted in a low gravity environment.

A simple and approximate criteria that the sedimentation process be stable and not bubble is that the Froude number remain less than unity. (Ref. 10).

The Froude number divided by the limiting velocity was calculated for the cases of n = 4.65 and n = 2 and is shown in Figures 3-22 and 3-23.

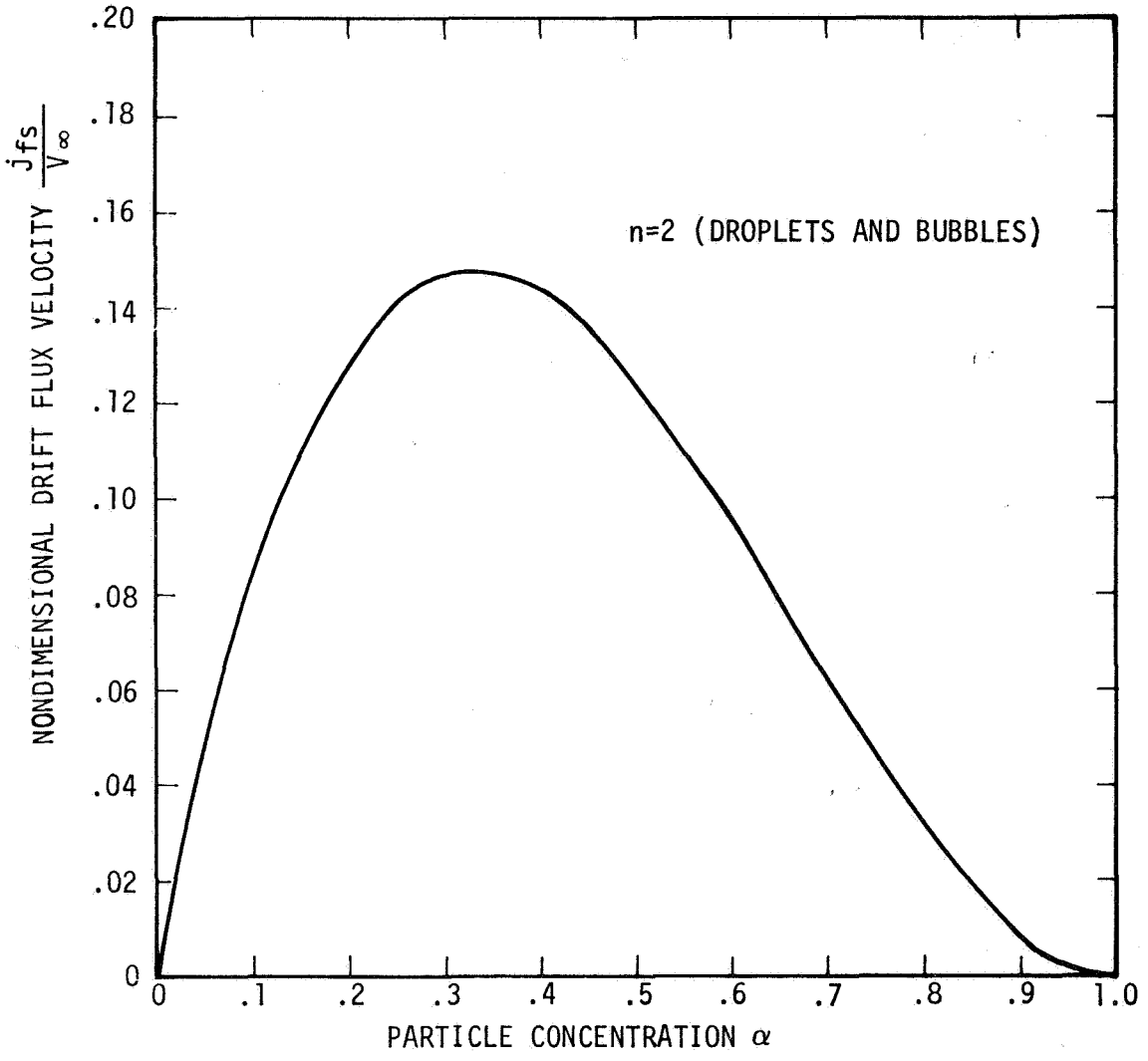

FIGURE 3-18. The drift flux velocity of droplets and bubbles as a function of volumetric concentration.

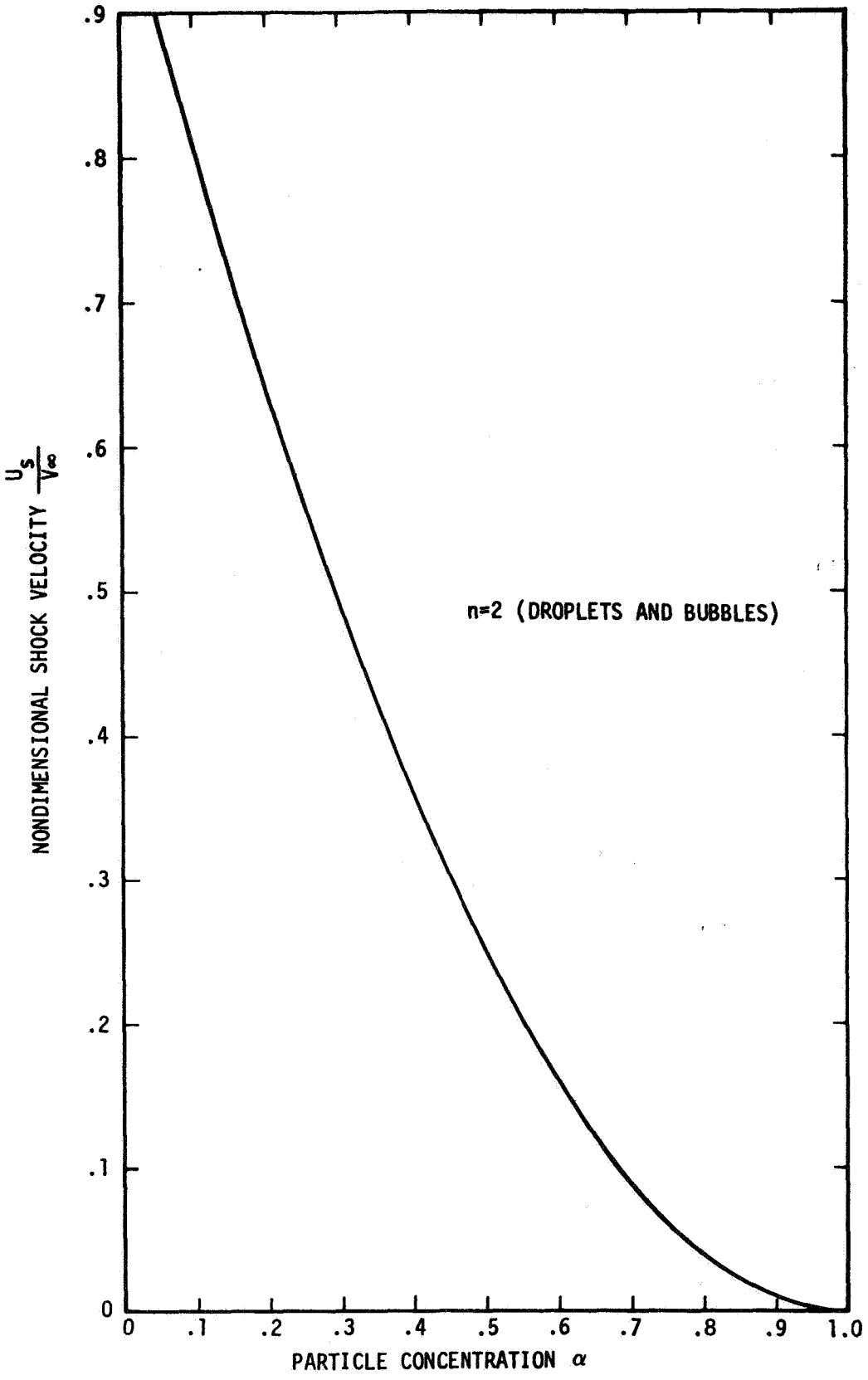

FIGURE 3-19. The concentration shock velocity of the interface AB as a function of volumetric concentration.

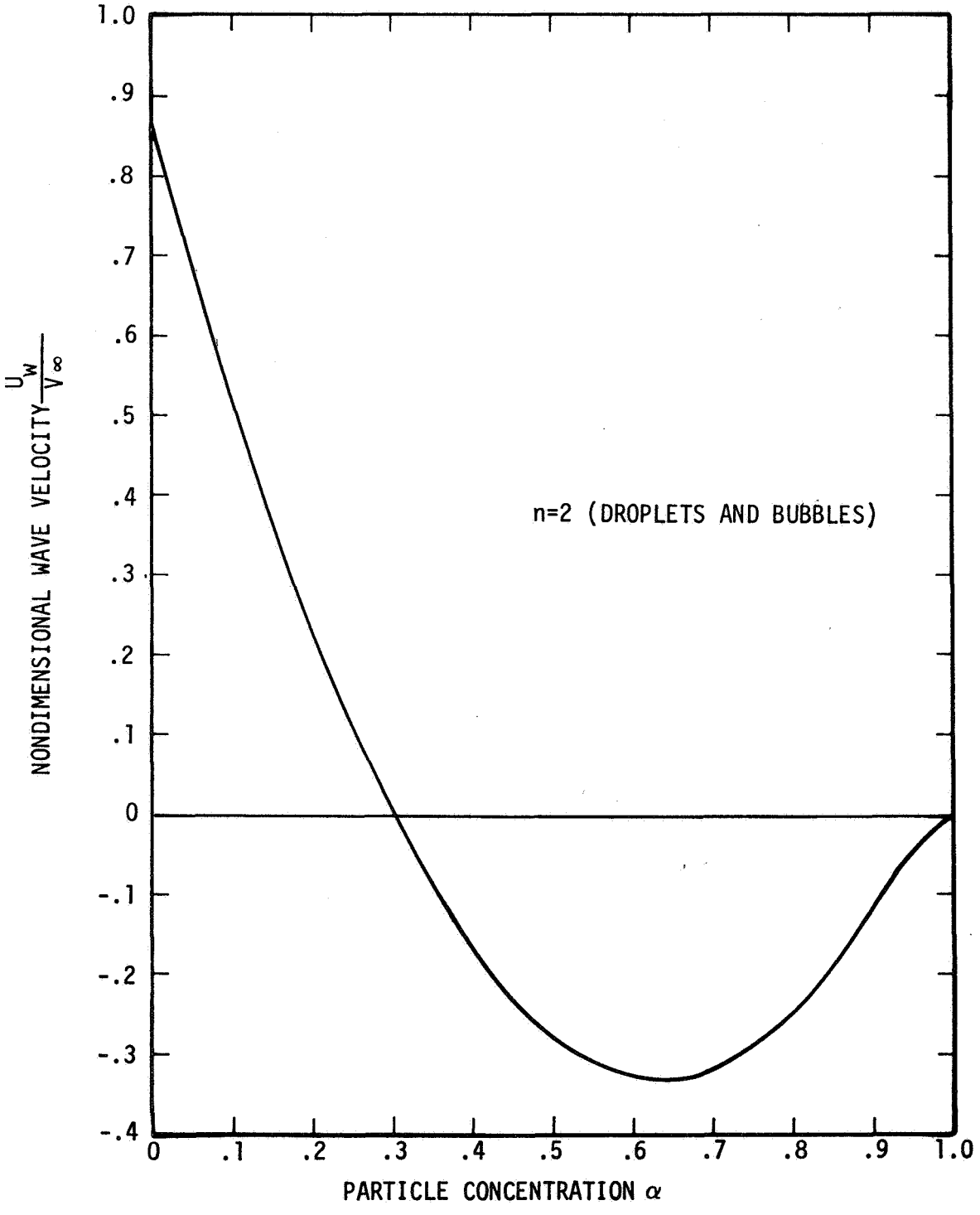

FIGURE 3-20. The continuity wave velocity as a function of volumetric concentration.

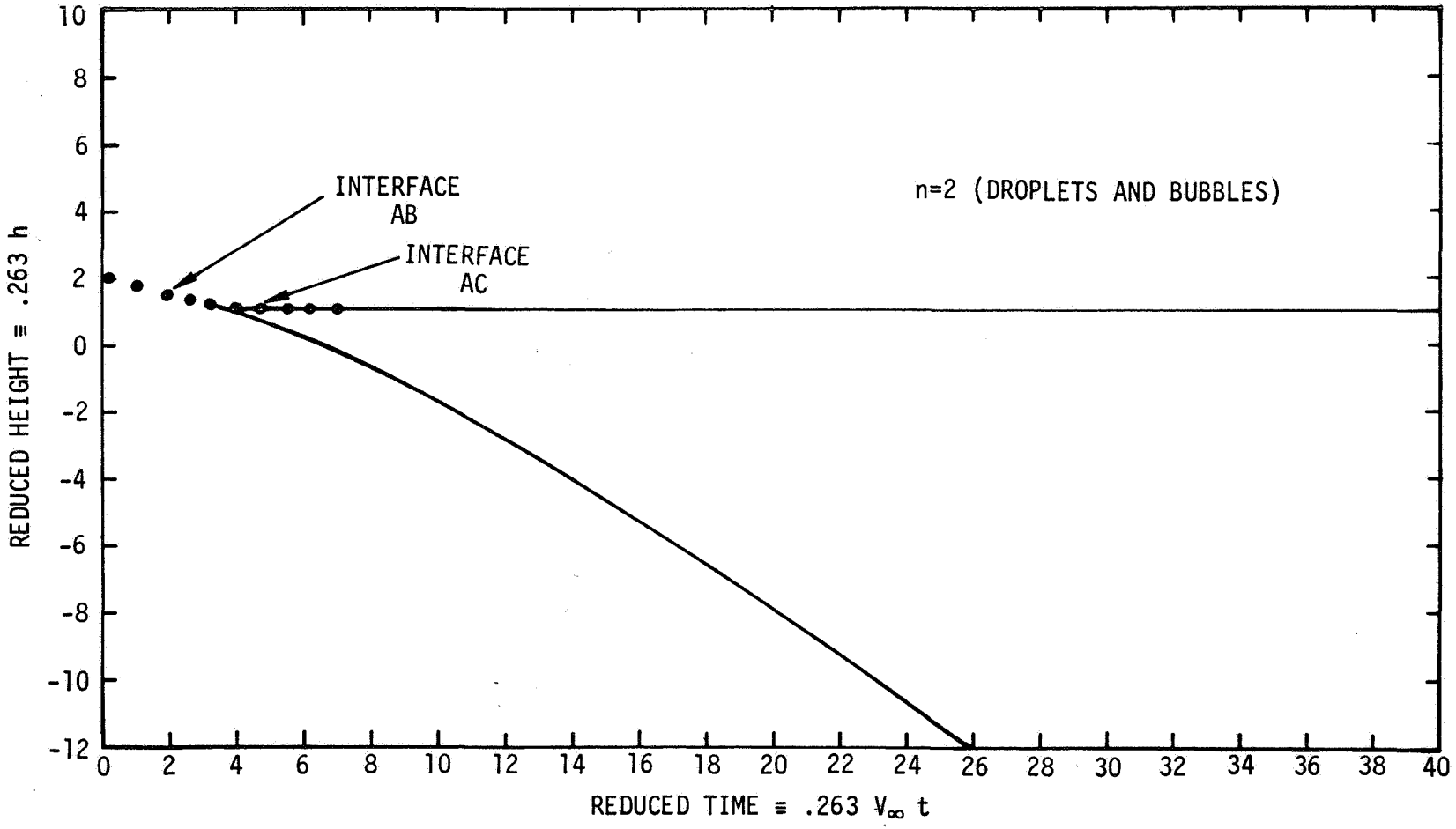

FIGURE 3-21. The time history of the settling of droplets or bubbles with an initial volumetric concentration of .5.

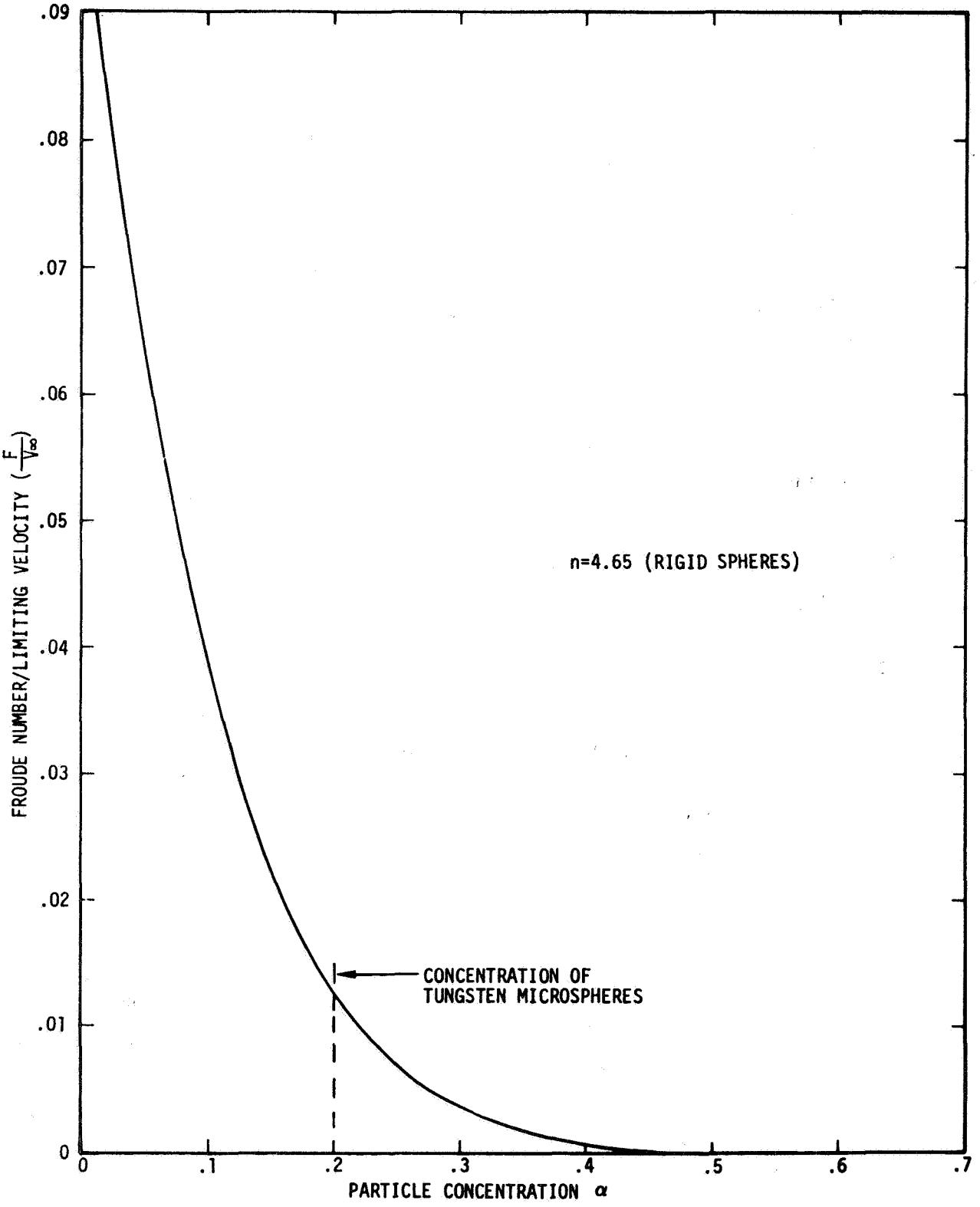

FIGURE 3-22. Froude number divided by limiting velocity as a function of volumetric concentration.

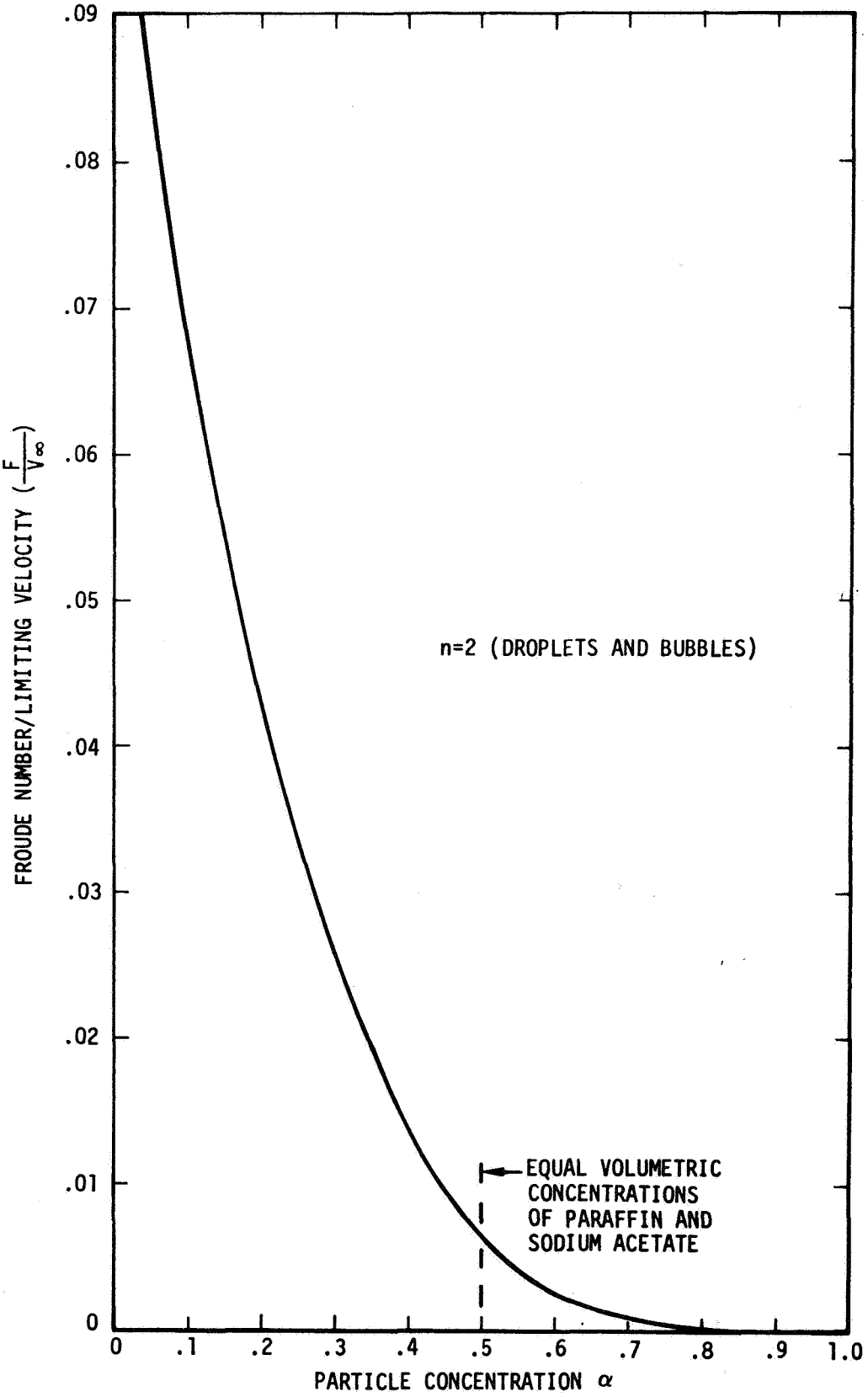

FIGURE 3-23. Froude number divided by limiting velocity as a function of volumetric concentration.

For the range of limiting velocities in both the control and flight experiments the Froude number was less than unity and therefore the sedimentation would be expected to be stable; i.e., the sedimentation would not exhibit any anomalous behavior such as streaming, layering, etc.

4.0 COMPARISON OF CALCULATED DATA WITH SPECIMEN EVALUATION

4.1 General

This comparison is based upon the interpreted experimental data of the specimens and theoretical fluid mechanical data computed for various droplet sizes, distributions and gravitational and thermal models of the materials. Due to the complex fluid, thermal and acceleration behavior of the materials, certain modeling simplifications were assumed. The most serious modeling limitations are in the treatment of the droplet behaviors of the materials during processing and subsequent cooldown. However, each of these areas were parametized with respect to observed phenomena and are discussed below, with the assumptions and limitations delineated.

4.2 Fluid Behavior

The calculated curves in Figure 3-1, Section 3.2 provide the characteristic times for viscous decay, spin-up and boundary layer growth for liquid sodium acetate and paraffin during the shaking period and after insertion on the cooling pin. A characteristic frequency of 1 sec^{-1} was used as the average shaking frequency used by the astronaut during the processing time. The curves show that boundary layer growth occurs rapidly and that viscous decay is constant for all frequencies. Spin-up time, which is assumed to be the upper bound for spin-down or the fluid deceleration time is relatively short, indicating that the fluids are in a turbulently mixed regime soon after the capsule is inserted on the cooling pin.

Boundary layers are evident on Flight Specimens 6 and 9, from the paraffin coating on 9 and the partial sodium acetate coating on the top half of 6. Flight Specimen 12 does not show a prominant boundary layer, although an outer layer is primarily sodium acetate. This may be due to the presence of the tungsten microspheres, which were preferentially wetted by the paraffin and thus may have affected the mean fluid properties of the paraffin-sodium acetate mixture.

Wall bound droplets were not observed in any of the specimens, as discussed in Section 3.2. The reason for this is not known, but the build-up of a

boundary layer during processing as well as droplet coalescence on the container wall may have prevented this phenomenon from occurring.

Examination of the Bond number indicates that the sodium acetate-paraffin system is capillary dominated for accelerations less than 10^{-2} g_e or 0.098 M/sec^2. In addition, the characteristic time for the system to revert to an equilibrium capillary configuration after an imposed body force is removed is small, on the order of 0.1 second. The calculated acceleration level at solidification from the capsule wall-paraffin interfaces for Flight Specimens 6 and 12 indicate 10^{-3} g_e or 0.0098 M/sec^2. The acceleration level may not have been as low as this during the complete solidification time, as indicated by the Reaction Control System firings during cooldown of Flight Specimen 12. The firing time coincides with the calculated solidification time in the thermal analysis.

4.3 Thermal Analysis

Figures 3-6 and 3-7 in Section 3.3 show the thermal history of Control Specimens 9C and 12C, measured at MSFC. The circled points are computed temperatures using the thermal properties of the materials. The measured and computed temperatures are in reasonably good agreement. Since the thermal properties of the materials dominate the transfer of heat from the capsule to the heat sink, the dotted line in Figures 3-8 and 3-9 showing the melting point of sodium acetate can be taken as a time-distance indicator of the solidification front. As an example, for Control Specimen 9C, approximately one-half of the specimen length was solidified at 720 seconds after insertion on the cooling pin. At the same cooling time, however, approximately 80 percent of the length of Control Specimen 12C was solidified.

The thermal curve for Control Specimen 6C was intermediate between the other two specimens, but approximated 12C. Thus complete solidification is estimated to have occurred between 800 and 1000 seconds for all specimens, or a mean of 900 seconds. The solidification time then was fastest for 12C, somewhat slower for 6C, and slowest for 9C. For the subsequent discussions, this same sequence will be assumed for the flight specimens.

4.4 Surface Tension and Bouyancy Driven Convection Force Analyses

Figures 3-10 and 3-11 in Section 3.4 illustrate the importance of considering both thermally dominated surface tension and gravity dominated regimes when dealing with two phase liquid behavior.

For sodium acetate droplets in paraffin, the droplet movement remains in the thermally dominated regime until the acceleration level becomes greater than 10^{-2} g_e. The droplets become gravity influenced as evidenced by lowering the limiting velocity in the thermal dominated regime. The direction of motion reverses in the gravity dominated regimes and the velocity increases with increasing g_e.

By contrast, in the case of paraffin droplets dispersed in sodium acetate, the droplet movement is always toward the region of higher temperature being in the thermally dominated regime. In a gravity field (10^{-2} g_e or greater), bouyancy forces further aid the surface tension driven convection forces to displace the droplets away from the gravity gradient.

In both cases, the droplet size is critical in determining both the limiting velocity and the behavior of the material. For dispersions containing a large variation in droplet sizes, a complex fluid motion would occur in which sedimentation, coagulation and agglomeration would play an increasingly larger role in the final configuration of the dispersed matrix.

4.5 Particle Motion

As mentioned in Section 4.2, the materials within the capsule are in a turbulent regime soon after the capsule is inserted on the cooling pin. This condition accentuates the dynamic dispersion of fluid droplets or solid particles in thermal/acceleration fields. Since the limiting velocities of groups of droplets or particles is appreciably slower as compared to single drops or particles, (Fig. 3-12), and the size distribution of the mixed materials also influences the limiting velocities, the final configuration of the dispersions is complex.

An initial equal particle concentration and mean particle size of sodium acetate and paraffin were assumed in calculating the sedimentation

behavior of this system. If incomplete mixing occurred, as is believed to be the case, causing a wide variation in droplet sizes, then the sedimentation behavior would be different from that modeled. This is due not only to the different velocities from the thermal and gravitational forces, but also to the influence on the various sedimentation velocities. Comparison of density and droplet distributions in Sections 2.4 and 2.5 and the thermal analysis in Section 3.4 indicates that incomplete mixing probably is the reason for the large droplets in all the flight specimens, and the non-uniform material concentrations in Flight Specimens 6 and 12. Flight Specimen 9 had the most homogeneous distribution, and also the slowest solidification rate, which may indicate that its thermal gradient was lower than the other two specimens. This postulation is corroborated by the larger number of duplex dispersions found in Flight Specimen 9 than in the other two specimens. Since duplex dispersions represent an unstable condition which exists only on Earth in emulsions undergoing reversion (Reference 12) they would be less likely to persist, the larger the thermal gradient.

5.0 CONCLUSIONS

Stable dispersions of immiscible materials processed in a low gravity environment have been demonstrated. The majority of the dispersions are between 25μm and 1 mm, although areas containing dispersions of 1μm or less and droplets of 1 cm have been observed in all three flight specimens.

Four stable types of dispersions have been observed in the specimens: sodium acetate in paraffin, paraffin in sodium acetate, a paraffin-tungsten microsphere blend in sodium acetate and sodium acetate in a paraffin-tungsten microsphere blend.

The last two dispersions were observed in Flight Specimen 12, predominantly the sodium acetate in the paraffin-tungsten microsphere blend. Since the tungsten microspheres are preferentially wetted by the paraffin, this phase tends to become the continuous phase, with sodium acetate the dispersed phase (Reference 13). The tendency of the system to stabilize in this mode was verified.

Stable duplex dispersions (and more complex forms) of either sodium acetate in paraffin or vice versa were observed in all three flight specimens, predominantly in Flight Specimen 9. Since this type of dispersion is unstable on Earth, this is a direct confirmation of the unique mixing of immiscible materials in a low gravity environment.

All three flight specimens displayed an axial gradation in density that was more gradual than the control specimens. None of the three flight specimens exhibited a homogeneous density distribution, indicating complete dispersion of the materials. However, the distribution in Flight Specimen 9 exhibited the best dispersions.

Examination of droplet size and distribution in the sectioned samples of all three flight specimens exhibited minimal radial differentiation, but droplet size increased longitudinally away from the heat sink end.

Comparison of the observed properties of the processed specimens with the theoretical analyses indicate the following general conclusions:

1. From the contact angle between the paraffin and the capsule wall on Flight Specimens 6 and 12, the acceleration level at solidification was approximately 10^3 g_e or 0.0098 M/sec^2.
2. Initial mixing was insufficient to thoroughly disperse the molten sodium acetate and paraffin.
3. The body force exerted on the specimens when they were inserted on the cooling pin had little or no effect on the distribution of the materials.
4. Since the cooling was essentially unidirectional, the surface driven convection forces were probably more predominant in causing fluid movement and droplet size and distribution differentiation than the acceleration forces present.
5. There is a possibility that some of the segregation of the materials in Flight Specimen 12 was caused by the Reaction Control System firings during capsule cooldown.
6. From the calculated limiting velocity and sedimentation curves, the critical droplet diameter is approximately 100μm. Droplets less than this size tend to be stable in a thermal or low gravity gradient. This was partially corroborated by the droplet distribution measurements for paraffin.

6.0 REFERENCES

1. Greenspan, "The Theory of Rotating Fluids", Cambridge Univ. Press, pg. 36.

2. W. Uterberg, J. Congelieve, "Zero Gravity Problems in Space Powerplants: A Status Survey", Am. Rocket Soc. J., Vol. 32, No. 6, June 1962, pg. 862-872.

3. C. E. Siegert, D. A. Petrash, and E. W. Otto, "Behavior of Liquid Vapor Interface of Cryogenic Liquids During Weightlessness", NASA TN D-2658, 1965.

4. W. C. Reynolds, M. A. Saad, and H. M. Satterlee, "Hydrostatic and Hydrodynamics at Low-g", Tech Rpt No. LG-3, Dept. Mech. Eng., Stanford Univ., Sept 1969.

5. D. A. Nield, Jour. Fluid Mech., Vol. 19, pg. 341, 1964.

6. J. F. Harper, D. W. Moore, JRA Pearson Jour. Fluid Mech., Vol 27, Part 2, pg. 361, 1967.

7. G. B. Wallis, "One Dimensional Two Phase Flow", McGraw-Hill, pg. 89, 1969.

8. G. W. Wallis, Symp. Interaction Fluids Particles, Inst. Chem. Engrs., London, pg. 9-16, 1962.

9. R. Gaylor, N. W. Roberts and H.R.C. Pratt, Trans. Inst. Chem. Engr., Vol. 31, pg. 57, 1953.

10. R. H. Wilhelm, M. Kwauk, Chem. Eng. Progr., Vol 44, pg. 201, 1948.

11. H. S. Carslan, J. C. Jaeger, Conduction of Heat in Solids, Oxford Press, 1959.

12. F. Seifriz, J. Phys. Chem. 29, 738 (1925).

13. J. J. Bickerman, Surface Chemistry, Academic Press, N.Y., N.Y., 377, 1958.

APPENDIX A
THERMAL ANALYSIS

The following model assumes the capsule, fluid mixture and copper sleeve can be represented by a finite homogeneous cylinder which is insulated on all sides except for the end connected to the heat sink. (This is called region 1.) Connected to the uninsulated end of region 1 is a semi-infinite insulated rod acting as a heat sink (region 2). The analysis assumes that at $t = 0$ the temperature is a constant θ_0 and uniform throughout region 1 and is zero in region 2.

The equations to be solved are in region 1,

$$\frac{\partial^2 \theta_1}{\partial X^2} - \frac{1}{K_1} \frac{\partial \theta_1}{\partial t} = 0 ,$$

and region 2,

$$\frac{\partial^2 \theta_2}{\partial X^2} - \frac{1}{K_2} \frac{\partial \theta_2}{\partial t} = 0 ,$$

where θ_1, θ_2 are the temperature, K_1, K_2 are the thermal diffusivities and x and t are the spatial coordinate and time respectively and k_1, k_2 are the thermal conductivities. (Ref. 11).
The above system will be solved by Laplace transforming the time variable and solving the resulting differential equation for the spatial variable. Transforming we have

$$\frac{d^2 \bar{\theta}_1}{dX} - \frac{p}{K_1} \bar{\theta}_1 + \frac{\theta_0}{K_1} = 0$$

which has a solution

$$\bar{\theta} = A \cosh q_1 (\ell + X) + B \sinh (\ell + X) + \frac{\theta_0}{p} ,$$